UNIVERSIDADE ESTADUAL DE CAMPINAS
FACULDADE DE ENGENHARIA MECÂNICA
E INSTITUTO DE GEOCIÊNCIAS

MOHAMMADREZA KESHAVARZ

A MODEL FOR ANALYSIS OF NON-NEWTONIAN FLUID FLOW IN NATURALLY-FRACTURED RESERVOIRS

UM MODELO PARA ANÁLISE DO FLUXO DE FLUIDOS NÃO-NEWTONIANOS EM RESERVATÓRIOS NATURALMENTE FRATURADOS

CAMPINAS
[2024]

MOHAMMADREZA KESHAVARZ

A MODEL FOR ANALYSIS OF NON-NEWTONIAN FLUID FLOW IN NATURALLY-FRACTURED RESERVOIRS

UM MODELO PARA ANÁLISE DO FLUXO DE FLUIDOS NÃO-NEWTONIANOS EM RESERVATÓRIOS NATURALMENTE FRATURADOS

Thesis presented to the Mechanical Engineering Faculty and Geosciences Institute of the University of Campinas in partial fulfillment of the requirements for the degree of Doctor of Philosophy in Petroleum Sciences and Engineering in the area of Reservoirs and Management.

Tese de Doutorado apresentada à Faculdade de Engenharia Mecânica e Instituto de Geociências da Universidade Estadual de Campinas como parte dos requisitos exigidos para obtenção do título de Doutor em Ciências e Engenharia de Petróleo, na área de Reservatórios e Gestão

Orientador: Prof. Rosângela Barros Zanoni Lopes Moreno

Este exemplar corresponde à versão final da Tese defendida pelo aluno MOHAMMADREZA KESHAVARZ e orientada pelo Prof. Rosângela Barros Zanoni Lopes Moreno.

CAMPINAS

[2024]

Ficha catalográfica
Universidade Estadual de Campinas
Biblioteca da Área de Engenharia e Arquitetura
Rose Meire da Silva - CRB 8/5974

K481m

Keshavarz, Mohammadreza, 1986-
A model for analysis of non-newtonian fluid flow in naturally-fractured reservoirs / Mohammadreza Keshavarz. – Campinas, SP : [s.n.], 2024.

Orientador: Rosângela Barros Zanoni Lopes Moreno.
Tese (doutorado) – Universidade Estadual de Campinas, Faculdade de Engenharia Mecânica.

1. Fluidos não-Newtonianos. 2. Reservatórios - Fratura. 3. Reservatórios de petróleo. 4. Reservatórios - Modelos matemáticos. 5. Poços de petróleo - Fluidos de perfuração. I. Moreno, Rosângela Barros Zanoni Lopes, 1966-. II. Universidade Estadual de Campinas. Faculdade de Engenharia Mecânica. III. Título.

Informações Complementares

Título em outro idioma: Um modelo para análise do fluxo de fluido não-newtoniano em reservatórios naturalmente fraturados
Palavras-chave em inglês:
Non-Newtonian fluids
Oil reservoir engineering
Reservoirs - Mathematical models
Drilling muds
Oil wells - Testing
Área de concentração: Reservatórios e Gestão
Titulação: Doutor em Ciências e Engenharia de Petróleo
Banca examinadora:
Rosângela Barros Zanoni Lopes
Joerg Dietrich Wilhelm Schleicher
Eduardo Cardoso de Abreu
Andre Leibsohn Martins
Tiago Luís Duarte Forti
Data de defesa: 02-02-2024
Programa de Pós-Graduação: Ciências e Engenharia de Petróleo

Identificação e informações acadêmicas do(a) aluno(a)
- ORCID do autor: https://orcid.org/0000-0002-7396-2919
- Currículo Lattes do autor: https://lattes.cnpq.br/4532920029339016

UNIVERSIDADE ESTADUAL DE CAMPINAS
FACULDADE DE ENGENHARIA MECÂNICA
E INSTITUTO DE GEOCIÊNCIAS

TESE DE DOUTORADO ACADÊMICO

A MODEL FOR ANALYSIS OF NON-NEWTONIAN FLUID FLOW IN NATURALLY-FRACTURED RESERVOIRS

Autor: Mohammadreza Keshavarz
Orientador: Prof. Rosângela Barros Zanoni Lopes Moreno

A Banca Examinadora composta pelos membros abaixo aprovou esta Tese:

Prof. Dr. Rosângela Barros Zanoni Lopes Moreno
UNICAMP

Prof. Dr. Joerg Dietrich Wilhelm Schleicher
UNICAMP

Prof. Dr. Eduardo Cardoso de Abreu
UNICAMP

Dr. Andre Leibsohn Martins
PETROBRAS

Dr. Tiago Luís Duarte Forti
SIMWORX

A Ata da defesa com as respectivas assinaturas dos membros encontra-se no processo de vida acadêmica do aluno

Campinas, 02 de Fevereiro de 2024.

DEDICATION

To the loves of my life — My father and mother. I would not be here without their support, encouragement, patience and most of all, their love.

ACKNOWLEDGEMENTS

I am profoundly grateful to the University of Campinas for providing me with the opportunity to undertake this research.

Special recognition goes to my advisor, Dr. Rosângela Barros Zanoni Lopez Moreno. Her unyielding support, academic rigor, and continuous encouragement throughout my PhD journey have been instrumental. Her inspiration, coupled with her kindness and empowering nature, have been invaluable. I am deeply thankful for her guidance in this research endeavor.

In summary, my sincere appreciation extends to both the University of Campinas and Dr. Moreno, for their crucial roles in making this scholarly journey possible.

RESUMO

Keshavarz, Mohammadreza, *UM MODELO PARA ANÁLISE DO FLUXO DE FLUIDOS NÃO-NEWTONIANOS EM RESERVATÓRIOS NATURALMENTE FRATURADOS*, Campinas, Faculdade de Engenharia Mecânica, Universidade Estadual de Campinas, 1993. 180 p. Dissertação (Doutorado)

A complexidade das operações de perfuração aumenta significativamente no contexto de reservatórios naturalmente fraturados (NFRs). A análise qualitativa e quantitativa das perdas de fluido de perfuração oferece critérios para algumas questões imperativas, como o projeto de fluido de perfuração não-Newtoniano que orienta ações corretivas precoces e o gerenciamento eficaz da pressão do poço. A pesquisa atual desenvolveu um modelo abrangente para abordar as limitações das metodologias pré-existentes. Este modelo leva em consideração as características dos NFRs, a reologia do fluido de perfuração, o fenômeno de perda de fluido e as condições do poço para prever a taxa e o volume de perda do fluido de perfuração até um grau aceitável. O modelo proposto é empregado para medir a taxa e o volume do fluido de perfuração não-Newtoniano escoando através de NFRs, levando em consideração a pseudo-plasticidade do fluido de perfuração não apenas para o sistema de fratura, mas também para o sistema de matriz sob pressão constante de poço (incorporando uma contribuição de matriz adimensional, D, na solução). A solução introduzida é eficaz em avaliar o progresso da fluido de perfuração tanto em NFRs quanto em reservatórios homogêneos. Esta metodologia desenvolvida é posteriormente aplicada para gerar curva-tipo para auxiliar nas análises qualitativas e quantitativas. A avaliação qualitativa é realizada para conduzir uma análise de sensibilidade em parâmetros de NFR e para examinar seu impacto no fenômeno de perda e no volume total de perda de fluidos do poço para o reservatório, enquanto a análise quantitativa mede as propriedades de NFR, o volume cumulativo total e o ROI (raio de invasão) em sistemas de unidades SI e de campo. A solução desenvolvida e as curvas-tipo são verificadas por dois métodos: primeiro, reduzindo-a a uma solução pré-existente (projetada para o caso do fluido Newtoniano) incorporando suas suposições; e segundo, aplicando-se dados de campo de medições de perda de um poço fraturado no Golfo do México. Casos sintéticos são utilizados para demonstrar a aplicação do fluxo de trabalho para medir propriedades de NFR, de taxa de perda de um fluido de perfuração e da perda total, e os resultados são comparados com modelos anteriores. O estudo destaca a influência das propriedades do NFR e da pseudo-plasticidade do fluido de perfuração (representada pelo índice de comportamento do fluxo, n) na taxa de perda de fluido de perfuração, volume total de perda e no fenômeno de perda de fluido, especialmente sob uma suposição de pressão constante dentro do poço. Este estudo sugere procedimentos práticos para ajustar as propriedades do fluido de perfuração e projetar tratamentos que interrompam perdas adicionais desse fluido. Nas condições estipuladas do poço, os operadores podem utilizar efetivamente a pseudo-plasticidade dos fluidos de perfuração como uma ferramenta para mitigar a perda de fluido de perfuração, especialmente através de NFRs com características de perda mais altas. O estudo identifica três períodos no fenômeno de perda de fluido de perfuração através dos NFRs, dependendo das propriedades deste, da reologia do fluido de perfuração e do coeficiente de perda: tempo inicial, período transiente e tempo tardio. Cada período requer um fluido de perfuração específico com pseudo-plasticidade distinta para mitigar a perda de fluido de perfuração e otimizar o desempenho da operação de perfuração. A pesquisa sugere que o projeto do fluido de perfuração deve garantir alta pseudo-plasticidade durante os tempos iniciais e finais e menor pseudo-plasticidade durante o período transiente. (Pode ser aplicado para técnicas de MPD* para perfurar perspectivas desafiadoras). Esta pesquisa aconselha a formulação de fluidos de perfuração para manter elevada pseudo-plasticidade nas fases inicial e final, e níveis baixos durante o período transiente. (Pode ser aplicado a técnicas de MPD para perfurar prospectos desafiadores). Os resultados também indicam que o período transiente desempenha um papel fundamental no fenômeno de perda de fluido de perfuração através de NFRs. Sugere-se manter este período curto enquanto se tenta manter uma taxa de invasão mais baixa do fluido de perfuração. A pseudo-plasticidade do fluido de perfuração pode desempenhar um papel crítico no controle deste período. A análise paramétrica revela um impacto significativo da pseudo-plasticidade do fluido de perfuração no volume cumulativo e no ROI em NFRs com pressão diferencial maior, perda e aberturas de fratura maiores. Além disso, o procedimento permite aos operadores determinar o ROI para os tempos de início e fim equivalentes do período transiente. O modelo proposto aprimora a conclusão de poços, a recuperação avançada de petróleo (EOR), a caracterização de NFR e as operações de perfuração ao facilitar a análise precisa das propriedades do reservatório e dos volumes de fluido em NFRs. Ele orienta os operadores na refinaria da reologia do fluido de perfuração para minimizar a perda de lama e melhorar a eficiência no flooding polimérico, otimizando assim o desempenho em reservatórios complexos.

Palavras-Chave: Fluidos não-Newtonianos; Reservatórios - Fratura; Reservatórios de petróleo; Reservatórios - Modelos matemáticos; Poços de petróleo - Fluidos de perfuração

* Managed Pressure Drilling ou Perfuração com Pressão Gerenciada

ABSTRACT

The complexity of drilling operations significantly intensifies in the context of naturally-fractured reservoirs (NFRs). Quantitative and qualitative analysis of drilling fluid losses offers a criterion for some imperative issues such as designing Non-Newtonian drilling fluid which guides early remedial actions and managing wellbore pressure effectively. In this study, I develop a comprehensive model to address the limitations of pre-existing methodologies. This model takes into account the characteristics of NFRs, the rheology of the mud, the leak-off phenomenon, and the wellbore conditions to predict the rate and volume of mud loss to an acceptable degree. The proposed model allows for gauging the rate and volume of Non-Newtonian drilling fluid through NFRs, taking into consideration the pseudo-plasticity of the drilling fluid not just for the fracture system, but also for the matrix system under constant wellbore pressure (incorporating a dimensionless matrix contribution, D, into the solution). The introduced solution is proficient in assessing drilling-fluid progress in both NFRs and homogeneous reservoirs. Subsequently, I apply it to generate type-curves to aid in quantitative and qualitative analyses. By utilizing qualitative evaluation, I conduct a sensitivity analysis on NFR parameters to examine their impact on the leak-off phenomenon and total loss volume, while a quantitative analysis measures NFR properties, total cumulative volume, and ROI in both SI and field unit systems. Next, I verify the solution and type-curves through two methods: first, by reducing it to the pre-existing solution (designed for the Newtonian fluid case) by incorporating their assumptions; and second, by applying field data of loss measurements from a fractured well in the Gulf of Mexico. Four cases demonstrate the application of the workflow to measure NFR properties, mud loss rate, and total loss, and allow the comparison of the results with previous models. The study underscores the influence of NFR properties and mud pseudo-plasticity (represented by the flow behavior index) on the drilling fluid loss rate, total loss volume, and the leak-off phenomenon, especially under a constant pressure assumption within the wellbore. The findings suggest practical procedures to adjust drilling-fluid properties and design remedial mud loss treatments to halt further drilling fluid loss. Under the stipulated wellbore conditions, operators can effectively utilize the pseudo-plasticity of drilling fluids as a tool to mitigate mud loss, particularly through NFRs with higher leak-off characteristics. The study identifies three periods in the mud loss phenomenon through NFRs, depending on their properties, mud rheology, and leak-off coefficient: early time, transient period, and late time. Each period requires a specific drilling fluid with distinct pseudo-plasticity to mitigate mud loss and increase performance. This research suggests that drilling-fluid design should ensure high pseudo-plasticity during early and late times and lower pseudo-plasticity during the transient period. (Can be applied for MPD* techniques to drill challenging prospects). The results also indicate that the transient period plays a pivotal role in the mud loss phenomenon through NFRs, and suggest decreasing this period while keeping the rate of mud advancement low. The pseudo-plasticity of drilling fluid can play a critical role in controlling this period. A parametric analysis reveals a significant impact of drilling-fluid pseudo-plasticity on cumulative volume and radius of invasion (ROI) in NFRs with higher differential pressure, leak-off, and larger fracture apertures. Additionally, the procedure allows operators to determine the ROI for equivalent starting and ending times of the transient period. The proposed model enhances well-completion, enhanced oil recovery (EOR), NFR characterization, and drilling operations by facilitating precise analysis of reservoir properties and fluid volumes in NFRs. It guides operators in refining drilling-fluid rheology to minimize mud loss and improve efficiency in polymer flooding, thereby optimizing performance in complex reservoirs.

Keywords: Non-Newtonian fluid; Oil reservoir engineering; Reservoirs – Mathematical models; Drilling muds; Oil wells - Testing

* Managed Pressure Drilling

LIST OF FIGURES

LIST OF TABLES

NOMENCLATURE

List of abbreviations and acronyms Units

A	Area, L2, [m2] or [ft2]
A_{m-f}	Cross-sectional area matrix to fracture, L2, [m2] or [ft2]
D	Dimensionless Matrix contribution, dimensionless
Ei	Exponential integral, dimensionless
I0	Modified Bessel Functions of the first kind, zero order, dimensionless
I1	Area, L2, [m2] or [ft2]
Iv	Modified Bessel Functions of the first kind, v order, dimensionless
K0	Modified Bessel Functions of the first kind, zero order, dimensionless
K1	Modified Bessel Functions of the first kind, first order, dimensionless
K_v	Modified Bessel Functions of the first kind, v order, dimensionless
L	Length, L, [m, cm] or [ft, in]
V	Velocity, L/t, [m/s] or [ft/s]
V_r	Rock volume, L3, [m3] or [ft3]
Y	Distance, L, [m] or [ft]
co	Fluid compressibility, (M/Lt2)-1, [Pa-1] or [psi-1]
cr	Formation compressibility, (M/Lt2)-1, [Pa-1] or [psi-1]
c_t	Total compressibility, (M/Lt2)-1, [Pa-1] or [psi-1]
h	Net pay thickness, L, [m] or [ft]
k	Permeability, L2, [mD] or [m2]
k_f	Fracture permeability, L2, [mD] or [m2]
k_m	Matrix permeability, L2, [mD] or [m2]
k_r	Radial Permeability, L2, [mD] or [m2]
n	Flow behavior index, dimensionless
p	Pressure, M/Lt2, [Pa] or [psi]
P_f	Pressure in the fracture, M/Lt2, [Pa] or [psi]
P_i	Initial pressure, M/Lt2, [Pa] or [psi]
p_m	Pressure in the matrix, M/Lt2, [Pa] or [psi]
P_D	Dimensionless pressure, dimensionless
P_{DNN}	Dimensionless Non-Newtonian pressure, dimensionless
P_{fD}	Dimensionless pressure in the fracture, dimensionless
P_{mD}	Dimensionless pressure in the matrix, dimensionless
P_{wD}	Dimensionless wellbore pressure, dimensionless
q	Flowrate, L3/t, [m3/sec] or [ft3/s]
q_m	Matrix flowrate, L3/t, [m3/sec] or [ft3/s]
q_D	Dimensionless flow rate, dimensionless
Q_D	Dimensionless cumulative volume (In this case cumulative mud loss or any other Non-Newtonian fluids), dimensionless
r	Radial distance, L, [m] or [ft]
t_D	Dimensionless time, dimensionless
t_{DNN}	Dimensionless Non-Newtonian time, dimensionless
ω	Storativity ratio, dimensionless
ΔL	Length, L, [m] or [ft]
Δp	Pressure differential, M/Lt2, [Pa] or [psi]
$\gamma^{\cdot}$	Shear rate, t-1, [s-1]]
μ	Newtonian Viscosity, M/Lt, [cp] or [lbm/ft.s]
μ_{eff}	Effective viscosity, M/Lt, [cp] or [lbm/ft.s]
λ	Interporosity flow parameter, dimensionless
ϕ	Porosity, fraction
ϕ_f	Fracture Porosity, fraction
ϕ_m	Matrix Porosity, fraction
ρ	Density, M/L3, [kg/m3] or [lbm/ft3]
τ	Shear stress M/Lt2, [N/m2] or [lbf /ft2]

α	Shape factor, dimensionless
DGD	Dual Gradient Drilling
DMTC	Derivative-based mud type-curves
LWD	Logging While Drilling
MPD	Managed Pressure Drilling
MTC	Mud type-curves
NFR	Naturally-fractured reservoir
TP	Transient period

TABLE OF CONTENT

Table of Contents

1 INTRODUCTION

Lost circulation is experienced in all types of reservoirs. However, naturally-fractured reservoirs (NFRs) are particularly prone to severe mud losses. Lost circulation into fractures has been the most serious formation-damage mode for the fractured reservoir (Carlson, 1999; Xu et al., 2016; Fakoya and Ahmed, 2018; Okoro et al., 2018; Mansour et al., 2019; Wu et al., 2020; Chan et al., 2022). It also presents challenges due to uncertainties in the fracture characteristics (notably fracture aperture) and loss rate. Natural fractures are recognized as beneficial for production; however, they introduce complications during drilling operations. A total-loss situation through NFRs under high downhole differential pressure can pose significant challenges. Consequently, it is imperative to address the loss before the continuation of drilling operations. A reliable estimate of NFR characteristics is required for the design of remedial drilling fluid loss treatments (Razavi et al., 2015, 2016, 2017a). Losses through NFR are controlled by the natural-fractured system, including fracture orientation, fracture density, fracture roughness, and distribution of fracture aperture; the losses through NFR also depend on other factors such as wellbore pressure, the drilling-fluid rheology and composition, the leak-off through the fracture walls, and filter-cake buildup inside the fracture. Severe mud losses can create subsequent problems such as well-control issues and formation damage. Therefore, loss circulation presents a key challenge to health and safety and the economic viability of drilling a well. Losses through matrix should be distinguished from losses through natural fractures. Dyke et al. (1995) demonstrated that mud loss through natural fractures can be distinguished from that through matrix pores. Mud loss through fractures initiates with pronounced losses that subsequently decline over time, whereas mud loss through pores commences slowly and intensifies gradually. A realistic procedure for assessing the mud-loss behavior of yield power-law drilling fluids in fractured formations must consider both leak-off and the transient period. NFRs are inherently heterogeneous across multiple scales, presenting unique challenges in reservoir characterization. Researchers identify these complexities as arising primarily from two relatively independent systems: the fracture system and the porous matrix system. Each system contributes uniquely to the reservoir's overall behavior, necessitating a comprehensive and multi-faceted approach for accurate analysis and prediction under different operational conditions. In academic literature, mathematical representations of these reservoirs are typically formulated as either single or double porosity models (Wennberg et al., 2006; Golghanddashti, 2011; Narr, 2011; Rezaee, 2015; Abbasi et al., 2017; Wang et al., 2018;).

In the endeavor to understand and measure loss through NFR, numerous researchers have developed both analytical and numerical models (Liétard et al., 1999; Lavrov, 2006; Majidi et al., 2010; Razavi et al., 2017b; Dokhani et al., 2019). Liétard et al., (1999) developed a mathematical model for an infinite fracture to predict the radial flow of Bingham-plastic drilling fluids. This model postulated that mud advancement would ultimately halt due to mud yield stress (Miska et al., 2008; Majidi et al., 2010). This approach informed an approximate formulation for predicting the lost circulation of yield power-law fluids in NFRs. It was found through a sensitivity analysis that increasing the yield stress or the flow-behavior index of the drilling fluid could mitigate mud losses. Razavi et al. (2017) presented a theoretical model for predicting the infiltration of drilling mud into NFRs. However, this model, like its predecessors, grappled with several issues including the over-simplification of complex physical processes and limited applicability across various types of NFRs. Bychina et al. (2017) introduced a versatile model that can manage different fluid rheologies, thereby eliminating the need for individual models for NFR tailored to each fluid type. Their model considers fracture deformation and both constant and variable leak-off rates into the formation. A sensitivity analysis was performed to discern the effects of variables such as fracture normal stiffness, leak-off rate, mud-yield stress, and aperture on mud losses. The model demonstrates that fracture deformation, leak-off pressure, and fluid yield stress significantly influence fluid loss in the formation. Dokhani et al., (2019) revisited the mud-loss issue by combing fracture deformation and leak-off from fracture surfaces to describe the mud-loss pattern through NFRs. The predictions of this numerical model reveal that, depending on the magnitude of the leak-off coefficient, it is possible to identify three major patterns for transient mud-loss data. Concurrently, several researchers have presented reservoir models that take into account flow behavior within a double-porosity reservoir. Warren and Root (1963) suggested a direct proportional relationship between the pressure difference in matrix-fracture systems and the fluid-flow transfer rate in fully-linked, regularly fractured media. Da Prat (1990) introduced the concept of outer bounded boundary and constant pressure conditions at the inner boundary for radial reservoirs, leading to the development of characteristic type curves, enabling analysis based on these assumptions. Garcia-Pastrana et al. (2017) assessed a reservoir model that considers Non-Newtonian behavior within a double-porosity reservoir. Their model revealed an inter-porosity transfer function for the pseudo-steady state by incorporating the dimensionless matrix contribution parameter. Unlike previous efforts, their approach focuses on Non-Newtonian fluid flow through NFRs and extends the model's applicability to most practical mud-loss measurement cases. A review of existing literature reveals that the effects of the leak-off phenomenon through NFRs, influenced by their natural characteristics, are not accurately considered. Further, the optimization of mud pseudo-plasticity for each scenario and period, which offers a criterion for designing loss preventative materials, and early remedial actions are the focal points of this study. In this thesis, we present an evaluated solution for the dual porosity diffusivity model (proposed by Garcia-Pastrana et al., 2017 in the literature) under a constant inner wellbore pressure. The solution, which considers the physics of pseudo-steady state inter-porosity transfer for Non-Newtonian fluids, gives the drilling fluid rate and invaded volume through NFRs (Keshavarz, M., & Moreno, R. B. Z. L. 2023). The solution in dimensionless terms is then numerically found using the inverse Laplace transform with the Stehfest algorithm (Stehfest, 1970). Additionally, unit conversion terms convert dimensionless terms into dimensional ones for drilling fluid rate, total loss volume, and wellbore differential pressure. By varying scenarios based on NFR properties and mud rheology, a series of type-curves are generated to perform qualitative and quantitative mud loss analyses. I validate the numerical solution for the diffusivity equation through two methods: first, by comparing the results with the solution obtained by Da Prat (1990) under the assumption of Newtonian reservoir fluid, and second, by using drilling fluid loss measurements from a fractured well in the Gulf of Mexico (Majidi et al., 2010). This work has practical implications for forecasting the rate and volume of Non-Newtonian fluids through NFRs, determining rock properties, and enhancing oil recovery mechanisms, such as polymer injection for oil production. By integrating the varied characteristics of NFR geology and fluid rheology, this research significantly enhances the reliability of these forecasts. These improvements are crucial for optimizing drilling operations and customizing oil recovery strategies to meet the unique challenges presented by NFRs.

1.1 Motivation

The study of drilling-fluid-loss models provides invaluable insights; however, these models are often accompanied by certain limitations. A critical deficiency arises from the lack of realistic characterization of Naturally Fractured Reservoirs (NFRs), which decreases the accuracy of mud-loss prediction, especially in complex cases. Traditionally, mud-loss models have been constructed based on the conservation of mass and momentum for transient radial flow in a variable-width fracture unit, or a single fracture. These models often overlook the important fact that an NFR comprises a system of matrix-fracture structures. Moreover, existing models tend to consider the Non-Newtonian behavior of drilling fluids throughout the fracture system, while neglecting the advancement of Non-Newtonian drilling flow through the matrix system. This oversight can lead to inaccurate predictions of reservoir behavior. The primary motivation of this research is to address these gaps. Our work presents an evaluated solution that not only takes into consideration the Non-Newtonian drilling-flow advancement through both the matrix and the total system but also aims to improve the characterization of drilling-fluid invasion into NFRs. Our approach aims to make models more geologically and rheologically consistent, thereby enhancing the predictive accuracy of mud-loss phenomena. Another key motivation for this research is the need for a robust methodology that can generate type-curves to facilitate both quantitative and qualitative analysis of drilling fluid loss. Such a methodology must consider the characteristics of NFRs, the rheology of drilling fluid, and wellbore conditions. Furthermore, our work also aims to categorize mud-loss phenomena from two distinct perspectives, bringing a new depth of understanding to this critical area. Ultimately, there is a pressing need for an efficient workflow that allows for real-time measurement of NFR properties during drilling operations, thereby substantially improving operational efficiency. This research is driven by the necessity for such an advanced workflow and the potential benefits it could bring to the field of drilling.

1.2 Objectives

The objective of this research is to derive a comprehensive and evaluated solution to quantify the drilling fluid loss rate, total loss volume, and NFR characteristics, incorporating the complexities of mud rheology and reservoir properties. Subsequently, the study aims to introduce a streamlined workflow that translates results from dimensionless terms to dimensional in real-time in both SI and field units. The specific objectives to fulfill this overarching goal are:

- ✓ Assess the significance of NFR characteristics and drilling-fluid pseudo-plasticity, and their interaction on the leak-off phenomenon, drilling fluid rate, and total loss volume. That includes a sensitivity analysis on these factors to propose practical procedures for modifying drilling-fluid properties and designing remedial mud-loss treatments for each scenario to curtail further drilling fluid loss.
- ✓ Evaluate the influence of NFR characteristics and drilling-fluid rheology on the transient period, a critical factor in the mud-loss phenomenon.
- ✓ Identify wellbore conditions that enable operators to utilize drilling-fluid rheology as an effective tool to control mud-loss progression through NFRs with different leak-offs.
- ✓ Provide a flexible and applicable solution for not only NFRs but also homogeneous reservoirs (after simplification) to measure drilling-fluid loss rate and volume. This allows for the comparison of the influence of mud pseudo-plasticity on loss volume between NFRs and homogeneous reservoirs.
- ✓ Improve the total loss-volume estimation by incorporating not just a unique fracture width, but also a matrix-fracture system that captures the physical phenomena of drilling-fluid progression through NFRs.
- ✓ Generate dimensionless type-curves to facilitate qualitative and quantitative analysis through NFRs, enabling the quantification of NFR properties (by applying curve-fitting techniques), drilling-fluid rate, total loss volume, and the performance of sensitivity analyses on NFR parameters to observe their influence on the leak-off phenomenon and total loss volume during different periods.
- ✓ Develop a workflow to simultaneously measure total loss volume and NFR properties during drilling.
- ✓ Quantify drilling-fluid volume through each specific period separately, particularly the early and transient periods.

- ✓ Determine the ROI for equivalent starting and ending times of the transient period.
- ✓ Identify and manage the transient period effectively to suggest drilling fluids with optimum rheology.
- ✓ Manage the leak-off phenomenon in NFRs through different periods.
- ✓ Identify the optimum differential pressure inside the wellbore to mitigate further loss.

Each of these objectives contributes to a broader understanding of mud-loss phenomena in both homogeneous reservoirs and NFRs and provides practical tools for its effective management.

1.3 Thesis outline

This dissertation is organized into seven chapters.

Chapter 1 serves as the introduction, setting the stage for the ensuing chapters.

Chapter 2 provides the theoretical background and reviews key bibliographic references that support the methodology of this study.

Chapter 3 delineates the general methodological procedures used to derive the evaluated solution and generate type-curves. This chapter also presents a workflow for quantifying and analyzing parameters for each case.

Chapter 4 assesses the applicability of the proposed workflow through four cases, working within the framework of the evaluated model. This section includes the validation of the model and a comparison of the results with existing models.

Chapter 5 discusses and presents the research results, divided into five sections. It includes a qualitative and quantitative analysis of NFR geology and fluid rheology, focusing on their impact on drilling fluid rate and volume. The key sections are as follows:

- The derivation of the evaluated solution to measure Non-Newtonian fluid rate and volume for two types of reservoirs.
- A comparison of drilling fluid rate and cumulative loss volume in homogenous and NFR settings, with an analysis of how drilling-fluid pseudo-plasticity affects drilling fluid rate and volume in these two types of reservoirs.
- A sensitivity analysis on NFR properties to observe their influence on Non-Newtonian fluid rate and volume through NFR with varying degrees of leak-off.
- An integrated evaluation of the simultaneous impact of two critical factors, mud rheology, and dimensionless matrix contribution, on the cumulative volume of Non-Newtonian fluid aims to elucidate their interactive effects on total cumulative volume measurement.
- An examination of the influence of wellbore boundary conditions on total cumulative volume, and the introduction of different criteria to categorize types of mud loss.

Chapter 6 presents the main accomplishments of the research and suggests potential applications of the findings.

Finally, Chapter 7 outlines future research directions, proposing methods to extend the model's applicability to different Non-Newtonian fluids through the COMSOL program. This chapter acts as a guide for subsequent researchers, offering insights into potential areas for further development and enhancement.

2 FUNDAMENTAL AND LITERATURE REVIEW

This chapter offers a comprehensive literature review and outlines the fundamentals of drilling fluid loss, the characteristics of naturally fractured reservoirs (NFRs), the leak-off phenomenon, and pre-existing models used to measure total loss volume. The primary emphasis of this review is on the aspects related to NFRs. The review will delve into an in-depth exploration of the current literature and prevailing theories in the field, along with an examination of the methodologies, findings, and conclusions drawn from past research. The objective is to illuminate the current understanding and prevailing knowledge gaps regarding the complex interplay between drilling fluid loss, NFR characteristics, and the leak-off phenomenon. This in-depth literature review will ultimately serve as a foundation upon which the subsequent chapters of this thesis are built.

2.1 Lost circulation

Lost circulation is one of the most troublesome drilling problems. In addition to mud loss itself, lost circulation can also lead to formation damage, wellbore instability and derivative issues (e.g., pack-offs, stuck pipe), and wellbore-control issues (Mahmoudi et al., 2016). As a consequence, the economic implications are substantial, largely stemming from the loss of expensive drilling fluid into the formation. This loss often accounts for a significant non-productive time dedicated to regaining circulation (Cook, 2011; Feng et al., 2015; Feng and Gray, 2018). Mud loss can be classified into four categories based on the severity of the losses, as detailed in Table 2.1.

Table 2.1: Mud loss classification (Guillot et al., 1990; Pilehvari and Nyshadham, 2002; Majidi et al., 2008; Razavi et al., 2014).

Classification of mud loss according to their severity			
loss rate less than 10 bbl/h, ie, below 1.6 m3/h Seepage losses	10-100 bbl/h, ie,1.6-16 m3/h Partial loss	More than 100 bbl/h, ie, above 16 m3/h Severe loss	No returns to the surface Total loss

Conventional drilling operations are commonly conducted under various circumstances and are classified according to Table 2.2.

Table 2.2: Conventional drilling operations (Rehm, 2012).

Three general regimes of drilling fluid density		
Overbalanced drilling	**Balanced pressure drilling**	**Underbalanced operations**
Uses fluid density that produces about 150 psi overbalance against borehole pressure (BHP)	Fluid column, either static or circulating, is balanced against BHP	Deliberately keeps the fluid column below BHP by including drilling with air or gas

Overbalanced drilling is achieved by using heavier drilling fluid to maintain wellbore pressure above formation pressure. Although this is done with the main purpose of killing the well, there are various problems accompanying overbalanced drilling which are detailed in Table 2.3.

Table 2.3: Disadvantageous of overbalanced drilling (Ostroot et al., 2007)

Overbalanced drilling disadvantages						
Loss circulation	Pipe sticking	Minimizing differential sticking	Formation damage	Reduction of well productivity due to skin	Disguise lithology changes and transition zones	Reduce the rate of penetration substantially

Avoiding and mitigating lost circulation requires well-thought-out strategies and thorough preparation, taking into account all crucial factors during the operation. Lost circulation can be addressed through both preventive and corrective procedures, as illustrated in Table 2.4.

Table 2.4: Procedures to mitigate lost circulation (Boukadi et al., 2004; Alsaba, 2014; Al-Hameedi et al., 2018; Elkatatny et al., 2020)

Actions to mitigate lost circulation (Preventive and Corrective Approach)								
Casing program optimization [2]	Precise controlled bottom hole pressure drilling [17]	Wellbore Pressure Containment Improvement (WPCI)	New organic salt drilling fluid system	Plug while drill	Compound plugged agent	Appropriate size for composite LCMs	Using compositions of LCM rather than just one type of them (Savari 2016)	Optimum particle size distribution which maximizes the Wellbore Strengthening (Razavi 2016)

Lost circulation is expected to occur in any type of lithology and formations as this issue has been encountered in many rock types at different depths. Table 2.5 classifies these types of formations.

Table 2.5: Susceptible formations prone to mud losses (Lavrov et al., 2016).

Susceptible formation for mud loss			
High-porosity high-permeability rocks such as sandstone	Unconsolidated sand or gravel and narrow fractures (natural or induced)	Unconsolidated sand or gravel and wider fractures (natural or induced)	Vugular or cavernous formations, heavily fractured rocks, and large fracture apertures
Seepage losses	Partial loss	Severe loss	Total loss

As noted earlier, mud loss varies across different types of formations. These formations are categorized in Table 2.6 below.

Table 2.6: Various formations for drilling (Lavrov et al., 2016).

Type of formations for drilling		
Unconsolidated formations	**Low to medium-strength formations**	**Medium to high-strength formations**
Gravel Sand Silt clay Sand with pebbles or boulders	Shale Sandstone	Limestone Igneous (granite,basalt) Metamorphic (Slate,gneiss)

Some common measures can be introduced to reduce lost-circulation incidents. They are categorized as shown in Table 2.7.

Table 2.7: Measures to mitigate the lost-circulation phenomenon (Boukadi et al., 2004; Moazzeni et al., 2012; Lavrov et al., 2016).

Three methods to solve the mud loss problem		
Operational procedure	**Optimize annulus fill-up rate**	**Bridging agents**
Float valves attached to the drill string act as a mechanical barrier to avoid influx entering the drill string		Combine the material such as tuff fiber cement pills to mud. The pore size needs to be larger than about three times the solid particle diameter for the mud to be able to enter the pore space [5]

There are numerous procedures and techniques to improve the interpretation of mud loss, in this regard, some of the common procedures are mentioned in Table 2.8.

Table 2.8: Technics for mud-loss interpretation (Boukadi et al., 2004).

Combination of procedures to improve interpretation of mud loss and its mechanism				
Core analysis	Logging	Monitoring operational drilling parameters	Pit level	Flow rate data

It should be noted that the implementation of preventive measures requires properly diagnosing the losses, both in terms of their mechanism and the location of the thief zone. Therefore, the characteristics of a formation dictate the type of treatment to control lost circulation. Selection of the proper solution depends on understanding the formation and identifying the type and cause of lost circulation. Table 2.9 provides some examples of diagnostic features of lost-circulation mechanisms through various formations.

Table 2.9: Formation types and diagnostic of lost circulation (Lavrov et al., 2016)

Formation types and diagnostics of lost circulation
High-porosity rock
* Losses start gradually * Loss flow rate increases gradually and may then gradually decrease as filter cake builds up
Vugular formation
* Loss starts suddenly * Severe or total loss * Impossible to cure with LCM * Loss in specific types of formations; eg, carbonates (karst) * Drill bit may drop a few meters when it hits the vug
Natural fracture
* Loss starts suddenly as fractures are intersected by the wellbore
Drilling-induced fracture
* Loss often accompanies pressure surges (eg, when running pipe in a hole or starting the pump)

The common model used to describe mud loss is Darcy's law, occasionally taking into account the filter-cake effect (Moore, 1986; Carlson et al., 1996). It is important to note that mud losses into the matrix primarily occur in high-permeability formations like sandstone. In such media, these losses can be controlled by building a low-permeability filter cake inside the wellbore, which mitigates further mud loss when the appropriate mud is utilized (Ziegler and Jones, 2014; Feng and Gray, 2018). In the case of caverns or vugs, there are no models to anticipate the mud-loss volume due to the easiness of mud advancement through their system without any confrontation.

2.2 Fractured reservoirs

According to the classification provided by Canson (1985) and further elaborated by Feng et al. (2015), fractures within geological formations can be categorized into four principal types: natural fractures, induced fractures, cavernous formations, and formations with high permeability. While natural fractures can be present in any formation, they are more commonly found in geologic settings with ongoing tectonic activity (Cook, 2011). Fractures can also be induced while drilling due to drilling dynamics such as the drilling speed and weight-on-bit but most commonly due to excessive mud weights or pressures in the wellbore. Therefore, proper planning is required to prevent inducing fractures by adjusting the drilling and hydraulic parameters, since once a fracture is induced, less pressure is needed to lengthen the fracture further into the formation. Cavernous or vugular zones are fractures that create a large pathway for all or nearly all drilling fluid to invade the formation resulting in total loss. These zones are difficult to seal and management of these zones often requires complex drilling strategies. Highly permeable zones are more prone to induced fractures and might result in forming large, connected networks that are difficult to seal. Also, it can be said that NFRs are composed of random distributions of fractures, vugs, and matrices. The distribution of fractures in the reservoir can be massive, localized, oriented, or clustered along a fault. The nature of the fractures and their distribution has considerable influence on the pressure response of a well in a test. NFR can be represented with different models based on the type and distribution of the fractures within the system. These representative models are homogeneous reservoir, multiple region or composite reservoir, anisotropic reservoir, single fracture reservoir, and double-porosity reservoir. The main types of fractures have been categorized in Fig 2.1.

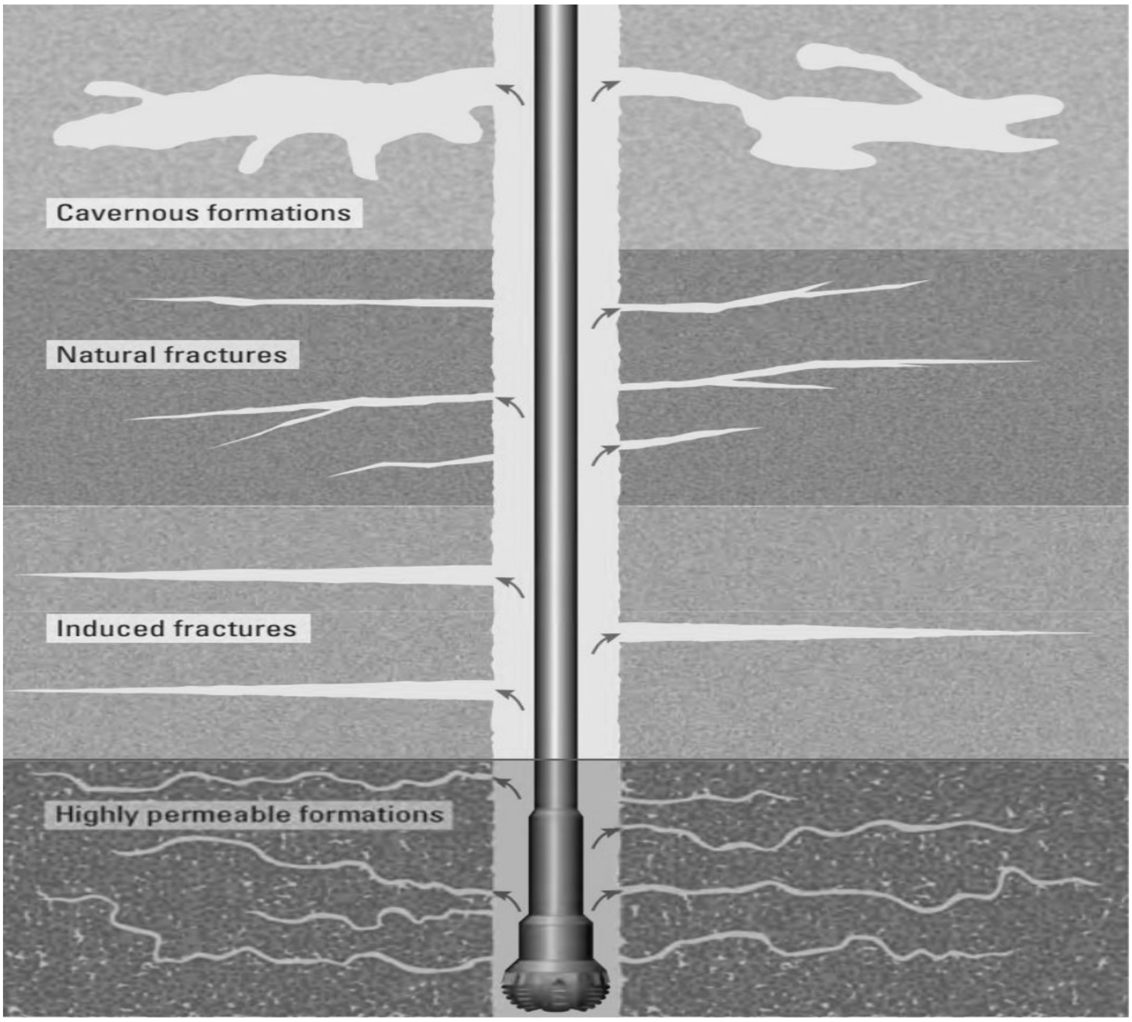

Fig 2.1 Main types of fractures (Alsaba, 2014).

The majority of lost circulation occurs through NFR, especially in drilling operations in deep water, depleted reservoirs, and fractured shale. Drilling through NFRs always presents challenges as a result of uncertainty in the loss rate and fracture sizes. However, offset well data should be applied to precisely anticipate the depths at which lost circulation is to be expected, which will help to plan accordingly. A total loss situation in an NFR that is highly pressurized can pose significant challenges. This loss situation must be addressed before drilling continues. In the case of drilling-induced fractures, Kostov et al. (2015) employed either a steady or time-variable injection rate at the wellbore as the boundary condition to initiate fractures. Yet, this model does not accurately reflect the actual conditions at the fracture mouth where, typically, a consistent bottom-hole pressure is maintained during drilling. This contrasts with a scenario where a constant flow rate is assumed at the well's inner boundary. Such differing boundary conditions can result in varying mud loss volumes, indicating that a constant rate model may not fully capture the complexities of the process. Furthermore, it is almost impossible to regain mud loss with an injection-rate boundary condition because all the injected fluid is forced into the fracture. A comprehensive lost circulation model should couple mud circulation in the wellbore for instantaneous anticipation of bottom hole pressure (BHP), instead of defining just an inner-boundary condition at the bottom hole. Therefore, the dynamic BHP and mud-loss flow can be measured.

2.3 Drilling operations and Bottom Hole Conditions

In the context of the solution presented in this study, it is imperative to maintain constant differential pressure intervals during drilling operations. To achieve this, a constant bottom hole pressure (CBHP) assumption is advocated, necessitating the use of an appropriate technique to keep the BHP constant. Maintaining BHP is a pivotal factor in drilling operations to ensure safety and efficiency. Various techniques are available to achieve constant BHP, including drilling with CBHP, managed pressure drilling (MPD), dual gradient drilling (DGD), and pressurized mud cap drilling (PMCD). The choice of the appropriate technique is contingent upon the specific drilling conditions and objectives, highlighting the significance of selecting the right method for maintaining constant BHP for the successful application of this model in drilling operations. The importance of maintaining constant pressure is underscored by its role in mitigating risks associated with differential pressure fluctuations. These fluctuations can lead to wellbore instability, drilling fluid losses, and even catastrophic blowouts. By applying the inner-constant pressure assumption, commonly utilized for water influx calculations in gas and oil reservoirs, we can also determine drilling-fluid loss volumes with greater accuracy. This principle further reinforces the necessity of constant BHP, as it provides a more stable drilling environment, optimizing operational safety and efficiency. Therefore, when selecting the appropriate technique to maintain constant BHP, criteria such as the geological conditions, well depth and configuration, and anticipated pressure variances must be thoroughly evaluated. This approach ensures that the selected method aligns with the specific requirements of the drilling operation, thereby enhancing its success rate. Fig 2.2 illustrates how an MPD system maintains wellbore pressure constancy across each interval, exemplifying the practical application of these concepts in real-world drilling scenarios.

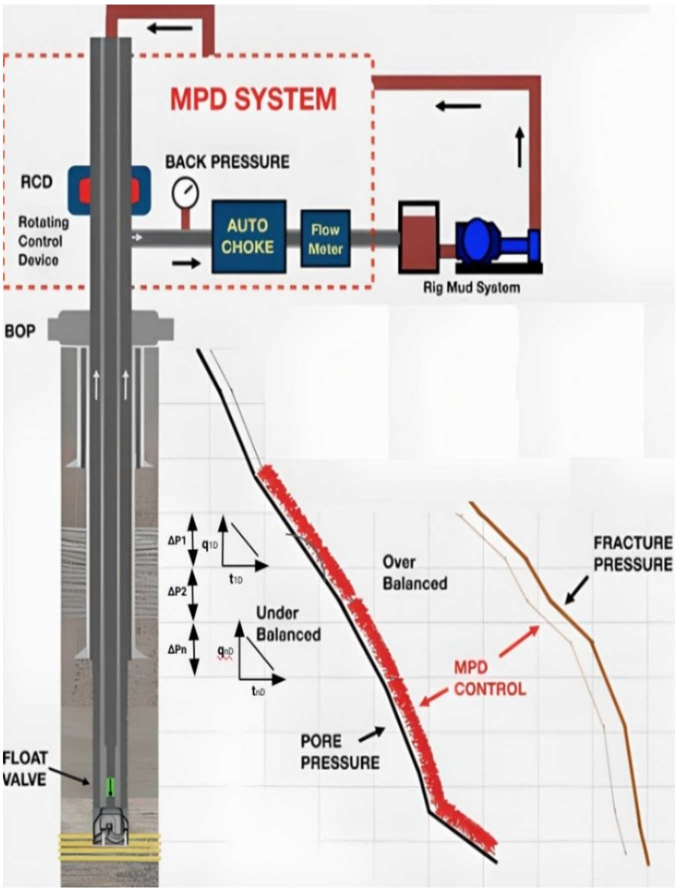

Fig 2.2 Illustration shows maintaining constant differential pressure intervals during drilling operations.

2.4 Mud classifications and existing drilling fluid-loss models

Drilling fluid, or mud, is a specialized fluid circulated through a wellbore to facilitate drilling operations. The choice of specific drilling fluid systems is optimized based on the characteristics of the targeted geological formation. Essential to its functionality, a drilling fluid must possess certain desirable physical properties. For instance, it must have a viscosity that permits easy pumping and circulation at pressures commonly used in drilling operations, without generating excessive differential pressure. Additionally, the fluid must exhibit sufficient thixotropic behavior to suspend cuttings within the borehole when the fluid circulation is halted. Drilling fluids can be categorized based on their mechanical and rheological responses to external pressure and shear stress. The first category considers the fluid’s resilience to the intense pressures deep within the wellbore, maintaining its structural integrity and flow characteristics. The second category focuses on the fluid's behavior under shear stress, which occurs when different fluid layers move at varying speeds, as seen during fluid circulation. This classification is critical for understanding how the fluid will perform, particularly its ability to carry drill cuttings to the surface amidst the mechanical forces of drilling operations. This classification is further illustrated in Fig 2.3.

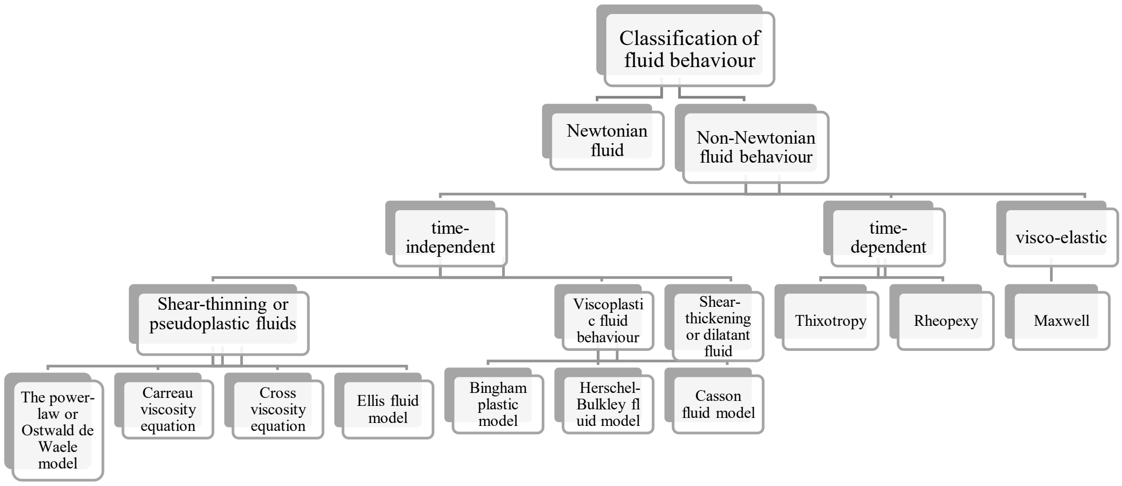

Fig 2.3 Fluid behavior classification

As another classification, drilling fluids can be categorized based on their base fluid, as shown in Table 2.10.

Table 2.10: Drilling fluid classification (Boukadi, 2010; Alsaba, 2014; Al-Hameedi, 2018; Elkatatny, 2020).

Drilling fluid systems	Water-Based Muds (WBM)
	Nonaqueous-Based Drilling Fluids (NADF)
	Pneumatic Systems

Several analytical and numerical models have been developed historically to estimate drilling fluid losses into formations. The advantages and disadvantages of each model are presented in Table 2.11 below.

Table 2.11: Comparative Analysis of Previous Models: Strengths and Weaknesses in Loss Volume Measurement.

MODEL	STRENGTH	WEAKNESSES
Sanfilippo et al. (1997)	Simple and flexible	Newtonian mud, non-deformable NFR, uniform aperture, do not consider leak-off
Lietard et al. (1999)	Evaluate the contribution of the natural fractures to the total permeability of a reservoir rock	Newtonian mud, non-deformable, constant aperture, incompressible mud, neglecting fracture deformation
Lavrov and Tronvoll (2003)	Considering the linear deformation of rock	Newtonian mud, linear fracture, finite length, Newtonian mud, constant leak-off from the walls of the fracture
Lavrov and Tronvoll (2004)	Power-law drilling fluid in deformable fracture, considering fracture aperture, borehole pressure, formation	Neglecting leak-off through walls of fracture
Majidi et al., (2008 and 2010)	The radial flow of a yield-power law fluid into an infinite fracture, effects of formation fluid into the model (if the ratio of formation fluid viscosity to drilling-fluid rheology is less than or equal to 0.01, the effects of formation fluids can be neglected)	non-deformable and constant aperture fracture, incompressible drilling fluid, no leak-off from the walls of the fracture
Shahri and Majidi (2011)	Applying exponential deformation function which replaced with linear deformation of rock.	Does not consider the permeability of the fracture walls and leak-off
Sun and Huang (2015)	Considering deformable fracture	The numerical stability of the explicit method requires very small-time steps especially when the flow behavior index deviates from the unity
Xia et al. (2015a and 2015b)	A complex methodology that couples the impacts of the formation matrix and the fracture, the methodology focuses on characterizing a network of natural fractures (as opposed to a single natural fracture,	Due to the complexity of developed model, it requires significant computational time which restricts the application of the developed model for most practical cases of mud-loss data analysis in real-time
Albattat and Hoteit (2019)	Using parabolic shape for deformation of upper plate in terms of hydraulic pressure	Applying parabolic shape for deformation of the upper plate in terms of hydraulic pressure, however, this treatment is not conclusive since several solid spacers were used to maintain a uniform gap
Albattat et al. (2022)	Using derivative-based solution to reduce uncertainty	Considering one hydraulic aperture rather than a system of matrix-fracture and neglecting mud infiltration in the porous media

2.5 Type-Curve analysis application

Type-curve analysis is a pivotal tool in reservoir engineering, particularly for evaluating well-test data in NFRs. Log-log type-curve matching to rate-time data provides insights into the reservoir's characteristics such as fracture-matrix interactions and storage capacities solely using drilling-fluid data. Originally developed for homogeneous systems (Sun, 2015), the technique was extended to NFRs by researchers like Da Prat (1990) and Sageev et al. (1985), accounting for the complex flow patterns in these reservoirs. These adaptations were necessary because NFRs behave differently from homogeneous systems due to the presence of matrix and fractures with distinct properties. Traditionally tailored for Newtonian fluids, type-curve analysis has been adjusted to handle Non-Newtonian fluids as well, where viscosity changes with flow conditions. This adaptability underscores the technique's versatility, allowing it to remain relevant for modern reservoir engineering applications. Type-curve analysis not only diagnoses the current state of a reservoir but also predicts future performance, guiding decisions for well interventions and recovery strategies. As such, it continues to be an indispensable method for well-test interpretation and reservoir management, balancing historical development with modern requirements for accuracy and applicability.

2.6 Theoretical foundation

There are various analytical and numerical models developed to model the dynamics of Non-Newtonian fluid flow from the wellbore to homogenous and NFR reservoirs. This section summarizes the models found in the literature to characterize the models applied to measure Non-Newtonian fluid rate and volume which can be categorized into two main procedures:

2.6.1 Non-Newtonian fluid volume measurement based on linear momentum

Lavrov and Tronvoll (2004) developed several theoretical models that considered mud losses (Non-Newtonian fluid) into a deformable fracture of finite length, then, Liétard et al., (1999) developed a model based on the radial flow of a Bingham-plastic fluid into an unlimited-extension fracture. Non-Newtonian fluid flow through fracture medium was described by the local pressure drop because of laminar flow in a slot of width w. According to the linear momentum equation, the pressure gradient and average velocity are interrelated (Liétard et al., 1999b; Majidi et al., 2010)

$$\frac{dP}{dr} = \frac{12\mu_p v}{w^2} + \frac{3\tau_y}{w} \quad \text{Eq 2.1}$$

where v, P, r, w, τ_y and μ_p are the average velocity, differential pressure, radial distance, fracture hydraulic width, yield stress, and plastic viscosity of the fluid, respectively. Considering constant overpressure established at the wall, Liétard et al., (1999) obtained a relationship for mud-invasion velocity versus time. This model predicted that the mud losses would eventually stop because of the yield stress of drilling fluid. The ultimate quantity of mud loss is a function of the yield value of the drilling fluid and the amount of overpressure. The model assumes a constant drilling overpressure (i.e., the difference between the circulating pressure and the static reservoir pressure does not change with time). The governing equation is derived by use of the principles of conservation of mass and conservation of linear momentum for transient radial flow in a fracture. Pilehvari and Nyshadham (2002) have shown the approximately steady-state laminar solution of the momentum-balance equation for radial flow is used to model mud flow in a single fracture but it has some restrictions such as does not consider the transient flow effects which are so important during the short times and is important for mud loss issues, particularly in fractured reservoirs; the other deficiency is neglecting the fluid leak-off through the walls of the natural fracture (Dual-porosity model) into formation for heterogeneous reservoirs; in reality, part of the advancing drilling fluid in the fracture may leak off into the reservoir rock, particularly when the permeability of the formation is high.

2.6.2 Non-Newtonian fluid volume measurement based on radial diffusivity equation

Building on the seminal work of Ikoku and Ramey (1979) on modeling Non-Newtonian fluid flow within homogeneous reservoirs, Olarewaju (1992) introduced a dual-porosity partial differential equation (PDE) for describing the radial flow of Non-Newtonian fluids through NFR. This work was further advanced by Escobar et al. (2011), who incorporated a pseudo-steady-state interporosity transfer function into the Non-Newtonian radial diffusivity equation, enhancing its ability to model Non-Newtonian fluid behavior in double porosity systems. This comprehensive modeling approach integrates mass conservation principles, transport equations, and state equations to formulate a PDE that effectively captures the time-dependent flow of Non-Newtonian fluids, such as drilling fluids, through porous media. The model utilizes a specialized interporosity transfer function that is designed to represent a "pseudosteady-state" flow regime within the reservoir matrix, a critical aspect considering that both pseudosteady-state and transient flow regimes play significant roles in describing fluid movement from the matrix to fractures. This thesis specifically focuses on the pseudosteady-state flow regime. This research aims to rigorously evaluate the PDE model for Non-Newtonian fluid flow within a dual-porosity reservoir, taking into account pseudo-steady-state interporosity transfer conditions, as outlined by Garcia-Pastrana et al. (2017). The foundational equations and the theoretical framework for this analysis are detailed in Table 2.12 (section II.2.8), which introduces eight distinct models, each tailored to specific fluid rheology and boundary conditions. These models are applied in various contexts, including well-test analysis and water influx measurement, highlighting the diverse applicability of the radial diffusivity equation. Table 2.12 provides a systematic categorization of these models into eight different cases.

Table 2.12: Radial diffusivity-based equation for various cases.

Radial diffusivity based equation for different cases	II.2.1 Flow of newtonian fluids through homogeneous reservoirs under constant rate
	II.2.2 Flow of newtonian fluid (mud) through homogeneous reservoirs under inner constant pressure
	II.2.3 Flow of Non-Newtonian fluids through homogeneous reservoirs under constant rate
	II.2.4 Flow of Non-Newtonian fluids through homogeneous reservoirs under inner constant pressure
	II.2.5 Flow of newtonian fluids through Natural fractured reservoir (double porosity model) with pseudosteady-state interporosity transfer under constant rate
	II.2.6 Flow of newtonian fluids through Natural fractured reservoir (double porosity model) with pseudosteady-state interporosity transfer under inner constant pressure
	II.2.7 Flow of Non-Newtonian fluids through NFR (double porosity model) with pseudosteady-state interporosity transfer under constant rate
	II.2.8 Flow of Non-Newtonian fluids through NFR (double porosity model) with pseudosteady-state interporosity transfer under inner constant pressure

3 MATHEMATICAL MODELING AND METHODOLOGY

This thesis focuses on measuring the cumulative volume of Non-Newtonian fluid flow through NFR (section 2.5.2 at Table 2.9). The aim is to analyze the flow across a specified inner radius over a given time interval in response to a specific differential pressure between an outer boundary and the specific inner radius. Additionally, simplifications particularize the applicability to homogeneous reservoirs. In this regard, the underlying equation is the partial differential equation for Non-Newtonian flow within a double porosity reservoir under pseudo-steady-state inter-porosity transfer conditions, as proposed by Garcia-Pastrana et al. (2017). The model core structure comprises a conservation of mass law, a transport equation, and an equation of state, and a diagram is provided below to outline the schematic of the model. To analyze Non-Newtonian fluid flow through NFR and homogeneous reservoirs, the proposed evaluated solution in this study is solved under a wellbore constant pressure assumption, resulting in both numerical and analytical solutions. The presented solution aims to quantify the drilling-fluid rate and cumulative loss volume at distinct time intervals for the NFR. The outer boundary is conceptualized as an infinite-acting reservoir condition. The inner-constant pressure assumption, frequently employed for water-influx calculations in gas and oil reservoirs, can similarly be used to determine drilling-fluid loss volumes. Although Da Prat (1990) proposed a solution for the dual-porosity model under a constant pressure drop at the wellbore, his methodology is based on the premise of Newtonian fluids. Such an assumption is not considered realistic for this study's objective, which focuses on assessing the flow of drilling fluid through the NFR. In this context, the influence of the outer boundary does not appear, positing that the infiltrating Non-Newtonian fluid does not interact with the outer boundary as it moves through the combined system (fracture+matrix).

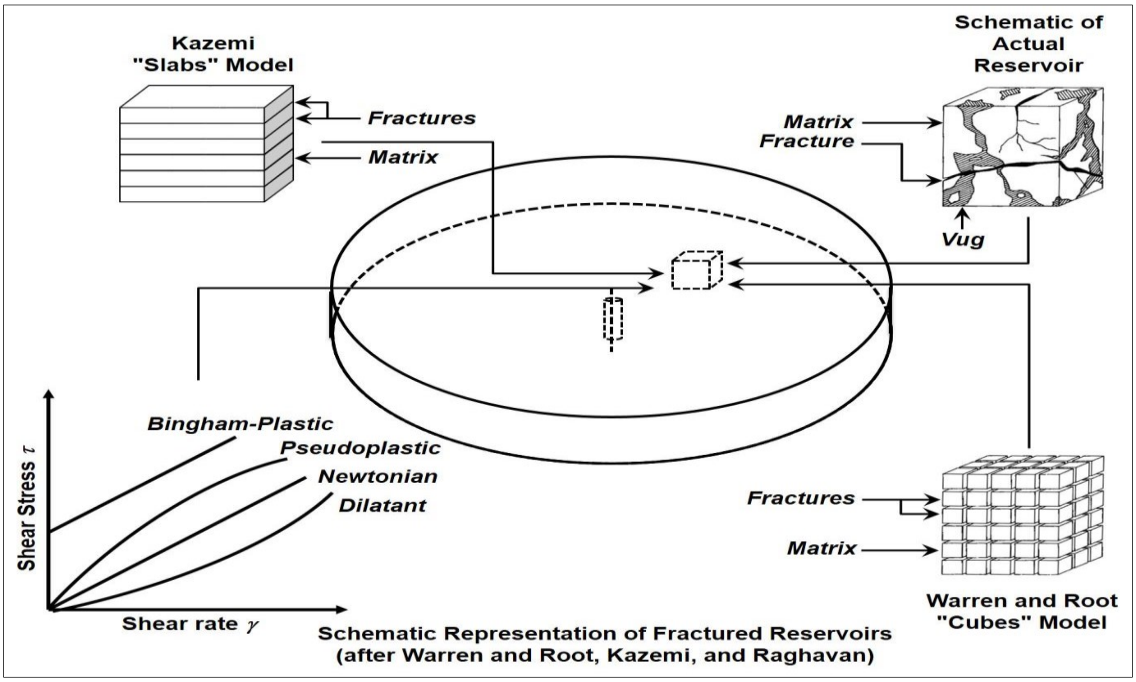

Fig 3.1 Schematic representation of the proposed model for fractured reservoir Garcia-Pastrana et al., (2017).

3.1 Assumptions

The assumptions listed for Non-Newtonian fluid flow through naturally fractured reservoirs are critical for the analytical tractability and simplification of the complex physical processes involved. These assumptions are made to strike a balance between mathematical rigor and the practical applicability of the model. While some assumptions, such as the homogeneity of matrix blocks and constant fracture porosity, might seem idealized, they are essential for developing a foundational understanding of fluid flow in NFRs. These assumptions are aligned with common practices in reservoir engineering, particularly when employing dual-porosity models, and are supported by existing literature in the field. The realism of these assumptions varies; however, they are constructed on the premise that simplifying complex reservoir characteristics enables the derivation of meaningful insights into fluid flow dynamics. The assumption of constant pressure within the wellbore, rather than a constant rate, for instance, reflects a practical approach to measuring fluid influx and reservoir management through techniques such as managed pressure drilling. This particular assumption is not only feasible but also common in dual-porosity modeling, facilitating the analysis of fluid flow under controlled conditions that closely mimic operational practices. The importance of these assumptions lies in their ability to define the scope and applicability of the model. They delineate the conditions under which the model's predictions are valid, guiding engineers in applying the model to real-world scenarios with similar characteristics. Violating these assumptions could lead to discrepancies between the model's predictions and actual reservoir behavior. For example, deviations from the assumed homogeneity and isotropy of matrix blocks, or changes in fracture porosity, could affect the radius of invasion and fluid flow patterns, potentially necessitating adjustments to the model or the application of different modeling techniques to accurately capture the observed dynamics. Therefore, while these assumptions simplify the modeling process, their limitations and the implications of their violation must be acknowledged and addressed through sensitivity analyses, comparative studies, or model refinement to ensure the model remains a valuable tool for understanding and managing Non-Newtonian fluid flow in NFRs.

- A vertical well penetrates the entire thickness of the reservoir.
- The reservoir thickness is uniform (constant).
- The matrix blocks are in a systematic array of identical rectangular parallelepipeds.
- The matrix blocks are homogeneous and isotropic.
- The matrix blocks have a constant porosity (Φ_m).
- The fracture network is arrayed as an orthogonal system of continuous and uniform fractures.
- The fracture porosity (Φ_f) is unique to the fracture system (i.e., is constant)
- The double porosity media is considered to be homogeneously distributed.
- Flow to the wellbore occurs only through the fracture network.
- Flow occurs only between the matrix blocks and fracture network (no flow between matrix blocks).
- The reservoir (matrix) and fracture permeabilities are constant.
- The system contains a slightly compressible fluid and Isothermal.
- The effects of gravity are negligible.
- The pressure gradients are small.
- Non-Newtonian fluids obey the Ostwald de Waele power law relationship over the flow regime of interest.
- The fluid is classified as pseudoplastic and exhibits time-independent behavior; the flow behavior index values range from zero to one, with a value of one corresponding to the case of a Newtonian fluid.

- Single phase flow

3.2 Diffusivity-based model for NFR

The partial differential equation evaluated in the literature, proposed by Garcia-Pastrana et al., (2017) is applied to describe the flow behavior of Non-Newtonian fluids as presented in Eq 3.1

$$\frac{\partial^2 p_f}{\partial r^2} + \frac{n}{r}\left[\frac{\partial p_f}{\partial r}\right] = \frac{n\mu_{eff}}{k_f} \cdot \left[\frac{q}{2\pi hr}\right]^{n-1} \cdot \left[(\varphi c_t)_f \frac{\partial p_f}{\partial t} + (\varphi c_t)_m \frac{\partial p_m}{\partial t}\right] \text{ .... Eq 3.1}$$

The source term equation, which adds the fluid from the fracture to the matrix is defined by

$$\frac{\partial p_m}{\partial t} = \frac{\alpha}{(\varphi c_t)_m} \frac{k_m}{\mu_{eff}} \left[\frac{q_m}{\Delta L^2}\right]^{1-n} \cdot (p_f - p_m) \text{ .... Eq 3.2}$$

Where p_f, p_m, r, t, k_f, k_m, α, q_m, φ, n, h, μ_{eff}, ΔL, and c_t represent the pressure drop in the fracture system, pressure drop in the matrix system, radius, time, fracture permeability, matrix permeability, shape factor, matrix flow rate, porosity, flow behavior index, reservoir height, effective viscosity, length, and total compressibility. Dimensionless variables, Eq 3.3 and Eq 3.4, as cited in the literature (Da Prat, 1990; Garcia-Pastrana et al., 2017a), are used to derive Eq 3.5. These dimensionless quantities allow for the comparison and interpretation of data across different wells, reservoirs, and operational conditions by normalizing the data against reference quantities. These variables are then applied to transform Eqs 3.1 and 3.2 into their dimensionless forms. The dimensionless pressure in the fracture network is

$$p_{fD} = \frac{(2\pi h)^n k_f (p_i - p_f)}{q^n \mu_{eff} r_w^{1-n}} \text{ .... Eq 3.3}$$

Here, p_i, r_w, and q represent the initial pressure, wellbore radius, and flow rate respectively. The dimensionless pressure in the matrix is

$$p_{mD} = \frac{(2\pi h)^n k_m (p_i - p_m)}{q^n \mu_{eff} r_w^{1-n}} \text{ .... Eq 3.4}$$

The dimensionless rate is derived as

$$q_D = \left[\frac{\mu_{eff}.r_w^{1-n}}{k_f.(2\pi h)^n.(p_i - p)}\right]^{\frac{1}{n}}.q \quad \text{.........Eq 3.5}$$

Dimensionless time

$$t_D = \frac{q^{1-n}k_f}{n(\varphi c_t)_t(2\pi h)^{1-n}\mu_{eff}r_w^{3-n}}.t \quad \text{.........Eq 3.6}$$

Where the total expansion of the reservoir is

$$(\Phi c_t)_t = (\Phi c_t)_f + (\Phi c_t)_m \quad \text{.........Eq 3.7}$$

and the dimensionless radius is

$$r_D = \frac{r}{r_w} \quad \text{.........Eq 3.8}$$

At the same time, there are three dimensionless terms have been introduced to describe the NFR characteristics which introduced below,

The storativity ratio is defined as

$$\omega = \frac{(\Phi V)_f}{(\Phi V)_f + (\Phi V)_m} \quad \text{.........Eq 3.9}$$

where interface inter-porosity coefficient λ defined as

$$\lambda = \alpha \frac{k_m}{k_f} r_w^2 \quad \text{.........Eq 3.10}$$

The dimensionless matrix contribution, D, is defined as

$$D = \frac{q_m}{q}\frac{2\pi h r_w}{\Delta L^2} \quad \text{.........Eq 3.11}$$

With these dimensionless variables, Eq 3.1 and Eq 3.2 can be written in the dimensionless form proposed by Escobar et al. (2011)

$$\frac{\partial^2 p_{fD}}{\partial r_D^2} + \frac{n}{r_D}\frac{\partial p_{fD}}{\partial r_D} = r_D^{1-n}\left(\omega\frac{\partial p_{fD}}{\partial t_D} + (1-\omega)\frac{\partial p_{mD}}{\partial t_D}\right), t_D > 0 \text{ ....Eq 3.12}$$

For the source term, the dimensionless form is defined by (Escobar et al. 2011)

$$\frac{\partial p_{mD}}{\partial t_D} = \frac{n\lambda}{(1-\omega)}.D^{1-n}.(p_{fD} - p_{mD}) \text{ ....Eq 3.13}$$

3.3 General and numerical solution

The study carried out in this thesis commences with a rigorous investigation of the solutions to fluid flow models within double porosity reservoirs, specifically under the operational paradigms of constant rate and constant pressure. Our inquiry begins with an analytical revisitation of the established Garcia-Pastrana et al. (2017) model, traditionally framed within a constant rate context. In a departure from the original study, we recalibrate the model to a constant pressure framework, an approach that aligns more closely with field-realistic scenarios (specifically the drilling-fluid loss phenomenon) and the operational parameters that define them. This adaptation is crucial, as it imparts a nuanced understanding of the pressure dynamics that are often paramount in reservoir management. Building on this groundwork, the study pivots to a focused analysis of Non-Newtonian fluid flow through NFR as delineated in Section 2.5.2 (Table 2.9). By measuring the cumulative volume of fluid over time and the response to differential pressure across a defined inner radius, we gain critical insights into the behavior of such fluids under specific conditions. The model is further refined with simplifications to render it applicable to homogeneous reservoirs, a common scenario in the field. Employing the foundational partial differential equation for Non-Newtonian flow within a double porosity reservoir, which encompasses pseudo-steady-state inter-porosity transfer conditions as proposed by Garcia-Pastrana et al., we extend the dialogue on reservoir characterization. To address the flow dynamics in NFR and homogeneous reservoirs, the proposed model within this study is resolved under a wellbore constant pressure assumption. The fruit of this labor is a set of both numerical and analytical solutions, which are meticulously derived and cataloged in Appendices A and B, respectively. These evaluated solutions form the bedrock for subsequent qualitative and quantitative analyses, providing a comprehensive framework to interrogate the mechanics of Non-Newtonian fluid flow in reservoirs. This chapter is structured to facilitate an in-depth understanding of these phenomena. The first section, "The Solution

Under Constant Rate Assumption," scrutinizes the constant rate condition, while the second, "The Solution Under Constant Pressure Assumption," delves into the particulars of maintaining a constant pressure. Each segment elaborates on the distinctive features and resultant dynamics specific to the condition in question, thus offering a robust conceptual toolkit for practitioners and researchers alike in the domain of reservoir petroleum engineering. In bridging the gap between the established insights of the Garcia-Pastrana model and the novel approaches introduced in this study, the chapter emphasizes a bifocal perspective that not only enriches the scholarly discourse but also informs the strategic development of more effective and predictive reservoir management techniques. Additionally, the findings hold particular relevance for drilling operations, offering pivotal knowledge that can aid in managing and mitigating drilling fluid loss, a critical operational challenge. This dual application showcases the practical implications of the research, underscoring its importance in both the optimization of reservoir exploitation and the enhancement of drilling efficiency.

3.3.1 The Solution Under Constant Rate Assumption for Non-Newtonian Fluids in NFRs

This section elucidates the solution methodology applied to the Garcia model for double porosity reservoirs characterized by Non-Newtonian fluid behavior. The analytical approach employs the Laplace transform to determine essential solutions. To achieve this, specific initial and boundary conditions have been meticulously established, which are crucial for the accurate depiction of the solution relevant to our scenario. The derived general solution of Garcia-Pastrana et al. (2017), expressed in a dimensionless format within the Laplace domain, is encapsulated by

$$p_{fDNN}(r_D, u) = r_D^{\frac{1-n}{2}}\left[C_1 I_{\frac{1-n}{3-n}}\left(\frac{2}{3-n}.\sqrt{u.g(u)}.r_D^{\frac{3-n}{2}}\right) + C_2 K_{\frac{1-n}{3-n}}\left(\frac{2}{3-n}.\sqrt{u.g(u)}.r_D^{\frac{3-n}{2}}\right)\right] \text{.......Eq 3.14}$$

It incorporates the modified Bessel functions of the first and second kinds, denoted by I and K respectively, with order ν. Here, 'u' symbolizes the Laplace transform variable, and the function 'g(u)' is defined as

$$g(u) = \frac{\omega(1-\omega)u + n\lambda D^{1-n}}{(1-\omega)u + n\lambda D^{1-n}} \text{ ....Eq 3.15}$$

The initial condition presumes a uniformly distributed pressure throughout the reservoir, which is mathematically articulated in Eq 3.16. In contrast, the inner boundary condition is established based on a constant flow rate, detailed in Eq 3.17, and it applies irrespective of the temporal frame under consideration.

$$p_{mDNN}(r_{mD},0) = p_{fDNN}(r_{fD},0) = 0 \quad \text{......Eq 3.16}$$

$$\left[r_D.\frac{d\hat{p}_{fD}(r_D,u)}{dr_D}\right]_{r_D=1} = -\frac{1}{u} \quad \text{......Eq 3.17}$$

As for the outer boundary condition, the model assumes the reservoir is infinite-acting, meaning the outer boundaries exert no influence. This translates to the condition

$$\lim_{r_D\to\infty} p_{fDNN}(r_D,t) = 0 \quad \text{......Eq 3.18}$$

Building upon these conditions, the solution within the Laplace domain for an infinite-acting reservoir, considering a constant flow rate at the wellbore, is precisely formulated as

$$\hat{p}_{fD}(r_D,u) = \frac{r_D^{\frac{1-n}{2}}.K_{\frac{1-n}{3-n}}\left(\frac{2.\sqrt{u.g(u)}}{3-n}.r_D^{\frac{3-n}{2}}\right)}{u.\sqrt{u.g(u)}.K_{\frac{2}{3-n}}\left(\frac{2.\sqrt{u.g(u)}}{3-n}\right)} \quad \text{......Eq 3.19}$$

Due to the complexities inherent in the equation, direct analytical inversion from the Laplace to the real domain is not feasible. As such, the Gaver-Stehfest numerical inversion algorithm is utilized to translate Eq 3.19 into a form that is applicable for practical use.

3.3.2 The Solution Under Constant Pressure Assumption for Non-Newtonian Fluids in Reservoirs

This section explores the solution for Non-Newtonian fluid flow in double porosity reservoirs under a constant pressure assumption, diverging from the constant rate conditions previously discussed in the literature and revisited above. This new approach mirrors practical wellbore conditions more accurately and allows for a deeper understanding of pressure-driven flow behavior in such reservoirs. The analytical solutions in the Laplace domain are modified to reflect these conditions and are numerically inverted to real-time domains to provide actionable insights for reservoir management and drilling operations. We divide this section into two parts. First, we discuss solutions for NFRs under constant pressure. Then, we examine solutions for homogeneous reservoirs, applying the same pressure conditions. These discussions are aimed at clarifying fluid behavior in each reservoir type, aiding in effective management and drilling practices.

3.3.2.1 The Solution for NFR

In this part of the study, we diverge from the dual-porosity model solutions provided by Garcia-Pastrana et al. (2017), which were based on a wellbore constant rate assumption suitable for well-test applications. Instead, our study employs a wellbore constant pressure approach to develop an appropriate solution for quantifying Non-Newtonian fluid volume. For quantifying the fluid volume, the procedure outlined by Archer has been utilized (Archer, 2000). To solve Eq 3.12 and Eq 3.13, initial and boundary conditions are considered as:

Initial Condition: uniform pressure distribution

$$p_{mDNN}(r_{mD}, 0) = p_{fDNN}(r_{fD}, 0) = 0 \quad \text{Eq 3.20}$$

Inner boundary condition: constant flow pressure

$$p_{fDNN}\text{-}\left(\frac{\partial P_{fD}}{\partial t_D}\right)=1 \quad \text{Eq 3.21}$$

The outer boundary condition is considered an infinite-acting reservoir, as shown below

$$\lim_{r_D \to \infty} p_{fDNN}(r_D, t) = 0 \quad \text{Eq 3.22}$$

After solving the double-porosity diffusivity model for Non-Newtonian fluids (Eq 3.12 and Eq 3.13), the general solution is presented in the literature (Arfken et al., 2013) in dimensionless form as modified Bessel functions of the first and second kind as shown above at Eq 3.14. Then, in this section, Eq 3.14 is solved under a wellbore constant pressure condition to derive the dimensionless pressure, as presented below

$$\hat{p}_{fD}(r_D, u) = \frac{r_D^{\frac{1-n}{2}} . K_{\frac{1-n}{3-n}}\left(\frac{2.\sqrt{u.g(u)}}{3-n} . r_D^{\frac{3-n}{2}}\right)}{u . K_{\frac{1-n}{3-n}}\left(\frac{2.\sqrt{u.g(u)}}{3-n}\right)} \quad \text{Eq 3.23}$$

In the literature, there are numerous algorithms designed for the numerical inversion of Laplace transforms. It is essential to focus on methods that are stable, accurate, and efficient. The Gaver-

Stehfest inversion method (Stehfest, 1970; Kuhlman, 2013) meets these criteria for a majority of practical cases encountered. Owing to its high accuracy and stability for most pressure solutions, it stands as one of the most widely adopted methods in this field (Kuhlman, 2013). Since Eq 3.23 is solved numerically by employing the Stehfest inverse algorithm to convert the solution in the Laplace domain to those in the real-time domain. The results indicate that the differential pressure remains constant at different times within the wellbore, confirming the observed case. These results are presented in Fig 3.2. According to the Darcy's law, it is feasible to relate dimensionless pressure with dimensionless rate as below

$$q_D = -r_D.\frac{\partial p_D}{\partial r_D} \qquad \text{Eq 3.24}$$

Subsequently, we utilize Eq 3.23 and incorporate it into Eq 3.24 to derive the dimensionless rate. The resulting equation, provided below, is used to measure the flow of Non-Newtonian fluid through the NFR

$$\hat{q}_D(r_D, u) = -r_D.\frac{\partial \hat{p}_D(r_D,u)}{\partial r_D} = -r_D.\frac{\partial}{\partial r_D}\left(\frac{r_D^{\frac{1-n}{2}}.K_{\frac{1-n}{3-n}}\left(\frac{2.\sqrt{u.g(u)}}{3-n}.r_D^{\frac{3-n}{2}}\right)}{u\,.K_{\frac{1-n}{3-n}}\left(\frac{2.\sqrt{u.g(u)}}{3-n}\right)}\right) =$$

$$\frac{(1-n).r^{\frac{1-n}{2}}.K_{\frac{1-n}{3-n}}\left(\frac{2.r^{\frac{3-n}{2}}.\sqrt{u.g(u)}}{3-n}\right)}{2.u.K_{\frac{1-n}{3-n}}\left(\frac{2.\sqrt{u.g(u)}}{3-n}\right)} -$$

$$\frac{r^{\frac{1-n}{2}+\frac{3-n}{2}}.\sqrt{u.g(u)}.\left[-K_{\frac{1-n}{3-n}-1}\left(\frac{2.r^{\frac{3-n}{2}}.\sqrt{ug(u)}}{3-n}\right)-K_{\frac{1-n}{3-n}+1}\left(\frac{2.r^{\frac{3-n}{2}}.\sqrt{ug(u)}}{3-n}\right)\right]}{2.u.K_{\frac{1-n}{3-n}}\left(\frac{2.\sqrt{u.g(u)}}{3-n}\right)} \qquad \text{Eq 3.25}$$

To measure Non-Newtonian fluid dimensionless rate through NFR, Eq 3.25 has been solved numerically by applying the inverse Laplace Transform by Gaver-Stehfest, (1970) algorithm (MATLAB application has been used for the calculation). Dimensionless rate versus time has been graphed in Fig 3.2. The cumulative drilling-fluid recovery is defined by (Archer, 2000)

$$Q_D(r_D, t_D) = \int_0^{t_D} q_D(r_D, t_D)\, dt_D \qquad \text{Eq 3.26}$$

Therefore, dimensionless Non-Newtonian fluid volume is measured below, (Appendix A)

$$Q_D(r_D,u) = \frac{1}{u}.q_D(r_D,u) = -\frac{(1-n).r^{\frac{1-n}{2}}.K_{\frac{1-n}{3-n}}\left(\frac{2.r^{\frac{3-n}{2}}.\sqrt{u.g(u)}}{3-n}\right)}{2.u^2.K_{\frac{1-n}{3-n}}\left(\frac{2.\sqrt{u.g(u)}}{3-n}\right)} -$$

$$\frac{r^{\frac{1-n}{2}+\frac{3-n}{2}}.\sqrt{u.g(u)}.[-K_{\frac{1-n}{3-n}-1}\left(\frac{2.r^{\frac{3-n}{2}}.\sqrt{ug(u)}}{3-n}\right)-K_{\frac{1-n}{3-n}+1}\left(\frac{2.r^{\frac{3-n}{2}}.\sqrt{ug(u)}}{3-n}\right)]}{2.u^2.K_{\frac{1-n}{3-n}}(\frac{2.\sqrt{u.g(u)}}{3-n})} \quad \text{Eq 3.27}$$

Eq 3.27 is numerically solved for NFR and drilling-fluid properties with specific values of λ = 5E-6, ω = 1E-3, n = 0.5, and D = 1E3. Under the assumption of constant wellbore pressure, the cumulative drilling-fluid loss versus time is illustrated in Fig 3.2.

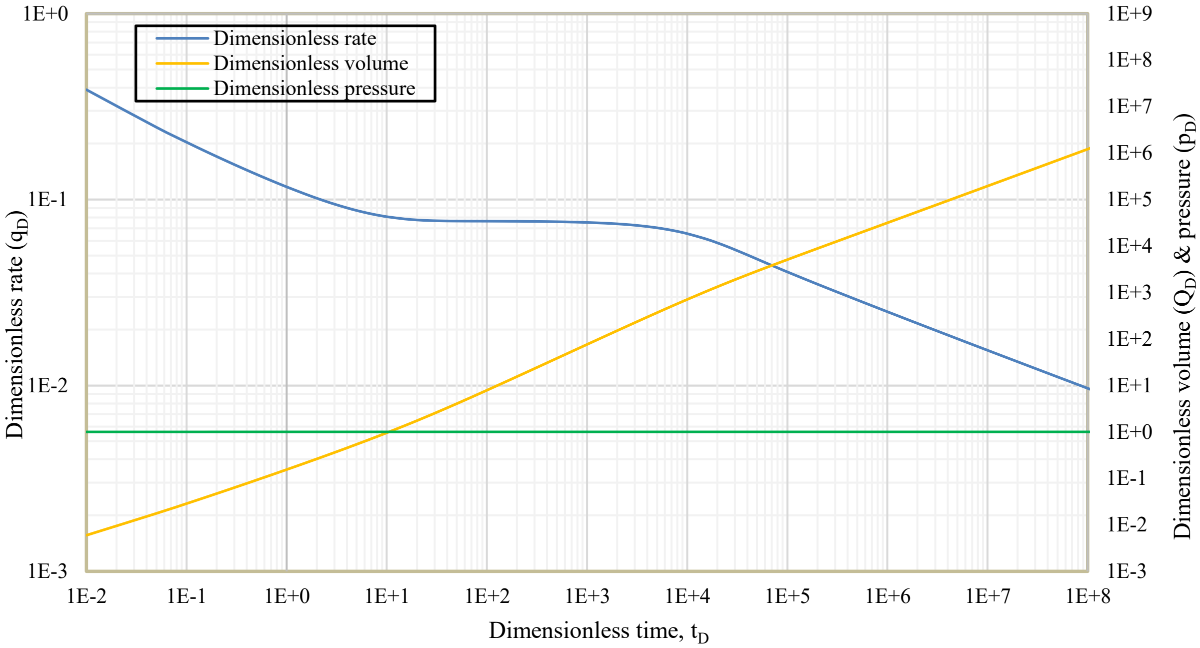

Fig 3.2 Measured dimensionless pressure, rate, and volume of drilling fluid by the proposed model.

3.3.2.2 The Solution for Homogenous reservoir (After simplification)

After simplifying the proposed complex solution for NFR (Eq 3.12 and Eq 3.13), it becomes applicable to describe the flow of a slightly compressible, Non-Newtonian, power-law fluid in a homogeneous porous medium proposed by Ikoku and Ramey, (1979). One initial and two boundary conditions in the dimensionless form are assumed to derive the evaluated solution for a homogenous reservoir under wellbore constant pressure.

$$p_{DNN}(r_D, 0) = 0 \quad \text{Eq 3.28}$$

$$p_{DNN}(1, t_D) = 1 \quad \text{Eq 3.29}$$

$$\lim_{r_D \to \infty} p_D(r_D, t_D) = 0 \ldots\ldots\ldots\ldots\ldots\ldots\ldots\ldots\ldots\ldots \text{Eq 3.30}$$

Thus, in this study, the solution for a homogeneous reservoir can be derived in the Laplace domain under wellbore constant pressure, as presented below

$$\hat{p}(r_D, u) = \frac{r_D^{\frac{1-n}{2}} . K_{\frac{1-n}{3-n}}\left(\frac{2}{3-n} . \sqrt{u} . r_D^{\frac{3-n}{2}}\right)}{u . K_{\frac{1-n}{3-n}}\left(\frac{2}{3-n} . \sqrt{u}\right)} \ldots\ldots\ldots\ldots\ldots\ldots\ldots\ldots\ldots\ldots \text{Eq 3.31}$$

To ensure the wellbore pressure is kept constant, equation Eq 3.31 must be solved numerically. The result is graphed in Fig 3.3. Similarly, while Darcy`s law applied, the dimensionless rate in the Laplace domain for Non-Newtonian fluid through homogenous reservoir derived as

$$q_D(r_D, u) = \frac{r^{2-n} . K_{\frac{2}{3-n}}\left(\frac{2 . r^{\frac{3-n}{2}} . \sqrt{u}}{3-n}\right)}{u^{0.5} . K_{\frac{n-1}{n-3}}\left(\frac{2 . \sqrt{u}}{3-n}\right)} \ldots\ldots\ldots\ldots\ldots\ldots\ldots\ldots\ldots\ldots \text{Eq 3.32}$$

Then, the dimensionless volume can be derived as

$$Q_D(r_D, u) = \frac{r^{2-n} . K_{\frac{2}{3-n}}\left(\frac{2 . r^{\frac{3-n}{2}} . \sqrt{u}}{3-n}\right)}{u^{1.5} . K_{\frac{n-1}{n-3}}\left(\frac{2 . \sqrt{u}}{3-n}\right)} \ldots\ldots\ldots\ldots\ldots\ldots\ldots\ldots\ldots\ldots \text{Eq 3.33}$$

Since Eq 3.33 is solved numerically, the cumulative fluid versus time is plotted in Fig 3.3.

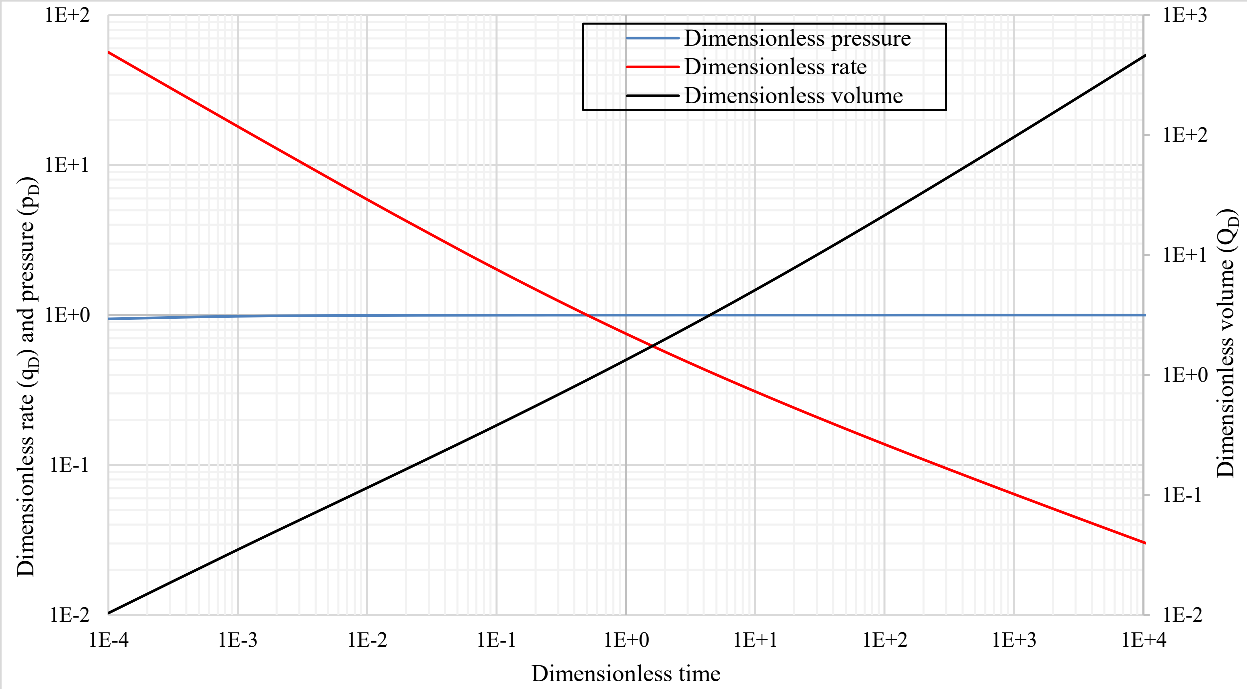

Fig 3.3 Dimensionless pressure, rate, and volume of Non-Newtonian fluid versus time in a homogenous reservoir under inner-constant pressure assumption (n=0.1).

3.3.2.2.1 Dimensionless rate early time (short-time approximation)

When the solution in Laplace space is derived for measuring Non-Newtonian fluid rate through a homogenous case, Hankel developed asymptotic (short argument) expansions can be applied to derive an analytical solution designed for a short time. Since Hankel expansion is applied to approximate Besselk for both the numerator and denominator of Eq 3.32, the equation is simplifying and taking Laplace inversion, consequently, dimensionless rate analytical solution for short time measured as below

$$q_D(r_D, t_D) = \frac{r^{(1.25-0.75n)} . e^{-\frac{(1-r_D^{(1.5-\frac{n}{2})})^2}{(n-3)^2 . t_D}}}{\sqrt{\pi} . \sqrt{t_D}} \quad \text{……………………..……...……...……………….Eq 3.34}$$

3.3.2.2.2 Dimensionless rate at late time (long-time approximation)

To derive the long-time behavior of dimensionless flow rates, developed asymptotic (Large argument) expansions by Hankel should be applied in both numerator and denominator to approximate modified Besselk terms for a long time, following simplifying the equation and taking LaPlace inversion, consequently, dimensionless rate analytical solution for long-time measured as below (Appendix B)

$$q_D(r_D, t_D) = \frac{(3-n)^{\frac{n+1}{3-n}}.r^{1-n}.t_D^{-\frac{2}{n-3}-1}}{\Gamma(\frac{n-1}{n-3})} \quad \text{..Eq 3.35}$$

3.3.2.2.3 Dimensionless volume at early time (short-time approximation)

To measure the early-time behavior of Non-Newtonian dimensionless fluid rates, Hankel developed asymptotic (short argument) expansions should be applied, as a result, approximation of Besselk for both numerator and denominator of Eq 3.33, then, taking the LaPlace inversion result in dimensionless analytical volume at a short time as below

$$Q_D(r_D, t_D) = -\frac{0.9\,.r_D^{2-n}.(r^w-1).(\frac{1.77245.t_D.|n-3|.1F1(-0.5;0.5;\frac{(r^w-1)^2}{(n-3)^2.t_D})}{|r^w-1|}-3.1416)}{\sqrt{3-n}\,.(n-3)} \quad \text{.........................Eq 3.36}$$

3.3.2.2.4 Dimensionless volume at a late time (long-time approximation)

To derive Non-Newtonian analytical fluid volume for a long time, similarly, developed asymptotic (small argument) expansions have been applied to approximate quantity of Besselk for both numerator and denominator, then, taking Laplace inversion of the result to achieve dimensionless analytical volume in real long-time

$$Q_D(r_D, t_D) = \frac{(3-n)^{\frac{n+1}{3-n}}.r^{1-n}.t_D^{-\frac{(5-n)}{n-3}-1}.\Gamma(\frac{2}{n-3})}{\Gamma\left(\frac{n-1}{n-3}\right).\Gamma(-\frac{5-n}{n-3})} \quad \text{..Eq 3.37}$$

3.4 Model validation

The proposed solution is validating by treating the fluid as Newtonian (n=1). This aligns with the solution reported by Da Prat (1990) for Newtonian fluid data. Fig 3.4 presents the results of the proposed solution for the dimensionless drilling fluid-loss rate through NFR, considering various inter-porosity flow coefficients under constant wellbore pressure conditions. These are compared with Da Prat's (1990) model for Newtonian fluid. The outcomes from our model closely match the data presented by Da Prat (1990) for Newtonian fluid flow. The specifications for NFR and mud pseudo-plasticity, employed to adjust both models, are λ=1E0, 1E-3, 1E-5, 1E-7, 1E-9; ω=0.01; n=1; and D=1. In the context of numerical inversion using the Stehfest algorithm, a distinct parameter n is utilized to denote the number of terms in the approximation for Laplace transform inversion. After careful analysis and experimentation, the optimal value for this specific application is found to be n=8, a choice that ensures a balance between computational efficiency and the desired level of accuracy. This parameter is maintained at 8 to solve both the Keshavarz-Moreno and Da Prat models. In Fig 3.4, our model's results are delineated by solid lines, while Da Prat's (1990) data is indicated by dashed lines. Close examination reveals a remarkable agreement between the two models.

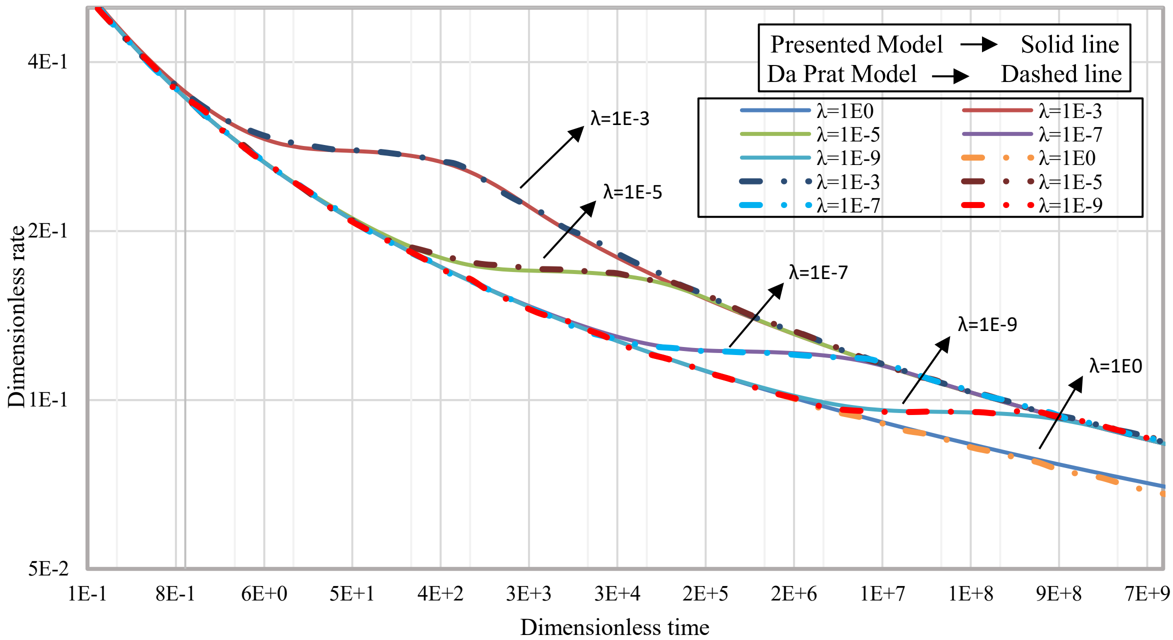

Fig 3.4 Comparison of presented solution with analytical one derived by Da Prat (1990).

3.5 Qualitative and quantitative analysis of drilling-fluid loss

The solution evaluated in the previous section serves as a foundational structure for generating specific type-curves for each scenario. These scenarios vary based on factors such as inter-porosity flow coefficient, storativity ratio, dimensionless matrix contribution, and flow behavior index, all of which are critical to this strategy. The following section describes how these type-curves facilitate analysis.

3.5.1 Qualitative analysis

The evaluated solution derived in the previous section is considered as a base structure to draw different type-curves for each specific scenario. Created type-curves are completely depend on inter-porosity flow coefficient, storativity ratio, dimensionless matrix contribution, and flow behavior index. These four parameters play an important role in this strategy. Due to the definition, these parameters can be measured since the operator has access to the reservoir properties such as porosity, permeability, and total compressibility. Various procedures exist to determine high-resolution reservoir properties, including logging while drilling (LWD) and drilling-cutting analysis. Once the type-curve for each specific scenario is created (according to the mentioned above parameters), the sensitivity analysis on two issues can be performed. The first sensitive analysis is being performed on NFR characteristics (including inter-porosity flow coefficient, storativity ratio, and dimensionless matrix contribution) and drilling-fluid pseudo-plasticity to observe how these factors affect the leak-off phenomenon and loss volume over different periods. In addition, two procedures can be used to measure the dimensionless loss volume for each scenario, which provides insights into how these parameters affect the total loss volume. The first method involves calculating the area under the dimensionless rate-time curve using the trapezoidal rule. The second method involves directly measuring the dimensionless loss volume by numerically solving the evaluated solution. The second sensitivity analysis is conducted on reservoir properties and wellbore conditions such as fracture permeability, total storativity, fracture storativity, wellbore differential pressure, fracture aperture, and radius of invasion to observe how they influence the drilling-fluid rate and loss volume.

3.5.2 Quantitative analysis

One of the main goals of this study is to present a procedure that facilitates the quantification of reservoir parameters and total loss volume. To accomplish this, the evaluated dual-porosity solution (Eqs 3.23, 3.25, 3.27), which is detailed in section 3.3.21, provides the essential framework for developing specific type-curves for each scenario, taking into account inter-porosity flow coefficient, storativity ratio, dimensionless matrix contribution, and flow behavior index. These generated type-curves are applied to estimate not only NFR parameters but also Non-Newtonian fluid rate and total cumulative volume. Two detailed procedures are described as follows: The first procedure employs type-curve matching for reservoir parameter estimation, while the second procedure not only quantifies drilling-fluid rate and total loss volume but also aids in categorizing them across three distinct periods in NFR, considering two different classification schemes. Additionally, the effects of NFR properties, wellbore differential pressure, and fracture aperture on a radius of invasion (ROI) and total cumulative volume are examined. The workflow for measuring parameters using these two procedures is further explained below.

3.5.2.1 Reservoir properties measurement by derived type-curves

The derived evaluated solution for NFR is applied to reproduce type-curves to use in this procedure. Since drilling-fluid data is available, the type-curve based on the storativity ratio and inter-porosity flow coefficient of the studied NFR case is graphed to measure reservoir properties such as fracture permeability, fracture storativity, and total storativity. In this process, drilling-fluid rate data is graphed as a function of time on tracing paper, and then it is placed over the desired type-curve to find the match point at the rate and time axis to put in Eq 3.38. As a result, fracture permeability can be measured by Eq 3.38 as shown in Table 3.1. To facilitate the process and directly measure fracture permeability from the total cumulative volume curve, the fracture permeability has also been derived based on this parameter according to Eq 3.39 as shown in Table 3.1. It should be noted that Eq 3.39 is presented to facilitate the process of directly measuring fracture permeability from the total cumulative volume curve. Similarly, total storativity can be calculated by matching the point of drilling-fluid time and dimensionless time by Eq 3.40 as illustrated in Table 3.1. The total storativity definition can be applied to determine fracture storativity (Da Prat, 1990) by Eq 3.41 as shown in Table 3.1. Eqs 3.38 to 3.40 are then transformed from the SI unit to the field unit and subsequently derived as Eqs 3.42 to 3.44, which have been added to Table 3.1. The dimensionless terms for both SI and Field unit are listed in Table 3.1 below,

Table 3.1: Dimensionless terms for the curve-fitting procedure.

Matching terms	SI unit	Field unit
Fracture permeability (Rate data) - k_f	$\left(\frac{\mu_{eff}.r_w^{1-n}}{(2\pi h)^n.(p_i-p)}\right).\left(\left[\frac{q}{q_D}\right]^n\right)_M$ (3.38)	$\left(\frac{\mu_{eff}*r_w^{1-n}}{(7.081*10^{-3}*h)^n*(p_i-p)}\right)*\left(\left[\frac{q}{q_D}\right]^n\right)_M,$ (3.42)
Fracture permeability (Loss volume data) - k_f	$\left[\frac{(2\pi h)^{\frac{n^2-n-1}{n}}.(p_i-p)^{\frac{-1}{n}}}{\mu_{eff}^{1-\frac{1}{n}}.n.(\varphi.c_t)_t.q^{n-1}.r_w^{4-\left(\frac{n^2+1}{n}\right)}}\right]^{\frac{n}{1-n}}.\left[\frac{Q}{Q_D}\right]_M^{\frac{n}{1-n}}$ (3.39)	$\left[\frac{7.081^n.h^{n-2}.(p_i-p)^{\frac{-1}{n}}}{(0.19).\mu_{eff}^{1-\frac{1}{n}}.n.(\varphi.c_t)_t.q^{n-1}.r_w^{4-\left(\frac{n^2+1}{n}\right)}}\right]^{\frac{n}{1-n}}.\left[\frac{Q}{Q_D}\right]_M^{\frac{n}{1-n}},$ (3.43)
Total Storativity - $[\varphi c_t]_t = [\varphi c_m + \varphi c_f]$	$\left(\frac{k_f.q^{1-n}}{n.(2\pi h)^{1-n}.\mu_{eff}.r_w^{3-n}}\right).\left(\frac{t}{t_D}\right)_M$ (3.40)	$\left(\frac{2.637*10^{-4}*k_f*q^{1-n}}{n*(h)^{1-n}*\mu_{eff}*r_w^{3-n}}\right)*\left(\frac{t}{t_D}\right)_M,$ (3.44)
Fracture storativity - φc_f	$[\varphi c_m + \varphi c_f].\omega$ (3.41)	$[\varphi c_m + \varphi c_f].\omega$

3.5.2.2 Cumulative volume measurement through NFR by real-time curves (after type-curve conversion)

This method concentrated on measuring Non-Newtonian fluid rate and volume by converting presented type-curves to dimensional real-time data curves (For each dimensionless rate, there is one equivalent rate in real time; the dimensionless time is measured through NFR and plot). In this regard, the type-curve for NFR with specific inter-porosity flow coefficient, storativity ratio, dimensionless matrix contribution, and flow behavior index graphed. The reservoir specification of this reservoir should then be put in Eqs 3.45 to 3.47 in Table 3.2 to measure drilling-fluid rate and volume versus time in a real-time graph (dimensional curve) for this type of NFR to convert the data to real-time data.

Table 3.2: Dimensional rate, volume, and time for both SI and field data.

Dimensional term	SI unit	Field unit
Drilling-fluid rate, q	$\left[\frac{\mu_{eff}.r_w^{1-n}}{k_f.(2\pi h)^n.(p_i-p)}\right]^{-\frac{1}{n}}.q_D$ (3.45)	$\left[\frac{\mu_{eff}.r_w^{1-n}}{k_f.(7.081*10^{-3}*h)^n.(p_i-p)}\right]^{-\frac{1}{n}}.q_D$ (3.48)
Loss volume, Q	$\left[\frac{\mu_{eff}^{1-\frac{1}{n}}.n.(\varphi.c_t)_t.q^{n-1}.r_w^{4-\left(\frac{n^2+1}{n}\right)}}{k_f^{\frac{n-1}{n}}.(2\pi h)^{\frac{n^2-n-1}{n}}.(p_i-p)^{\frac{-1}{n}}}\right].Q_D$ (3.46)	$\left[\frac{(0.19).r^{4-\left(\frac{n^2+1}{n}\right)}.\mu_{eff}^{1-\frac{1}{n}}.q^{n-1}.(\varphi.c_t)_t}{k^{1-\frac{1}{n}}.0.007081^n.h^{n-2}.n.(p_i-p)^{\frac{-1}{n}}}\right].Q_D$ (3.49)
Time, t	$\left[\frac{n.(\varphi.c_t)_t.(2\pi h)^{1-n}.\mu_{eff}.r_w^{3-n}}{k_f.q^{1-n}}\right].t_D$ (3.47)	$\left[\frac{n.(\varphi.c_t)_t.(h)^{1-n}.\mu_{eff}.r_w^{3-n}}{2.637*10^{-4}.k_f.q^{1-n}}\right].t_D$ (3.50)

Eqs 3.45 to 3.47 are converted from the SI unit to the field unit and further derived as Eqs 3.48 to 3.50. These equations have been included in Table 3.2. The table lists dimensionless terms for rate, volume, and time in both SI and field units. The procedure presented in this study enables the measurement and analysis of Non-Newtonian fluid cumulative volume for each specific NFR in real time by generating a predictive curve for each scenario. The process flowchart is illustrated in Fig 3.5.

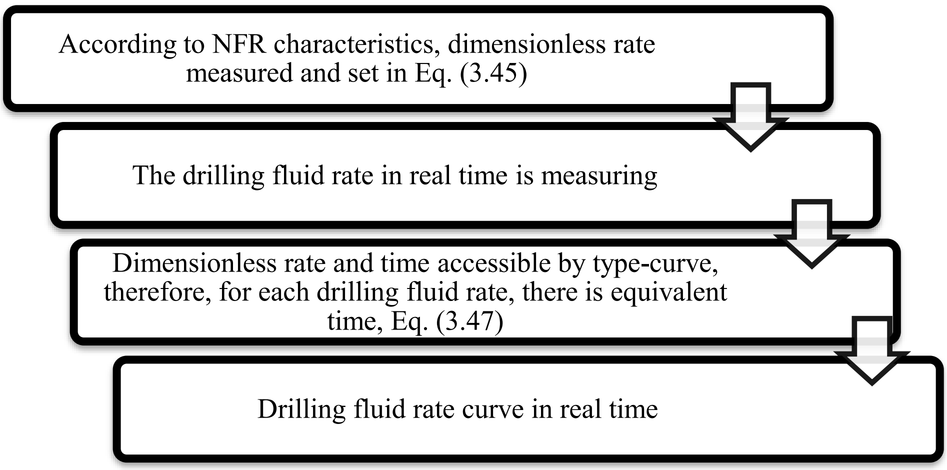

Fig 3.5 Type-curve conversion to real-time data process (since reservoir parameters are available).

It is worth noting that additional conversion factors from Table 3.3 are required to be added to Eqs 3.38 to 3.41 and Eqs 3.45 to 3.47 to render them applicable to field data. Four cases (with field data) are presented in the application section of this study to clarify and confirm the applicability of the presented procedure. This procedure can be applied in conditions where drilling-fluid field data is unavailable.

Table 3.3: Conversion constants for dimensionless pressure and time functions (Dake, 2001; Lee et al., 2003).

Constant	Darcy Units	Field Units	SI Units
$\mathbf{t_{Dc}}$	1	2.637E-4	3.557E-6
$\mathbf{p_{Dc}}$	2π	7.081E-3	5.356E-4
$\mathbf{p_{Dcr}=\frac{1}{p_{Dc}}}$	$1/(2\pi)$	141.2	1867.1

4 APPLICATION

In unconventional reservoirs, several enhanced oil recovery (EOR) projects are being executed to extract heavy hydrocarbon resources, along with drilling fluid loss mitigation projects to mitigate further loss. This section introduces four case studies to illustrate the applicability and efficacy of the proposed methodology and workflow. The aim is to validate the proposed procedure using two distinct sets of field data: data from the Machar-20 field in the UK central North Sea (Liétard et al., 1999b; Li´etard et al., 2002; Albattat et al., 2022) and loss measurements data from a fractured well in the Gulf of Mexico (Majidi et al., 2010). These datasets have been utilized to substantiate the effectiveness of the proposed solution. The objectives of these case studies are to: (1) determine NFR characteristics, such as fracture permeability and storativity as well as total storativity by type-curve matching; (2) quantify the rate and volume of Non-Newtonian fluid in real-time to predict the total cumulative volume; (3) classify drilling fluid rate and volume based on two criteria; (4) conduct a sensitivity analysis of reservoir and fluid properties, as well as differential wellbore pressure, to evaluate their impact on total cumulative volume; (5) measure the equivalent ROI for starting and ending transient periods through NFR; and (6) determine the total loss volume for each period. The following section presents these case studies in detail.

4.1 Case 1

In the first case, Machar-20 field data (Sanfilippo et al., 1997; Liétard et al., 1999; Albattat et al., 2022) in the literature is applied to demonstrate the application of the type-curve matching procedure to determine fracture permeability, total storativity, and fracture storativity for a Non-Newtonian drilling fluid within a double porosity reservoir model under wellbore constant pressure conditions. The drilling fluid and reservoir data are presented in Table 4.1 a, while mud-loss rate data for the Machar-20 field are reported in Table 4.1 b. In addition, the dimensionless rate and volume are graphed for the NFR properties (λ, ω, and D) and pseudo-plastic mud in Fig. 4.1

Table 4.1: Input parameters of base scenario, Machar 20 field data, (b) Drilling fluid report for Machar 20 field (Albattat et al., 2022; Liétard et al., 1999).

(a)

Parameter	Value	Parameter	Value
n	0.375	ω	1E-3
h, ft	0.00203412	μ, cp	30.5
Overpressure, Δp, psi	1120	r_w	0.36
λ	9E-1	D	6E-6

(b)

Time, day	Loss volume, bbl	Rate, bbl/day	Time, day	Loss volume, bbl	Rate, bbl/day
0.0064	17.60	2734.59	0.2536	231.88	914.11
0.0122	29.19	2375.33	0.2704	240.63	889.63
0.0222	48.35	2177.57	0.2899	246.36	849.58
0.0277	55.41	1993.82	0.3232	256.06	792.09
0.0393	74.85	1902.25	0.3576	266.66	745.50
0.0491	87.13	1773.27	0.3808	272.88	716.41
0.0612	100.24	1635.85	0.4089	282.55	690.84
0.0732	113.21	1544.97	0.4300	286.23	665.59
0.0864	125.20	1449.07	0.4571	292.75	640.38
0.0988	137.69	1392.61	0.4897	297.96	608.43
0.1129	147.14	1303.22	0.5212	301.11	577.62
0.1250	157.97	1263.42	0.5494	305.77	556.54
0.1422	170.25	1196.90	0.5824	309.45	531.34
0.1583	179.33	1132.19	0.6115	315.11	515.29
0.1731	190.42	1099.94	0.6337	319.38	503.92
0.1900	199.79	1051.20	0.6537	325.49	497.90
0.2063	208.48	1010.09	0.6570	323.82	492.83
0.2298	221.14	962.20			

Initially, the dimensionless rate as a function of time is plotted for the corresponding inter-porosity flow parameter, dimensionless storage coefficient, and flow behavior index (after numerically solving the evaluated model for NFR). Subsequently, it is placed over Machar 20 field data (Table 4.1 b), enabling the determination of NFR parameters, as illustrated in Fig 4.1.

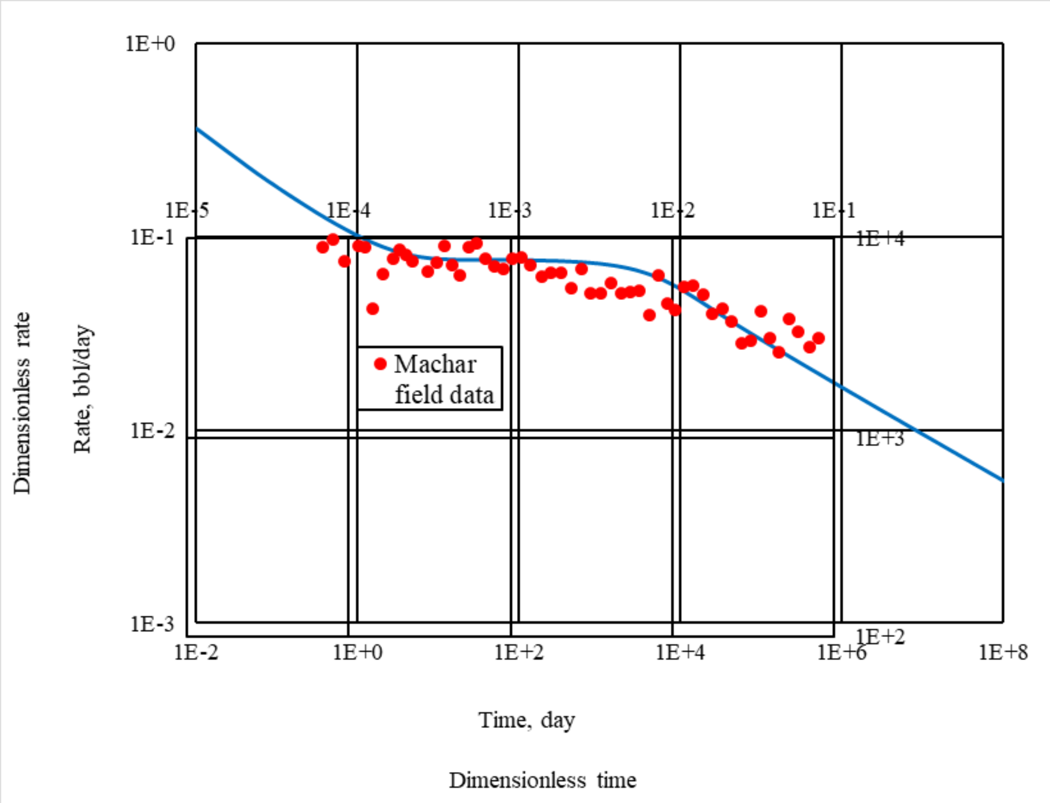

Fig 4.1 Dimensionless type-curve and real time data matching.

As the two graphs are found to match, the corresponding fractions are obtained from Fig 4.1. The resulting fractions are presented in Table 4.2.

Table 4.2: Measured ratio for this scenario.

Parameter	Quantity
$\frac{\mathbf{q}}{\mathbf{q_D}}$	$\frac{1E3}{1.5E-2}$
$\frac{\mathbf{t}}{\mathbf{t_D}}$	$\frac{1E-1}{1E6}$

Considering both reservoir and drilling fluid data, Eqs. 3.41, 3.42, and 3.43 are utilized to determine fracture permeability, storativity, and total storativity. In this context, fracture permeability is evaluated as

$$k_f = \left(\frac{30.5 * (0.36)^{1-0.375}}{(7.081 * 10^{-3} * 0.00203412)^{0.375} * (1120)}\right) * \left(\left[\frac{1E3}{1.5E-2}\right]^{0.8}\right)_M = 60.5 \text{ mD}$$

The relative permeability can also be directly measured using the dimensionless cumulative volume while applying Eq. 3.42. Additionally, the total storativity can be measured using Eq. 3.43 as shown below,

$$(\phi C_t)_{\mathrm{t}} = \left(\frac{2.637*10^{-4}*60.5*(1000)^{1-0.375}}{0.375*(0.00203412)^{1-0.375}*30.5*0.36^{3-0.375}}\right)*\left(\frac{1\mathrm{E}-1}{1\mathrm{E}6}\right)_{\mathrm{M}} = 1.7\mathrm{E}-4\ \mathrm{psi}^{-1}$$

It is crucial to emphasize that the time variable in Eq 3.43, which is a dimensional equation, should be quantified in hours. Additionally, after determining the total storativity, the storativity specific to fractures is assessed. This measurement, indicative of the fractures' capacity to retain drilling fluid, is determined to be 6.1E-5. Previous studies in the literature, such as Da Prat (1990), have employed Newtonian fluids to determine fracture permeability, total storativity, and fracture storativity parameters. In contrast, this study applies a Non-Newtonian fluid to ascertain these three parameters in NFR, with the results falling within the acceptable range for NFR reservoirs.

4.2 Case 2

In this section, we use the Machar-20 filed data to describe the workflow for measuring drilling fluid rate and volume by generated type-curve. If Non-Newtonian fluid field data is unavailable, this procedure can be utilized for real-time measurement of Non-Newtonian fluid rate and volume. When NFR characteristics and drilling-fluid rheology data are available, it is possible to convert the dimensionless drilling fluid rate and volume data into real-time data. This can be presented in the form of a real-time graph for a particular NFR, which can be subjected to quantitative analysis to predict Non-Newtonian fluid rate, cumulative loss volume, ROI, start and end of the transient period, the cumulative loss in each period, and classification of the mud loss. In addition, the drilling fluid (which is a Non-Newtonian fluid) rate and total loss volume have been categorized using two distinct criteria to differentiate the type of drilling fluid loss and observe it during separate intervals. The procedure is described as follows: Firstly, a type-curve is graphed for a specific inter-porosity flow parameter, storativity ratio, flow behavior index, and dimensionless matrix contribution, according to Table 4.1 a, and the result is depicted in Fig 4.1 (solid line). Secondly, to convert the dimensionless type-curve into a real-time curve, Eqs. 3.47 to 3.49 are utilized by incorporating the reservoir characteristic data (Table 4.1 a) to measure the drilling fluid rate and loss volume in real time. By following this procedure, the Non-Newtonian fluid rate and loss volume for each NFR can be measured in real time over different periods. The drilling fluid rate is measured and depicted in Fig 4.2 with respect to reservoir properties, drilling-fluid rheology, and wellbore condition. Then, Nayberg & Petty's (1986) description is applied to classify the drilling fluid loss. Fig 4.2 presents the outcome of applying this criterion to the drilling fluid rate over time, as demonstrated below

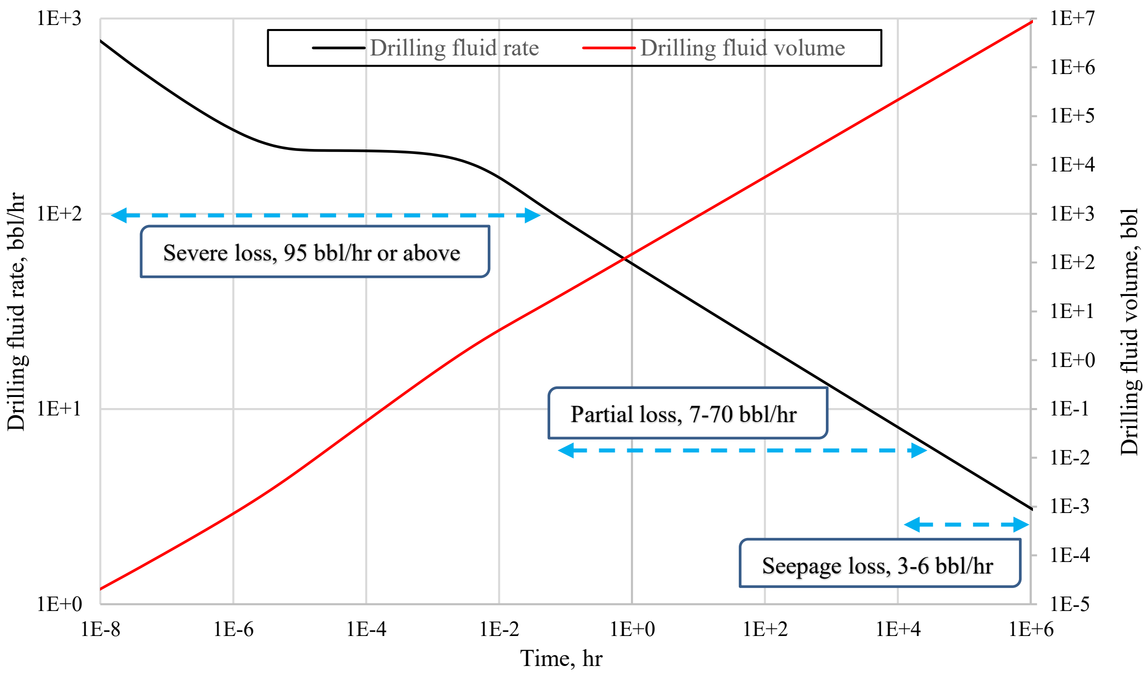

Fig 4.2 Categorization of drilling fluid loss based on Nayberg and Petty's (1986) standard.

In Fig 4.2, a severe loss is observed to occur at early times, which continues into the transient period. At later stages, partial and seepage losses are noted. The duration of drilling fluid loss, dictated by its severity, is presented in Table 4.3 and is illustrated in Fig 4.2.

Table 4.3: Mud-loss duration according to Nayberg and Petty's (1986) categorization.

Parameter	Severe loss	Partial loss	Seepage loss
Duration of mud loss Categorized by severity, min (time changed from hr to min)	3.54 min	2E6 min	5.25E7 min

The total cumulative loss can be measured in two ways: by applying the trapezoidal rule to Fig 4.2 or by directly utilizing Eq 3.48. In this section, Eq 3.49 is used, and the resulting graph of the total loss volume is displayed in Fig 4.3. As another categorization, the total loss volume, along with the drilling fluid rate, is divided into three phases: early time, transient time, and late time. These divisions are highlighted in Fig 4.3.

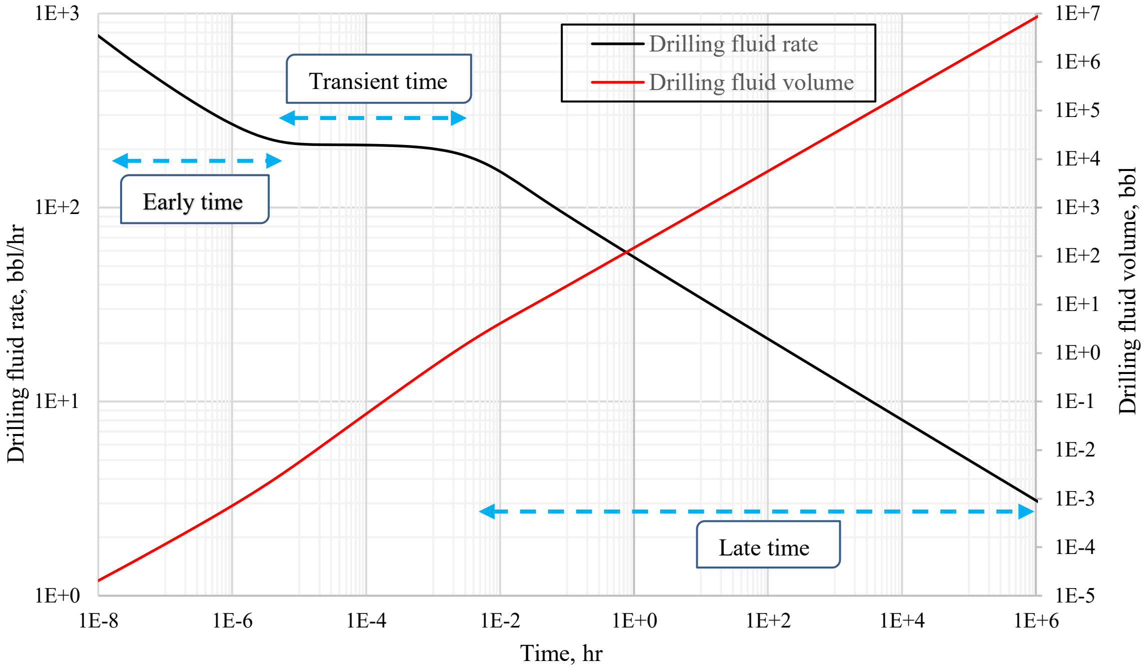

Fig 4.3 Drilling fluid rate and loss volume versus time in the dimensional curve.

In the given scenario, the cumulative loss volume from t=1.5E-8 to t=1.36E6 hours for each phase (early, transient, and late time) is meticulously calculated using Eq 3.49. This approach enables the detailed measurement of the total loss volume within each period, applying the reservoir parameters and adjusting dimensionless parameters λ, ω, n, and D, as depicted by the red solid line in Fig 4.3. Furthermore, Table 4.4 elaborates on the quantity and duration of loss for each period separately. Such detailed quantification lays a robust foundation for operators to effectively manage the overall loss volume, taking into consideration the characteristics of the NFR. This methodological approach not only ensures accurate measurement but also facilitates a comprehensive understanding and management of loss volumes in relation to NFR properties.

Table 4.4: Mud-loss volume and duration time in each section

Parameter	Early time	Transient time	Late time
Drilling-fluid loss volume (bbl) and period time (hour)	3.7E-3 bbl - 6.47E-6 hr	3.336 bbl - 7.77E-3 hr	7.6E6 bbl – 9E5 hr

Fig 4.4 illustrates the early-time behavior of the ROI as the drilling fluid invades through the NFR, for the specific reservoir characteristics. The figure demonstrates how this procedure can aid in identifying the ROI during each period, and also enables the operator to determine the

corresponding ROI at the beginning and end of the transient period. The three distinct periods are differentiated in the figure using different colors, as shown below.

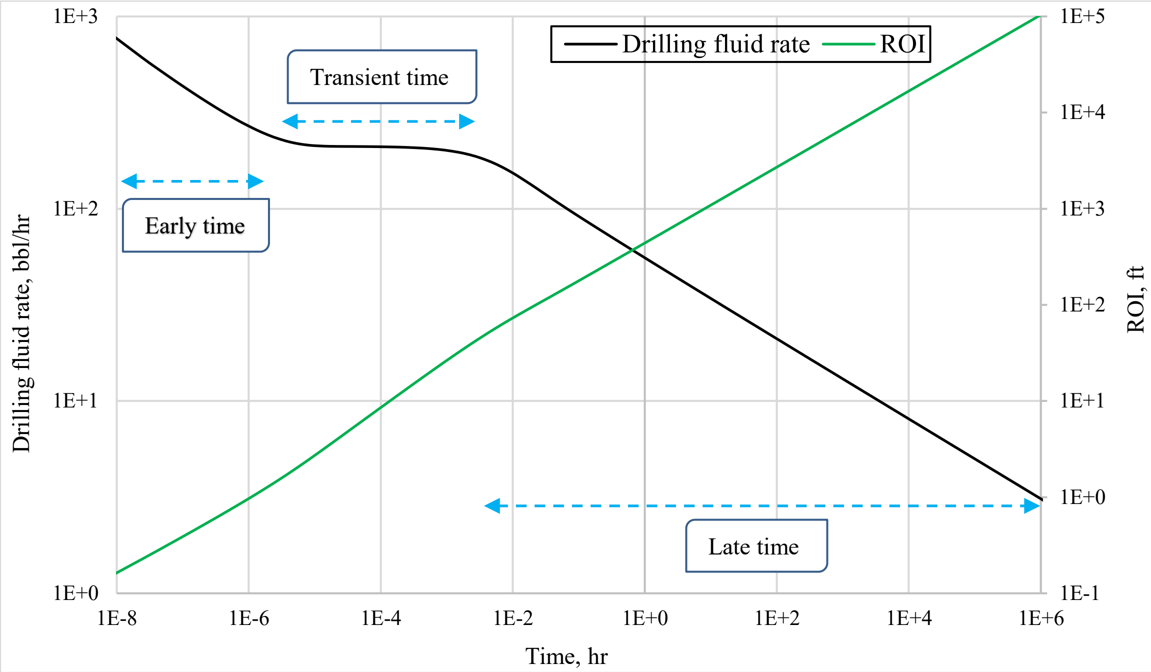

Fig 4.4 Categorization of the radius of invasion and drilling fluid rate.

Measuring the ROI at the beginning and end of each period aids in better characterizing the mud loss phenomenon, thereby assisting operators in mitigating mud loss at earlier times. In this case, the ROI at the start and end of the transient period is measured and displayed in Table 4.5.

Table 4.5: Radius of invasion for the start and end of the transition period.

Time, hour	Radius of invasion, ft
3.6E-6	2
9E-3	70

When drilling fluid invades through the NFR, the total loss volume corresponding to each ROI is measured based on the properties of both the reservoir and the Non-Newtonian fluid. Fig 4.5 illustrates the ROI and the equivalent cumulative volume at the onset of the transient period. The period time in Fig 4.5 is determined by measuring the corresponding ROI for each time interval. It is observed that, when the drilling-fluid front reaches 2 ft through the NFR (marking the commencement of the transient period), the total loss volume stands at 3.5E-3 bbl. This continues until it reaches 2.8 bbl at a distance of 60 ft, marking the conclusion of the transient period.

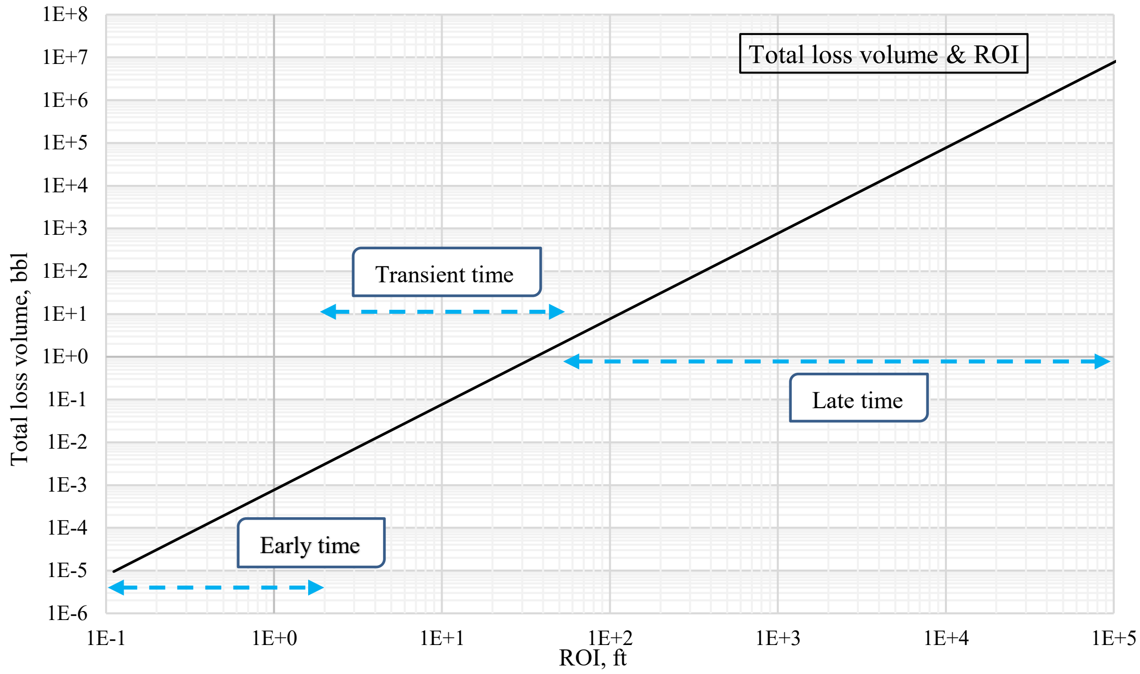

Fig 4.5 Drilling-fluid total loss volume for the equivalent radius of invasion through NFR.

To demonstrate the significance of Non-Newtonian fluid pseudo-plasticity in NFR with different fracture apertures (considered as reservoir thickness within the matrix-fracture system), four cases varying in fracture aperture and fluid pseudo-plasticity were analyzed. The findings indicate that the impact of drilling-fluid rheology in NFR is considerably more pronounced for higher fracture apertures than for lower ones, especially at later times. Therefore, this parameter can play a crucial role in decreasing the drilling fluid invasion rate. While the fracture aperture does not inherently alter the duration of the transient period, it modulates the rate at which this period occurs, either intensifying or attenuating it. Additionally, an increase in fracture aperture leads to an increase in the total cumulative fluid volume. The proposed analytical framework enables operators to precisely gauge the fracture aperture. This is achieved by taking into account both the inherent properties of the NFR and the fluid's pseudo-plasticity within the fracture and porous medium, utilizing the available differential pressure inside the wellbore. Table 4.6 provides detailed reservoir and drilling-fluid information, while Fig 4.6 illustrates the obtained results. In Fig 4.6, the drilling-fluid rate is represented by a solid line and the cumulative volume by a dotted line.

Table 4.6: Well, reservoir, and drilling fluid information applied in the calculations

Parameter	Value	Parameter	Value
n	0.375 & 0.6	μ, cp	30.5
h, ft	0.001 & 0.009	r_w, ft	0.36
Δp_w, psi	1120	k_f, md	60.5
λ	9E-01	$[\phi c_t]_t$, psi^{-1}	1.75E-4
ω	1E-3	ϕ	0.12

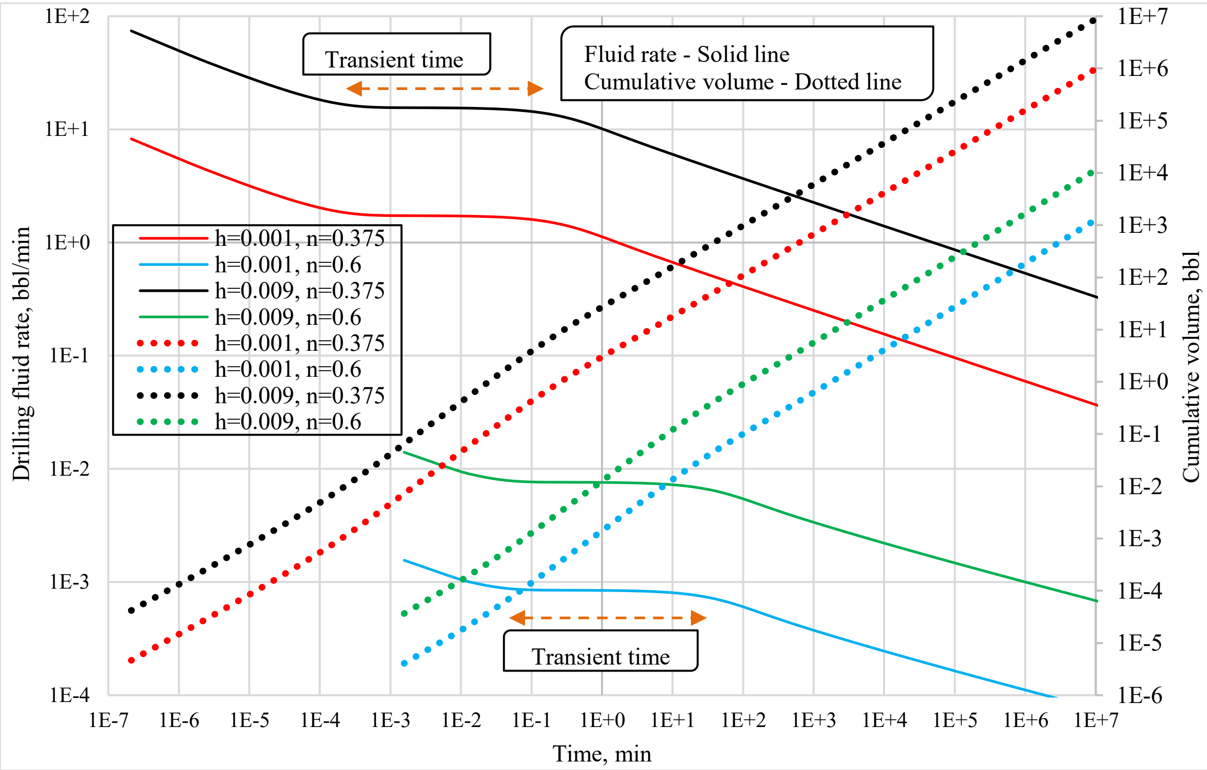

Fig 4.6 Mud-rheology influence on total cumulative volume through NFR with different fracture aperture (reservoir thickness, matrix-fracture system.

To validate and showcase the applicability of the model introduced here (Keshavarz-Moreno model), we compared its predictions of drilling fluid rate and volume in NFR with the Majidi model and the field data (Gulf of Mexico) from an actual mud-loss incident (Majidi et al., 2010; Razavi et al., 2017b). The comparison is depicted in Fig 4.7. The Keshavarz-Moreno model is specifically designed to simulate pseudo-plastic fluid flow through NFR. In contrast to earlier studies that attempted to incorporate yield stress to simulate drilling-fluid invasion, the Keshavarz-Moreno model prioritizes the consideration of drilling-fluid pseudo-plasticity (power law model) during the early stages of drilling-fluid invasion. This approach results in a high degree of accuracy, emphasizing the importance of focusing on pseudo-plasticity rather than yield stress in the initial stages of drilling-fluid invasion. In practice, early-time behavior of drilling fluid is typically a concern, and remedial actions are implemented to mitigate losses.

The significance of the presented result in precisely simulating the drilling fluid rate of invasion at earlier times can be observed. Input parameters for the base scenario are provided in Table 4.7.

Table 4.7: Well, reservoir, and drilling-fluid information applied in the calculations.

Parameter	Value	Parameter	Value
n	0.41	ω	1E-3
h, ft	2.9E-3	μ, cp	30.5
Overpressure, Δp, psi	800	r_w	0.36
λ	8E-4	$[\varphi c_t]_t$, psi^{-1}	1.5E-4
ϕ	0.12	k, md	300
D	9E-4		

An overpressure ranging from approximately 700 to 800 psi was estimated through equivalent circulating density (ECD) calculations, as detailed in Majidi et al. (2010). This estimation was further elucidated by comparing the observed rate of losses with the loss volume predicted by the model, as depicted in Fig 4.7. Within the same figure, the Keshavarz-Moreno model is shown to have been adapted to align with field data, yielding an average fracture width measurement of 2.9E-3 ft. Notably, this measurement is congruent with the findings presented in the Majidi model, where the average hydraulic width was measured at 2.88E-3 ft. Unlike pre-existing models, the model introduced in this study precisely characterizes the period during which the drilling fluid occurs, thus setting it apart from previous approaches. The results of the presented model are further compared with the Majidi model, emphasizing the importance of yield stress at late times. Therefore, in the context of drilling-fluid phenomena, the presented model is noteworthy; although it considers only pseudoplasticity, it remains functional for drilling fluid with yield stress. In this case, as can be seen, the yield stress takes effect during the late period time at t=1E3 minutes.

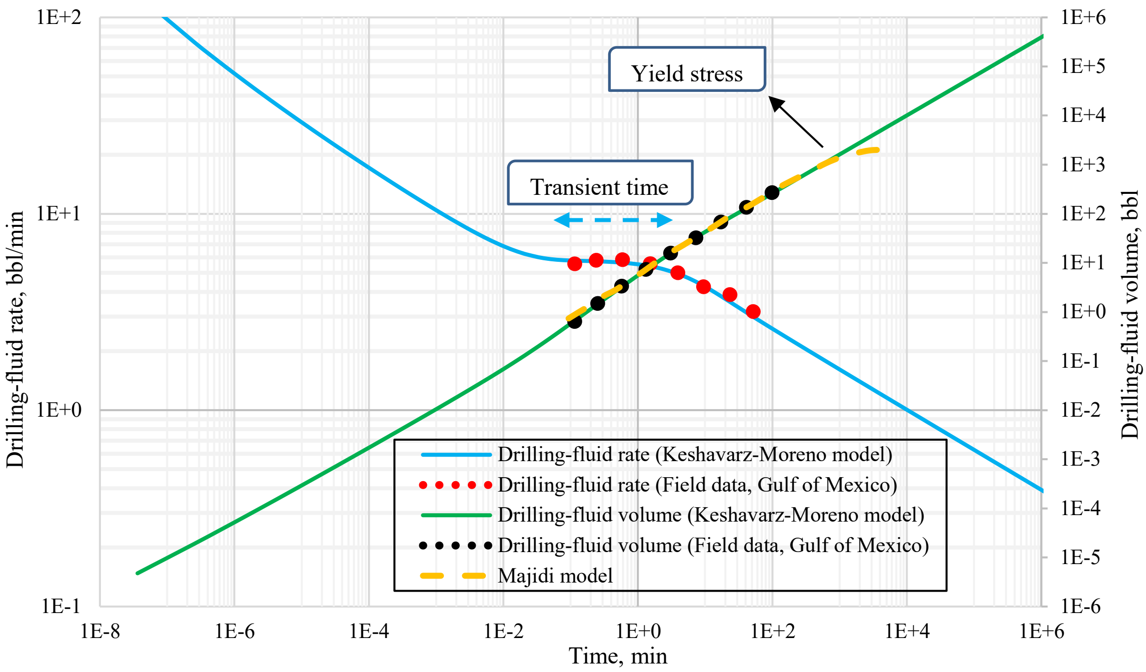

Fig 4.7 The predictions of the Keshavarz-Moreno model is compared with the Majidi model and field data of a real-life mud-loss phenomenon.

4.3 Case 3

In this section, two critical issues are examined. The first issue focuses on the impact of wellbore differential pressure on the rate of drilling fluid loss. The subsequent analysis investigates the influence of drilling-fluid rheology under both higher and lower differential wellbore pressures. Relevant data on the reservoir and drilling fluid are provided in Table 4.8.

Table 4.8: Well, reservoir, and drilling fluid information applied in the calculations.

Parameter	Value	Parameter	Value
n	0.375 & 0.6	ω	1E-3
h, ft	0.00203412	μ, cp	30.5
Overpressure, Δp, psi	1120 & 2000	r_w	0.36
λ	9E-1	$[\varphi c_t]_t$, psi^{-1}	1.75E-4
ϕ	0.12	k, md	60.5
D	6E-6		

The drilling fluid rate is measured at two distinct wellbore pressures: 1120 psi and 2000 psi. As illustrated in Fig 4.8, the rheology of the drilling fluid is found to be pivotal in mitigating mud-loss volume when the differential pressure inside the wellbore increases. This emphasizes the significance of the pseudoplasticity of drilling fluids during deepwater drilling. Furthermore, an increase in wellbore differential pressure is observed to result in a higher drilling fluid rate. It is noteworthy that while an elevated differential pressure inside the wellbore is not shown to influence the duration of the transition period, the transient period is found to occur at higher rates.

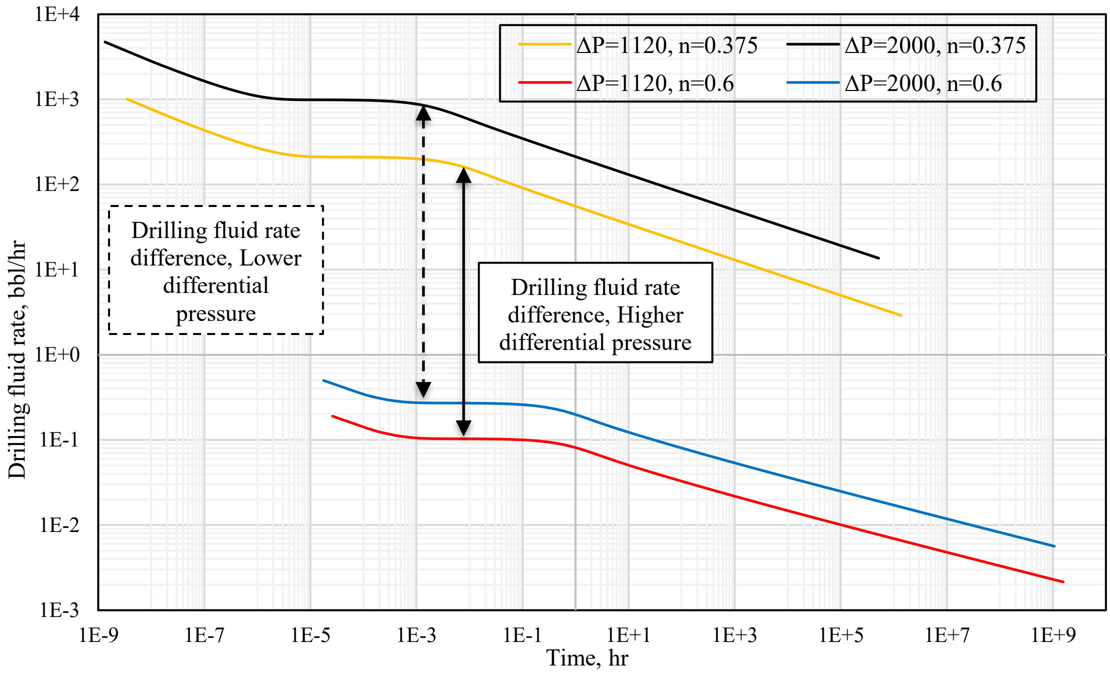

Fig 4.8 Drilling fluid rate under two different wellbore differential pressures.

4.4 Case 4

To examine the impact of drilling-fluid rheology on the ROI and total cumulative volume, four cases with different inter-porosity flow parameters and pseudo-plasticity are analyzed and depicted in Figs 4.9 and 4.10, as illustrated below. The reservoir and fluid details are summarized in Table 4.9.

Table 4.9: Well, reservoir, and drilling fluid information applied in the calculations.

Parameter	Value	Parameter	Value
n	0.375 & 0.6	μ, cp	30.5
h, ft	0.00203412	r_w	0.36
Δp_w	1120	k_f	60.577
λ	1E-3 & 1E-9	$[\phi c_t]_t$, psi^{-1}	1.75E-04
ω	3.5E-2	ϕ	0.12

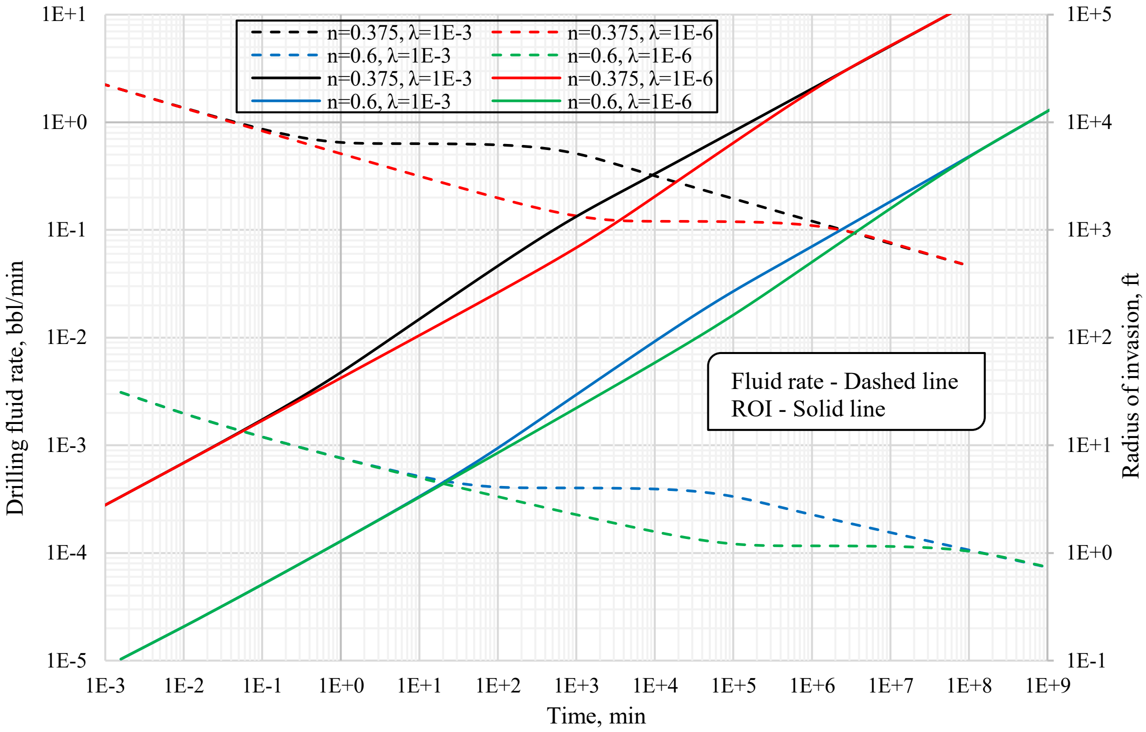

Fig 4.9 Radius of invasion comparison for two different fluid pseudo-plasticity and inter-porosity flow parameters.

In Figs 4.9 and 4.10, the results indicate that the inter-porosity flow parameter significantly influences ROI and total loss volume, especially when drilling fluids with higher pseudo-plasticity are used compared to those with lower pseudo-plasticity. This underscores the pivotal role of drilling-fluid rheology in NFRs with heightened leak-off. Notably, NFRs characterized by higher inter-porosity flow parameters exhibit increased drilling fluid loss and ROI, particularly during the transient period. This trend is more pronounced when drilling fluids with greater pseudo-plasticity are employed. For NFRs with elevated leak-off, a rapid increase in ROI is observed, which becomes even more pronounced during the transient period. Furthermore, Fig 4.9 provides a means to measure the ROI from the beginning to the end of the transient period, ranging in this case from 30ft to 2E4 ft, respectively.

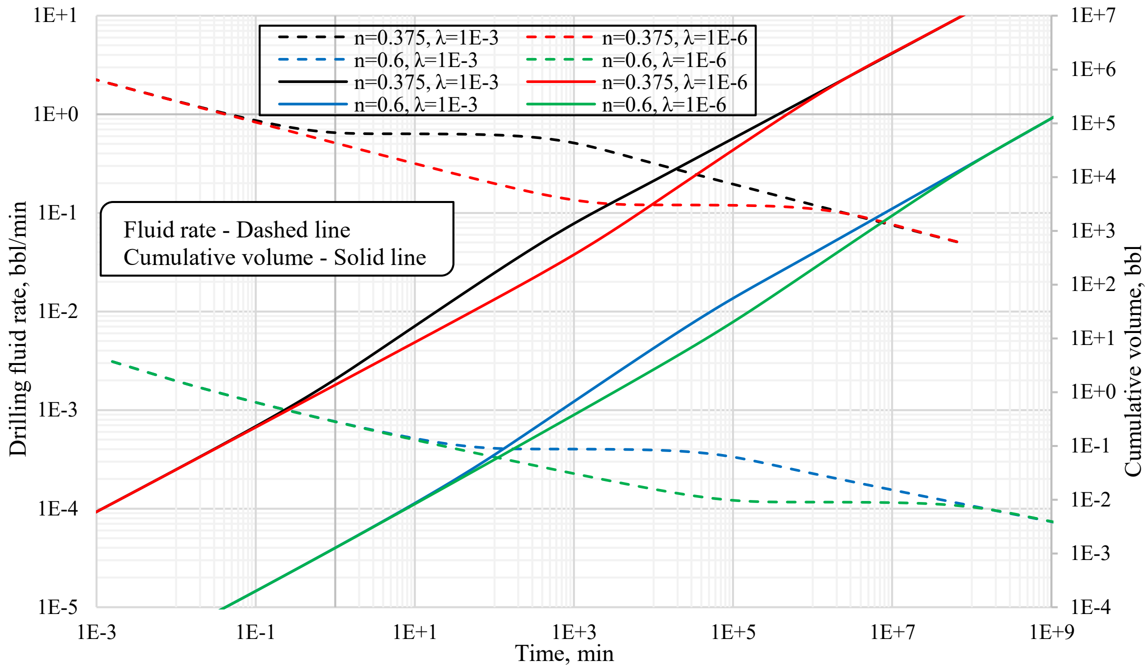

Fig 4.10 Total loss volume comparison for two different fluid pseudo-plasticity and inter-porosity flow parameters.

5 RESULT AND DISCUSSION

In this chapter, we synthesize the findings from our evaluated solution model as applied to NFRs. Following this, we illustrate the utility of the derived type-curves through a sensitivity analysis, the outcomes of which are extensively discussed in this section. Additionally, we have successfully identified and categorized various dimensionless terms, which have subsequently been introduced. In essence, this chapter encapsulates the key findings and implications drawn from our research and discusses them in detail.

5.1 Derived solution

In this study, we utilize the radial diffusivity equation as the foundational framework to analyze mud loss in both homogeneous formations and Naturally Fractured Reservoirs (NFRs). Upon solving the radial diffusivity equations with the assumption of constant wellbore pressure, we present the solutions for both scenarios as follows:

- For Non-Newtonian drilling fluid advancing through an NFR with a constant inner wellbore pressure, we derive dimensionless rates and volumes as expressed in Equations 3.25 and 3.27, respectively.
- For a homogeneous reservoir, considering the simplifications made for dimensionless rates through an NFR, we present the dimensionless rate and volume equations for measuring the advancement of Non-Newtonian drilling fluids under a constant inner wellbore pressure as Equations 3.32 and 3.33, respectively.

To enhance understanding, we have compiled two tables that systematically present the drilling fluid model for various scenarios under two distinct inner-boundary conditions. These tables detail the drilling-fluid flow models, evaluated solutions, their boundary conditions, and dimensionless equations for pressure, rate, and loss volume, along with the generated dimensionless terms.

Table 5.1: Diffusivity-based equations, boundary conditions, and solutions under wellbore constant pressure for both NFR and homogenous reservoir (Da Prat, 1990; Dake, 2001; Lee et al., 2003).

Fluid type and reservoir type	Newtonian, homogenous (Lee, John B, & Spivey, 2003)	Newtonian, NFR reservoir (DA PRAT, 1990)	Non-Newtonian, homogenous (Ikoku & Ramey Jr, 1979)	Non-Newtonian, NFR reservoir
Dimensionless equation in matrix	$\frac{1}{r_D}\frac{\partial}{\partial r_D}(r_D\frac{\partial p_D}{\partial r_D})=\frac{\partial p}{\partial t_D}$	$(1-\omega)\frac{\partial p_{Dm}}{\partial t_D}=\lambda(p_{Df}-p_{Dm})$	$\frac{\partial^2 p_{DNN}}{\partial r_D^2}+\frac{n}{r_D}\frac{\partial p_{DNN}}{\partial r_D}=r_D^{1-n}\left(\frac{\partial p_{DNN}}{\partial t_{DNN}}\right)$	$\frac{\partial p_{Dm}}{\partial t_D}=\frac{n\lambda}{(1-\omega)}.D^{1-n}.(p_{fD}-p_{mD})$
Dimensionless equation in fracture+matrix (total system)	……….	$\frac{\partial^2 p_{fD}}{\partial r_D^2}+\frac{1}{r_D}\frac{\partial p_{fD}}{\partial r_D}=\left(\omega\frac{\partial p_{fD}}{\partial t_D}+(1-\omega)\frac{\partial p_{mD}}{\partial t_D}\right)$	………	$\frac{\partial^2 p_{fD}}{\partial r_D^2}+\frac{n}{r_D}\frac{\partial p_{fD}}{\partial r_D}=r_D^{1-n}\left(\omega\frac{\partial p_{fD}}{\partial t_D}+(1-\omega)\frac{\partial p_{mD}}{\partial t_D}\right), t_D>0$
Initial boundary	$p_D(r_D,0)=0$	$p_{mD}(r_{mD},0)=p_{fD}(r_{fD},0)=0$	$p_{DNN}(r_D,0)=0$	$p_{mDNN}(r_{Df},0)=p_{fDNN}(r_{Df},0)=0$
Inner boundary	$p_D(1,t_D)=1$	$p_{fD}-S(\frac{\partial p_{fD}}{\partial t_D})=1$	$P_{DNN}(1,t_D)=1$	p_{fDNN}-$S(\frac{\partial p_{fD}}{\partial t_D})$=1
Outer boundary	$\lim_{r_D\to\infty} p_D(r_D,t)=0$	$\lim_{r_D\to\infty} p_{DNN}(r_D,t)=0$	$\lim_{r_D\to\infty} p_D(r_D,t)=0$	$\lim_{r_D\to\infty} p_{fDNN}(r_D,t)=0$
Dimensionless equation in matrix in laplace space	$\frac{1}{r_D}\frac{d}{dr_D}(r_D\frac{dp_D}{dr_D})=up_D$	$\acute{p}_{mD}(r_D,u)=\frac{\lambda}{u.(1-\omega)+\lambda}.\acute{p}_{fD}(r,u)$	$\frac{d^2 p_{DNN}}{dr_D^2}+\frac{n}{r_D}\frac{dp_{DNN}}{dr_D}=u.r_D^{1-n}.p_{DNN}$	$\acute{p}_{Dm}(r_D,u)=\frac{n\lambda D^{1-n}}{u.(1-\omega)+n\lambda D^{1-n}}.\acute{p}_{fD}(r_D,u)$
Dimensionless equation in fracture+matrix (total system) Laplace space		$\frac{1}{r_D}\frac{d}{dr_D}\left[r_D\frac{d\acute{p}_{fD}(r_D,u)}{dr_D}\right]=u.f(u).\acute{p}_{fD}(r_D,u)$ $f(u)=\frac{\omega(1-\omega)u+\lambda}{(1-\omega)u+\lambda}$		$\frac{d^2\acute{p}_{fD}(r_D,u)}{\partial r_D^2}+\frac{n}{r_D}\frac{d\acute{p}_{fD}(r_D,u)}{dr_D}=r_D^{1-n}[u.g(u).\acute{p}_{fD}(r_D,u)]$ $g(u)=\frac{\omega(1-\omega)u+n\lambda D^{1-n}}{(1-\omega)u+n\lambda D^{1-n}}$
Inner boundary in ls	$\acute{p}_D(1,u)=\frac{1}{u}$	$\acute{p}_{fD}-S(\frac{\partial p_{fD}}{\partial r_D})_{r_D=1}=\frac{1}{u}$	$\acute{p}_D(1,u)=\frac{1}{u}$	$\acute{p}_{fD}-S(\frac{\partial p_{fD}}{\partial rD})_{r_D=1}=\frac{1}{u}$
Outer boundary in ls	$\lim_{r_D\to\infty}\acute{p}_D(r_D,u)=0$	$\lim_{r_D\to\infty}\acute{p}_{DNN}(r_D,u)=0$	$\lim_{r_D\to\infty}\acute{p}_D(r_D,u)=0$	$\lim_{r_D\to\infty}\acute{p}_{fDNN}(r_D,u)=0$
General solution in Laplace domain	$p_D(r_D,u)=I_0(r_D\sqrt{u})+K_0(r_D\sqrt{u})$	$p_{fD}(r_D,u)=AI_0\left(r_D\sqrt{u.f(u)}\right)+BK_0(r_D\sqrt{u.f(u)})$	$p_D(r_D,u)=r_D^{\frac{1-n}{2}}[BI_{\frac{1-n}{3-n}}(\frac{2}{3-n}.\sqrt{u}.r_D^{\frac{3-n}{2}})+CK_{\frac{1-n}{3-n}}(\frac{2}{3-n}.\sqrt{u}.r_D^{\frac{3-n}{2}})]$	$p_{fD}(r_D,u)=r_D^{\frac{1-n}{2}}[C_1I_{\frac{1-n}{3-n}}(\frac{2}{3-n}.\sqrt{u.g(u)}.r_D^{\frac{3-n}{2}})+C_2K_{\frac{1-n}{3-n}}(\frac{2}{3-n}.\sqrt{u.g(u)}.r_D^{\frac{3-n}{2}})]$
Interporosity flow function		$f(u)=\frac{\omega(1-\omega)u+\lambda}{(1-\omega)u+\lambda}$		$g(u)=\frac{\omega(1-\omega)u+n\lambda D^{1-n}}{(1-\omega)u+n\lambda D^{1-n}}$
Solution after imposing boundary condition	$\acute{p}_D(r_D,u)=\frac{K_0(r_D.\sqrt{u})}{u.K_0(\sqrt{u})}$	$\acute{p}_{fD}(r_D,u)=\frac{K_0(\sqrt{u.f(u)}.r_D)}{u.K_0(\sqrt{u.f(u)})}$	$\acute{p}(r_D,u)=\frac{r_D^{\frac{1-n}{2}}.K_{\frac{1-n}{3-n}}(\frac{2}{3-n}.\sqrt{u}.r_D^{\frac{3-n}{2}})}{u.K_{\frac{1-n}{3-n}}(\frac{2}{3-n}.\sqrt{u})}$	$\acute{p}_{fD}(r_D,u)=\frac{r_D^{\frac{1-n}{2}}.K_{\frac{1-n}{3-n}}(\frac{2.\sqrt{u.g(u)}}{3-n}.r_D^{\frac{3-n}{2}})}{u.K_{\frac{1-n}{3-n}}(\frac{2.\sqrt{u.g(u)}}{3-n})}$
Dimensionless rate in Laplace domain (Vaneverdingen procedure)	$\hat{q}_D(r_D,u)=\frac{K_0(\sqrt{u})}{u.K_0(r_D.\sqrt{u})}$	$\hat{q}_{fD}(r_D,u)=\frac{K_0(\sqrt{u.f(u)})}{u.K_0(\sqrt{u.f(u)}.r_D)}$	$\hat{q}_D(r_D,u)=\frac{K_{\frac{1-n}{3-n}}(\frac{2}{3-n}.\sqrt{u})}{u.r_D^{\frac{1-n}{2}}.K_{\frac{1-n}{3-n}}(\frac{2}{3-n}.\sqrt{u}.r_D^{\frac{3-n}{2}})}$	$\hat{q}_{fD}(r_D,u)=\frac{K_{\frac{1-n}{3-n}}(\frac{2.\sqrt{u.g(u)}}{3-n})}{u.r_D^{\frac{1-n}{2}}.K_{\frac{1-n}{3-n}}(\frac{2.\sqrt{u.g(u)}}{3-n}.r_D^{\frac{3-n}{2}})}$
Dimensionless rate in Laplace domain (Rosalind Archer-Jim Lamber`s procedure)	$q_D(r_D,u)=\frac{r_D}{\sqrt{u}}\frac{K_1(r_D.\sqrt{u})}{K_0(\sqrt{u})}$	$\hat{q}_{fD}(r_D,u)=\frac{r_D.\sqrt{u.f(u)}.K_1[r_D.\sqrt{u.f(u)}]}{u.K_0\left[\sqrt{u.f(u)}\right]}$	$q_D(r_D,u)=\frac{r^{2-n}.K_{\frac{2}{3-n}}(\frac{2.r^{\frac{3-n}{2}}.\sqrt{u}}{3-n})}{u^{0.5}.K_{\frac{n-1}{n-3}}(\frac{2.\sqrt{u}}{3-n})}$	$q_D(r_D,u)=-\frac{(1-n).r^{\frac{1-n}{2}}.K_{\frac{1-n}{3-n}}\left(\frac{2.r^{\frac{3-n}{2}}.\sqrt{u.g(u)}}{3-n}\right)}{2.u.K_{\frac{1-n}{3-n}}\left(\frac{2.\sqrt{u.g(u)}}{3-n}\right)}-\frac{r^{\frac{1-n}{2}+\frac{3-n}{2}}.\sqrt{u.g(u)}.[-K_{\frac{1-n}{3-n}-1}\left(\frac{2.r^{\frac{3-n}{2}}.\sqrt{ug(u)}}{3-n}\right)}{2.u.K_{\frac{1-n}{3-n}}(\frac{2.\sqrt{u.g(u)}}{3-n}}$
Dimensionless rate in real short-time approximation (Rosalind Archer-Jim Lamber`s procedure)	$q_D(r_D,t_D)=\frac{\sqrt{r_D}}{\sqrt{\pi.t_D}}.e^{-\frac{(r_D-1)^2}{4.t_D}}$	$q_D=\frac{\sqrt{\pi}}{\pi}.(\frac{t_D}{\omega})^{-\frac{1}{2}}$	$q_D(r_D,t_D)=\frac{r^{(1.25-0.75n)}.e^{-\frac{(1-r_D^{(1.5-\frac{n}{2})})^2}{(n-3)^2.t_D}}}{\sqrt{\pi}.\sqrt{t_D}}$	---------

Dimensionless rate in real long-time approximation (Rosalind Archer's and Jim Lambers procedure)	---------	$q_D = \frac{2}{\ln t_D + 0.80907}$	$q_D(r_D, t_D) = \frac{(3-n)^{\frac{n+1}{3-n}} . r^{1-n} . t_D^{-\frac{2}{n-3}-1}}{\Gamma(\frac{n-1}{n-3})}$	-----------
Dimensionless accumulation in Laplace domain (Vaneverdingen procedure)	$\hat{Q}_D(r_D, u) = \frac{K_0(\sqrt{u})}{u^2 . K_0(r_D.\sqrt{u})}$	$\hat{Q}_{fD}(r_D, u) = \frac{K_0(\sqrt{u.f(u)})}{u^2 . K_0(\sqrt{u.f(u)}.r_D)}$	$\hat{Q}_D(r_D, u) = \frac{K_{\frac{1-n}{3-n}}(\frac{2}{3-n}.\sqrt{u})}{u^2 . r_D^{\frac{1-n}{2}} . K_{\frac{1-n}{3-n}}(\frac{2}{3-n}.\sqrt{u}.r_D^{\frac{3-n}{2}})}$	$\hat{Q}_{fD}(r_D, u) = \frac{K_{\frac{1-n}{3-n}}(\frac{2.\sqrt{u.g(u)}}{3-n})}{u^2 . r_D^{\frac{1-n}{2}} . K_{\frac{1-n}{3-n}}(\frac{2.\sqrt{u.g(u)}}{3-n}.r_D^{\frac{3-n}{2}})}$
Dimensionless accumulation in Laplace domain (Rosalind Archer's and Jim Lambers procedure)	$Q_D = \frac{r_D}{u^{1.5}} . \frac{K_1(r_D.\sqrt{u})}{K_0(\sqrt{u})}$	$Q_D(r_D, u) = \frac{r_D.\sqrt{u.f(u)}.K_1[r_D.\sqrt{u.f(u)}]}{u^2 . K_0\left[\sqrt{u.f(u)}\right]}$	$Q_D(r_D, u) = \frac{r^{2-n} . K_{\frac{2}{3-n}}(\frac{2.r^{\frac{3-n}{2}}.\sqrt{u}}{3-n})}{u^{1.5} . K_{\frac{n-1}{n-3}}(\frac{2.\sqrt{u}}{3-n})}$	$Q_D(r_D, u) = -\frac{(1-n).r^{\frac{1-n}{2}}.K_{\frac{1-n}{3-n}}\left(\frac{2.r^{\frac{3-n}{2}}.\sqrt{u.g(u)}}{3-n}\right)}{2.u^2.K_{\frac{1-n}{3-n}}\left(\frac{2.\sqrt{u.g(u)}}{3-n}\right)} - \frac{r^{\frac{1-n}{2}+\frac{3-n}{2}}.\sqrt{u.g(u)}.[-K_{\frac{1-n}{3-n}-1}\left(\frac{2.r^{\frac{3-n}{2}}.\sqrt{ug(u)}}{3-n}\right)}{2.u^2.K_{\frac{1-n}{3-n}}(\frac{2.\sqrt{u.g(u)}}{3-n}}$
Dimensionless accumulation in real short-time approximation(Rosalind Archer's and Jim Lambers procedure)	$Q_D(r_D, t_D) = \sqrt{r_D}\{2.\sqrt{\frac{t_D}{\pi}}.e^{-\frac{(r_D-1)^2}{4.t_D}} - (r_D - 1)\mathrm{erfc}(\frac{r_D-1}{2\sqrt{t_D}})\}$	$Q_D = \frac{2\sqrt{\pi}}{\pi}.(\omega t_D)^{\frac{1}{2}}$	$Q_D(r_D, t_D) = -\frac{0.9 . r_D^{2-n}.(r^w - 1).(\frac{1.77245.t_D.\lvert n-3\rvert.1F1}{\lvert r^w}}{\sqrt{3-n}.(n -}$	--------------
Dimensionless accumulation in real long-time approximation (Rosalind Archer's and Jim Lambers procedure)	-----------	------------	$Q_D(r_D, t_D) = \frac{(3-n)^{\frac{n+1}{3-n}} . r^{1-n} . t_D^{-\frac{(5-n)}{n-3}-1} . \Gamma(\frac{}{n}}{\Gamma\left(\frac{n-1}{n-3}\right) . \Gamma(-\frac{5-n}{n-3})}$	----------
Dimensionless Pressure of matrix	$p_D = \frac{(p_i - p)}{p_i - p_w}$	$p_{mD} = \frac{(p_i - p_m)}{\frac{q}{2\pi h)} \frac{\mu_{eff}.B}{k_m}}$	$p_{DNN} = \frac{p - p_i}{(\frac{q}{2\pi h})^n . \frac{\mu_{eff}.r_w^{1-n}}{k_r}}$	$p_{mD} = \frac{(p_i - p_m)}{(\frac{q}{2\pi h})^n \frac{\mu_{eff}.r_w^{1-n}}{k_m}}$
Dimensionless Pressure of fracture	………	$p_{fD} = \frac{2\pi k_f h(p_i - p_f)}{q\mu B}$	……….	$p_{fD} = \frac{k_f(p_i - p_f)}{(\frac{q}{2\pi h})^n \frac{\mu_{eff}.r_w^{1-n}}{k_f}}$
Dimensionless Time	$t_D = \frac{kt}{\Phi\mu c_t r_w^2}$	$t_D = \frac{\mu . r_w^2}{[(\Phi C_t)_m + (\Phi C_t)_f]K_f} . t$	$t_{DNN} = \frac{t}{G.r_w^{3-n}}$ $G = \frac{n\Phi c_t \mu_{eff}}{k_r}(\frac{2\pi h}{q})^{1-n}$	$t_D = \frac{q^{1-n}k_f}{n(\varphi c_t)_t(2\pi h)^{1-n}\mu_{eff} r_w^{3-n}} . t$
Dimensionless rate	$q_D(t_D) = -\left(\frac{\partial p_D}{\partial r_D}\right)_{r_D=1}$	$q_D(t_D) = -\left(\frac{\partial p_D}{\partial r_D}\right)_{r_D=1}$	$q_D(t_D) = -\left(\frac{\partial p_D}{\partial r_D}\right)_{r_D=1} = \frac{q}{q_{ref}} = \frac{q}{2\pi h[\frac{k}{\mu_{eff}.r_w^{1-n}}.\Delta p_{ref}]^{\frac{1}{n}}}$	$q_D = \left[\frac{\mu_{eff}.r_w^{1-n}}{k_f.(2\pi h)^n.(p_i - p)}\right]^{\frac{1}{n}} . q$
Dimensionless radius	$r_D = \frac{r}{r_w}$	$r_D = \frac{r}{r_w}$	$r_D = \frac{r}{r_w}$	$r_D = \frac{r}{r_w}$
Cumulative volume	$Q_D = \int_0^{t_D} q_D . dt_D$	$Q_D = \int_0^{t_D} q_D . dt_D$	$Q_D = \int_0^{t_D} q_D . dt_D = \frac{Q}{Q_{ref}} = \frac{Q}{q_{ref}.t_{ref}} = \frac{Q}{2\pi h^{2-n}.\frac{k}{\mu}^{\frac{1-n}{n}}.q^{n-1}.r_w^{\frac{2n-n^2+1}{2}}.\Delta p}$	$Q_D = \int_0^{t_D} q_D . dt_D$ (Measuring by Trapezoidal rule)
Dimensionless matrix contribution				$D = \frac{q_m}{q} . \frac{2\pi h r_w}{\Delta L^2}$
Storage		$\omega = \frac{(\Phi V)_f}{(\Phi V)_f + (\Phi V)_m}$	$\omega = \frac{(\Phi V)_f}{(\Phi V)_f + (\Phi V)_m}$	$\omega = \frac{(\Phi V)_f}{(\Phi V)_f + (\Phi V)_m}$
Interporosity flow		$\lambda = \alpha\frac{K_m}{K_f}r_w^2$	$\lambda = \alpha\frac{K_m}{K_f}r_w^2$	$\lambda = \alpha\frac{K_m}{K_f}r_w^2$

Table 5.2: Diffusivity-based equations, boundary conditions, and solutions under wellbore constant rate assumption for both NFR and homogenous reservoir (Da Prat, 1990; Dake, 2001; Lee et al., 2003).

Fluid type and reservoir type	Newtonian, homogenous (Lee, John B, & Spivey, 2003)	Newtonian, NFR reservoir (DA PRAT, 1990)	Non-Newtonian, homogenous (Ikoku & Ramey Jr, 1979)	Non-Newtonian, NFR reservoir (Garcia-Pastrana, Valdes-Perez, & Blasingame, 2017)
Dimensionless equation in matrix	$\frac{1}{r_D}\frac{\partial}{\partial r_D}(r_D\frac{\partial p_D}{\partial r_D})=\frac{\partial p_D}{\partial t_D}$	$(1-\omega)\frac{\partial p_{mD}}{\partial t_D}=\lambda(p_{fD}-p_{mD})$	$\frac{\partial^2 p_{DNN}}{\partial r_D^2}+\frac{n}{r_D}\frac{\partial p_{DNN}}{\partial r_D} = r_D^{1-n}\left(\frac{\partial p_{DNN}}{\partial t_{DNN}}\right)$	$\frac{\partial p_{mD}}{\partial t_D}=\frac{n\lambda}{(1-\omega)}.D^{1-n}.(p_{fD}-p_{mD})$
Dimensionless equation in fracture+matrix (total system)	………	$\frac{\partial^2 p_{fD}}{\partial r_D^2}+\frac{1}{r_D}\frac{\partial p_{fD}}{\partial r_D} = \left(\omega\frac{\partial p_{fD}}{\partial t_D}+(1-\omega)\frac{\partial p_{mD}}{\partial t_D}\right)$	………	$\frac{\partial^2 p_{fD}}{\partial r_D^2}+\frac{n}{r_D}\frac{\partial p_{fD}}{\partial r_D}=r_D^{1-n}\left(\omega\frac{\partial p_{fD}}{\partial t_D}+(1-\omega)\frac{\partial p_{mD}}{\partial t_D}\right), t_D>0$
Initial boundary	$P_D(r_D,0)=0$	$p_{mD}(r_{mD},0)=p_{fD}(r_{fD},0)=0$	$p_{DNN}(r_D,0)=0$	$p_{mDNN}(r_{mD},0)=p_{fDNN}(r_{fD},0)=0$
Inner boundary	$(\frac{\partial p_D}{\partial r_D})_{r_D=1}=-1$	$(\frac{\partial p_{fD}}{\partial r_D})_{r_D=1}=-1$	$(\frac{\partial p_{DNN}}{\partial r_D})_{r_D=1}=-1$	$(\frac{\partial p_{fDNN}}{\partial r_D})_{r_D=1}=-1$
Outer boundary	$\lim_{r_D\to\infty} p_D(r_D,t)=0$	$\lim_{r_D\to\infty} p_{DNN}(r_D,t)=0$	$\lim_{r_D\to\infty} p_D(r_D,t)=0$	$\lim_{r_D\to\infty} p_{fDNN}(r_D,t)=0$
Dimensionless equation in matrix in Laplace space	$\frac{1}{r_D}\frac{d}{dr_D}(r_D\frac{dp_D}{dr_D})=up_D$	$\acute{p}_{mD}(r_D,u)=\frac{\lambda}{u.(1-\omega)+\lambda}.\acute{p}_{fD}(r,u)$	$\frac{d^2p_{DNN}}{dr_D^2}+\frac{n}{r_D}\frac{dp_{DNN}}{dr_D}=u.r_D^{1-n}.p_{DNN}$	$\acute{p}_{mD}(r_D,u)=\frac{n\lambda D^{1-n}}{u.(1-\omega)+n\lambda D^{1-n}}.\acute{p}_{fD}(r_D,u)$
Dimensionless equation in fracture+matrix (total system) Laplace space		$\frac{1}{r_D}\frac{d}{dr_D}\left[r_D\frac{d\acute{p}_{fD}(r_D,u)}{dr_D}\right]=u.f(u).\acute{p}_{fD}(r_D,u)$ $f(u)=\frac{\omega(1-\omega)u+\lambda}{(1-\omega)u+\lambda}$		$\frac{d^2\acute{p}_{fD}(r_D,u)}{\partial r_D^2}+\frac{n}{r_D}\frac{d\acute{p}_{fD}(r_D,u)}{dr_D}=r_D^{1-n}[u.g(u).\acute{p}_{fD}(r_D,u)]$ $g(u)=\frac{\omega(1-\omega)u+n\lambda D^{1-n}}{(1-\omega)u+n\lambda D^{1-n}}$
Inner boundary in laplace domain	$(\frac{d\acute{p}_D}{dr_D})_{r_D=1}=-\frac{1}{u}$	$(\frac{d\acute{p}_{fD}}{dr_D})_{r_D=1}=-\frac{1}{u}$	$(\frac{d\acute{p}_{DNN}}{dr_D})_{r_D=1}=-\frac{1}{u}$	$(\frac{d\acute{p}_{fDNN}}{dr_D})_{r_D=1}=-\frac{1}{u}$
Outer boundary in laplace domain	$\lim_{r_D\to\infty}\acute{p}_D(r_D,u)=0$	$\lim_{r_D\to\infty}\acute{p}_{DNN}(r_D,u)=0$	$\lim_{r_D\to\infty}\acute{p}_D(r_D,u)=0$	$\lim_{r_D\to\infty}\acute{p}_{fDNN}(r_D,u)=0$
General solution in laplace domain	$p_D(r_D,u)=I_0(r_D\sqrt{u})+K_0(r_D\sqrt{u})$	$p_{fD}(r_D,u)=AI_0\left(r_D\sqrt{u.f(u)}\right)+BK_0(r_D\sqrt{u.f(u)})$	$p_D(r_D,u)=r_D^{\frac{1-n}{2}}[BI_{\frac{1-n}{3-n}}(\frac{2}{3-n}.\sqrt{u}.r_D^{\frac{3-n}{2}})+CK_{\frac{1-n}{3-n}}(\frac{2}{3-n}.\sqrt{u}.r_D^{\frac{3-n}{2}})]$	$p_{fD}(r_D,u)=r_D^{\frac{1-n}{2}}[C_1I_{\frac{1-n}{3-n}}(\frac{2}{3-n}.\sqrt{u.g(u)}.r_D^{\frac{3-n}{2}})+C_2K_{\frac{1-n}{3-n}}(\frac{2}{3-n}.\sqrt{u.g(u)}.r_D^{\frac{3-n}{2}})]$
Interporosity flow function		$f(u)=\frac{\omega(1-\omega)u+\lambda}{(1-\omega)u+\lambda}$		$g(u)=\frac{\omega(1-\omega)u+n\lambda D^{1-n}}{(1-\omega)u+n\lambda D^{1-n}}$
Solution after imposing boundary condition	$\acute{p}_D(r_D,u)=\frac{K_0(r_D.\sqrt{u})}{u^{1.5}.K_1(\sqrt{u})}$	$\acute{p}_{fD}(r_D,u)=\frac{K_0(\sqrt{u\,f(u)}.r_D)}{u.\sqrt{u.f(u)}.K_1(\sqrt{u.f(u)})}$	$\acute{p}(r_D,u)=\frac{r_D^{\frac{1-n}{2}}.K_{\frac{1-n}{3-n}}(\frac{2}{3-n}.\sqrt{u}.r_D^{\frac{3-n}{2}})}{u^{1.5}.K_{\frac{2}{3-n}}(\frac{2}{3-n}.\sqrt{u})}$	$\acute{p}_{fD}(r_D,u)=\frac{r_D^{\frac{1-n}{2}}.K_{\frac{1-n}{3-n}}((\frac{2.\sqrt{u.g(u)}}{3-n}).r_D^{\frac{3-n}{2}})}{u.\sqrt{u.g(u)}.K_{\frac{2}{3-n}}(\frac{2.\sqrt{u.g(u)}}{3-n})}$
Dimensionless rate in laplace domain (Vaneverdingen procedure)	$q_D(r_D,u)=\frac{1}{u^{0.5}}.\frac{K_0(r_D.\sqrt{u})}{K_1(\sqrt{u})}$	$q_D(r_D,u)=\frac{\sqrt{f(u)}.K_1[\sqrt{u.f(u)}]}{u^{0.5}\{K_0\left[\sqrt{u.f(u)}.r_D\right]\}}$ $f(u)=\frac{\omega(1-\omega)u+\lambda}{(1-\omega)u+\lambda}$	$q_D(r_D,u)=\frac{K_{\frac{2}{3-n}}(\frac{2.\sqrt{u}}{3-n})}{u^{0.5}.r_D^{\frac{1-n}{2}}.K_{\frac{1-n}{3-n}}(\frac{2.\sqrt{u}.r_D^{\frac{3-n}{2}}}{3-n})}$	$q_D(r_D,u)=\frac{\sqrt{g(u)}.K_{\frac{2}{3-n}}[\frac{2.\sqrt{u.g(u)}}{3-n}]}{u^{0.5}.r_D^{\frac{1-n}{2}}.\{K_{\frac{1-n}{3-n}}\left[\frac{2.\sqrt{u.g(u)}}{3-n}.r_D^{\frac{3-n}{2}}\right]\}}$
Dimensionless rate in Laplace domain (Sina procedure)	$q_D(r_D,u)=\frac{r_D}{u}.\frac{K_1(r_D.\sqrt{u})}{K_1(\sqrt{u})}$	$q_D(r_D,u)=\frac{r_D.K_1[r_D.\sqrt{u.f(u)}]}{u.K_1\left[\sqrt{u.f(u)}\right]}$ $f(u)=\frac{\omega(1-\omega)u+\lambda}{(1-\omega)u+\lambda}$	$q_D(r_D,u)=\frac{-1}{2.u^{2.5}.K_{-\frac{2}{n-3}}\left(-\frac{2.\sqrt{u}}{n-3}\right)}.r^{-n}[-($ $-1).u.r^{\frac{n+1}{2}}.K_{\frac{n-1}{n-3}}\left(-\frac{2.r^{1.5-\frac{n}{2}}.\sqrt{u}}{n-3}\right.$ $-r^2.u^{1.5}.K_{\frac{2}{n-3}}\left(-\frac{2.r^{1.5-\frac{n}{2}}.\sqrt{u}}{n-3}\right)$ $-r^2.u^{1.5}.K_{\frac{2(n-2)}{n-3}}(-\frac{2.r^{1.5-\frac{n}{2}}.\sqrt{u}}{n-3})]$	$q_D(r_D,u)=-\frac{(1-n).r^{\frac{1-n}{2}}.K_{\frac{1-n}{3-n}}\left(\frac{2.r^{\frac{3-n}{2}}.\sqrt{u.g(u)}}{3-n}\right)}{2.u.\sqrt{u.g(u)}.K_{\frac{2}{3-n}}\left(\frac{2.\sqrt{u.g(u)}}{3-n}\right)}$ $-\frac{r^{\frac{1-n}{2}+\frac{3-n}{2}}.[-K_{\frac{1-n}{3-n}-1}\left(\frac{2.r^{\frac{3-n}{2}}.\sqrt{ug(u)}}{3-n}\right)-K_{\frac{1-n}{3-n}+1}}{2.u.K_{\frac{2}{3-n}}(\frac{2.\sqrt{u.g(u)}}{3-n})}$

Dimensionless rate in real short-time approximation				
Dimensionless rate in real long-time approximation				
Dimensionless accumulation in Laplace domain (Vaneverdingen procedure)	$Q_D(r_D,u) = \frac{1}{u^{1.5}}.\frac{K_1(\sqrt{u})}{K_0(r_D\sqrt{u})}$	$Q_D(r_D,u) = \frac{\sqrt{f(u)}.K_1[\sqrt{u.f(u)}]}{u^{1.5}\{K_0\left[\sqrt{u.f(u)}.r_D\right]\}}$	$Q_D(r_D,u) = \frac{K_{\frac{2}{3-n}}(\frac{2.\sqrt{u}}{3-n})}{u^{1.5}.r_D^{\frac{1-n}{2}}.K_{\frac{1-n}{3-n}}(\frac{2.\sqrt{u}.r_D^{\frac{3-n}{2}}}{3-n})}$	$Q_D(r_D,u) = \frac{\sqrt{g(u)}.K_{\frac{2}{3-n}}[\frac{2.\sqrt{u.g(u)}}{3-n}]}{u^{1.5}.r_D^{\frac{1-n}{2}}.\{K_{\frac{1-n}{3-n}}\left[\frac{2.\sqrt{u.g(u)}}{3-n}.r_D^{\frac{3-n}{2}}\right]\}}$
Dimensionless accumulation in Laplace domain (Sina procedure)	$Q_D(r_D,u) = \frac{r_D}{u^2}.\frac{K_1(r_D.\sqrt{u})}{K_1(\sqrt{u})}$	$q_D(r_D,u) = \frac{r_D.K_1[r_D.\sqrt{u.f(u)}]}{u^2.K_1\left[\sqrt{u.f(u)}\right]}$	$Q_D(r_D,u) = \frac{-1}{2.u^{3.5}.K_{-\frac{2}{n-3}}\left(-\frac{2.\sqrt{u}}{n-3}\right)}.r^{-n}[-($ $-1).u.r^{\frac{n+1}{2}}.K_{\frac{n-1}{n-3}}\left(-\frac{2.r^{1.5-\frac{n}{2}}.\sqrt{u}}{n-3}\right.$ $-r^2.u^{1.5}.K_{\frac{2}{n-3}}\left(-\frac{2.r^{1.5-\frac{n}{2}}.\sqrt{u}}{n-3}\right)$ $-r^2.u^{1.5}.K_{\frac{2(n-2)}{n-3}}(-\frac{2.r^{1.5-\frac{n}{2}}.\sqrt{u}}{n-3})]$	$Q_D(r_D,u) = -\frac{(1-n).r^{\frac{1-n}{2}}.K_{\frac{1-n}{3-n}}\left(\frac{2.r^{\frac{3-n}{2}}.\sqrt{u.g(u)}}{3-n}\right)}{2.u^2.\sqrt{u.g(u)}.K_{\frac{2}{3-n}}\left(\frac{2.\sqrt{u.g(u)}}{3-n}\right)}$ $-\frac{r^{\frac{1-n}{2}+\frac{3-n}{2}}.[-K_{\frac{1-n}{3-n}-1}\left(\frac{2.r^{\frac{3-n}{2}}.\sqrt{ug(u)}}{3-n}\right)-K_{\frac{1-n}{3-n}+1}}{2.u^2.K_{\frac{2}{3-n}}(\frac{2.\sqrt{u.g(u)}}{3-n})}$
Dimensionless accumulation in real short-time approximation				
Dimensionless accumulation in real long-time approximation				
Dimensionless Pressure of matrix	$p_D = \frac{(p_i-p)}{p_i-p_w}$	$p_{mD} = \frac{2\pi K_m h(p_i-p_m)}{q\mu B}$	$p_{DNN} = \frac{p-p_i}{(\frac{q}{2\pi h})^n.\frac{\mu_{eff}.r_w^{1-n}}{k_r}}$	$p_{mD} = \frac{(2\pi h)^n k_m(p_i-p_m)}{q^n\mu_{eff}r_w^{1-n}}$
Dimensionless Pressure of fracture	………	$p_{fD} = \frac{2\pi k_f h(p_i-p_f)}{q\mu B}$	………	$p_{fD} = \frac{(2\pi h)^n k_f(p_i-p_f)}{q^n\mu_{eff}r_w^{1-n}}$
Dimensionless Time	$t_D = \frac{kt}{\Phi\mu c_t r_w^2}$	$t_D = \frac{\mu.r_w^2}{[(\Phi C_t)_m+(\Phi C_t)_f]K_f}.t$	$t_{DNN} = \frac{t}{G.r_w^{3-n}}$ $G=\frac{n\Phi c_t\mu_{eff}}{k_r}(\frac{2\pi h}{q})^{1-n}$	$t_D = \frac{q^{1-n}k_f}{n(\varphi c_t)_t(2\pi h)^{1-n}\mu_{eff}r_w^{3-n}}.t$
Dimensionless Rate	$q_D(t_D) = -\left(\frac{\partial p_D}{\partial r_D}\right)_{rD=1}$	$q_D(t_D) = -\left(\frac{\partial p_D}{\partial r_D}\right)_{rD=1}$	$q_D(t_D) = -\left(\frac{\partial p_D}{\partial r_D}\right)_{rD=1} = \frac{q}{q_{ref}} = \frac{q}{2\pi h[\frac{k}{\mu_{eff}.r_w^{1-n}}.\Delta p_{ref}]^{\frac{1}{n}}}$	$q_D(t_D) = -\left(\frac{\partial p_D}{\partial r_D}\right)_{rD=1}$
	$r_D = \frac{r}{r_w}$	$r_D = \frac{r}{r_w}$	$r_D = \frac{r}{r_w}$	$r_D = \frac{r}{r_w}$
Cumulative production	$Q_D=\int_0^{t_D} q_D.dt_D$	$Q_D=\int_0^{t_D} q_D.dt_D$	$Q_D = \int_0^{t_D} q_D.dt_D = \frac{Q}{Q_{ref}} = \frac{Q}{q_{ref}.t_{ref}} = \frac{Q}{2\pi h^{2-n}.\frac{k}{\mu}^{\frac{1-n}{n}}.q^{n-1}.r_w^{\frac{2n-n^2+1}{2}}.\Delta P}$	$Q_D=\int_0^{t_D} q_D.dt_D$
Dimensionless matrix contribution				$D = \frac{q_m}{q}.\frac{2\pi h r_w}{\Delta L^2}$
Storage		$\omega = \frac{(\Phi V)_f}{(\Phi V)_f+(\Phi V)_m}$		$\omega = \frac{(\Phi V)_f}{(\Phi V)_f+(\Phi V)_m}$
Interporosity flow		$\lambda = \alpha\frac{K_m}{K_f}r_w^2$		$\lambda = \alpha\frac{K_m}{K_f}r_w^2$

5.2 Quantitative analysis on drilling fluid rate and volume

The dimensionless terms derived and stated, not only measure NFR properties but also quantify drilling fluid rate and volume. It also makes the operator capable of measuring NFR properties (while drilling) by applying a curve-fitting procedure on both rate-time and volume-time graphs. Moreover, this procedure decreases non-productive time by determining NFR properties while drilling.

5.3 Qualitative analysis on drilling fluid rate and volume

This section presents and describes the achievements that result from the evaluated solution model for NFR and the methodological approach proposed in this work. In this regard, type-curves resulting from the solution have been employed to do sensitive analysis on NFR parameters, mud rheology, and wellbore boundary conditions to better understand the mechanism of drilling fluid loss in NFR. The influence of each parameter on drilling fluid rate and volume is investigated and explained below.

5.3.1 Mud rheology and NFR properties influence on leak-off and total loss volume under constant wellbore pressure

The scenario that follows in this study, takes into account the leak-off phenomenon through NFR which is modeled by the evaluated dual-porosity model. The governing evaluated solution leads to the conclusion that NFR characteristics and drilling-fluid rheological properties directly influence the leak-off phenomenon and total loss volume. The following has demonstrated how the leak-off phenomenon affects the drilling fluid rate and total loss volume in NFRs with different reservoir parameters. This section also has demonstrated how drilling-fluid pseudo-plasticity affects the drilling-fluid advancement through NFR at early, transient, and late periods. Additionally, it has demonstrated how operators can control the leak-off phenomenon and total loss volume effectively, by establishing constant pressure inside the wellbore. It should be noted that these four contributing elements can potentially increase the leak-off influence on total loss volume in the earlier times through NFR. How these elements have an impact is discussed in the following sections.

5.3.1.1 Storativity Ratio Impact on Leak-off and Total Loss Volume

The present section illustrates the considerable influence of the relative storage and expansion capacity of fractures and matrix medium (as measured by the storativity ratio parameter), on the short-term deliverability of NFR, as well as the drilling fluid rate and the total loss volume. NFRs with a higher potential to store drilling fluid in the fractured medium, which has a lower storage capacity in the matrix medium, display different drilling fluid rates and volume characteristics compared to those with a greater potential to store drilling fluid in the matrix medium. Sensitive analysis on this parameter and its influence on the drilling fluid rate reveals that the higher the storativity ratio, the dimensionless rate drops abruptly due to the predominant flow of mud through the fractured medium. As NFR with a lower storativity ratio can primarily store drilling fluid through the porous medium, its dimensionless rate occurs at lower values, particularly during the initial times, and its transient period starts earlier and lasts longer. It should be noted, at ω=1 which means all the expansion in the reservoir is attributed to the fracture expansion, transient period disappearing. After t_D=1E1, the total system almost acts as a homogenous system, and the rate of mud advancement decreases equally, due to the existence of a homogenous system. As observed, during the initial times, the mud loss primarily occurred in the fractured medium. For example, for ω=1E-1, the mud loss in fractured medium occurring between t_D=1E-2 to t_D=1E-1, following a transient period that began between t_D=1E-1 to t_D=1E1, and the mud loss inside fractured medium passes through a porous medium. Since equilibrium has been established between fracture and matrix, mud loss has continued to infiltrate through the entire system. The dual porosity model assumes that the matrix has low permeability but a large storage capacity compared to the fractured system, whereas the fractured medium has high permeability but low storage capacity relative to the natural fracture system. Thus, it is imperative to consider the storativity ratio as a parameter that introduces storage capacity and analyzes how it affects total loss volume in NFR while constant pressure is established inside the wellbore. In this regard, sensitivity analysis is performed on this parameter, revealing that increasing the storativity ratio results in greater drilling-fluid storage in the fractured medium and consequently leads to higher cumulative loss at earlier times. In the case of NFR with a lower storativity ratio, a larger quantity of mud can be stored in the matrix medium, leading to reduced drilling-fluid invasion, particularly during the early times. Additionally, the distinction in cumulative loss among various storativity ratios is more pronounced during the early time; however, once t_D=3E1 is surpassed, the mud-loss volume reaches equilibrium for the entire system. Consequently, this factor plays a vital role mainly during the earlier times. Dimensionless cumulative volume can be calculated by measuring the area under each dimensionless rate curve separately by applying the trapezoidal rule for these four different storativity ratios (ω=1E0, ω=1E-1, ω=1E-2, ω=1E-3) to perform sensitivity analysis and observe how this parameter affects cumulative loss volume. This is illustrated in Fig 5.1. Other NFR characteristics held constant during the analysis include λ= 5E-6, n=0.8, and D=1. The dotted line in Fig 5.1 represents the transient period during dimensionless rate and volume for NFR with various storativity ratios.

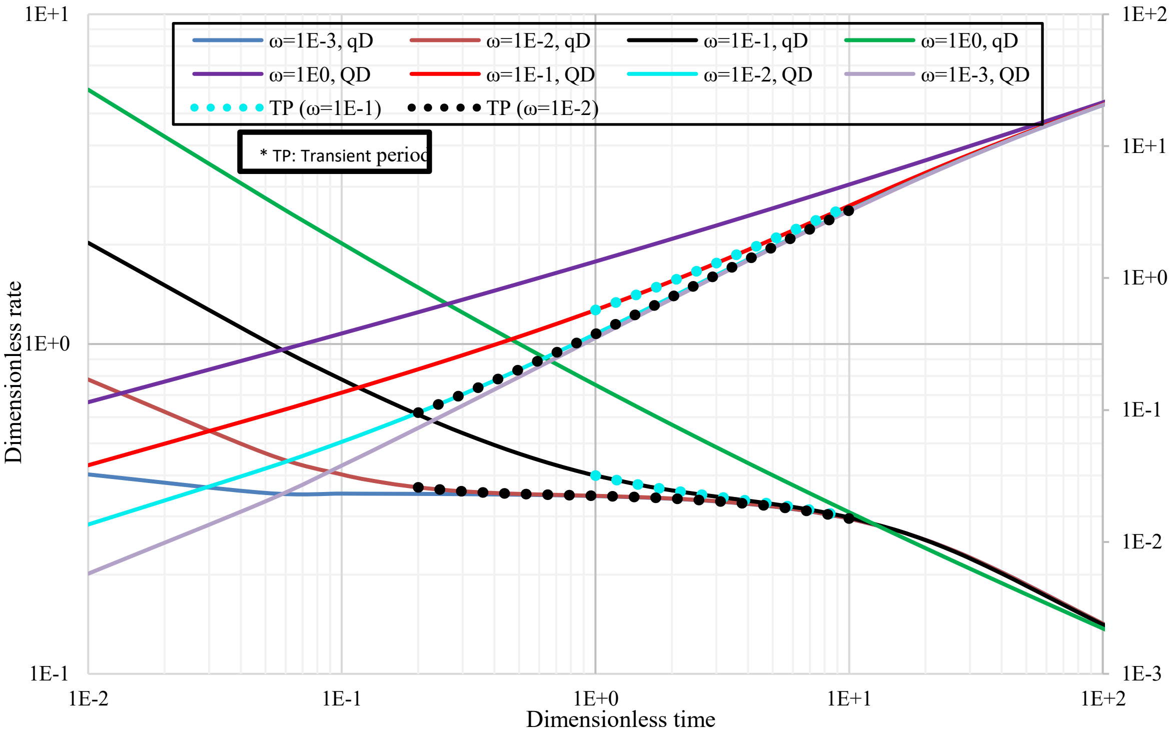

Fig 5.1 Dimensionless rate and volume for NFR with different interporosity flow coefficient.

5.3.1.2 Interporosity Coefficient Impact on Leak-off and Total Loss Volume

In this section, it has investigated how matrix-fracture communication (exchange of mud between the fracture and the matrix systems) affects the leak-off phenomenon and drilling fluid. This is studied under constant wellbore pressure as Non-Newtonian drilling fluid invaded through NFR. Sensitivity analysis is conducted on the inter-porosity flow coefficient, which is an important characteristic of NFR, to observe how the drilling fluid loss rate and volume vary for NFR with different quantities of matrix-fracture communication. The analysis reveals that the higher the matrix-fracture communication, the earlier the transition period begins, resulting in a higher constant drilling fluid rate due to higher acceptance of drilling fluid by matrix medium during this period. After the equilibrium condition is established, a decreasing trend in the dimensionless rate is observed. As an example, when λ=1E-6, the drilling-fluid flows through the fractured medium between t_D=1E-2 and t_D=1E+1, leading to an abrupt decrease in the mud-loss rate. This is followed by a transient period between t_D=1E+1 and t_D=1E4. After the equilibrium condition is established, the decreasing trend in the mud-loss rate in the total system continues. Fig 5.2 depicts the outcome. Subsequently, a sensitivity analysis is performed on the inter-porosity coefficient to evaluate its impact on drilling-fluid volume in NFR. The outcome indicates that an increase in the inter-porosity flow coefficient leads to a sudden surge in the cumulative loss at early times, and there is a significant increase in mud advancement during the transition period. As an example, in the case of NFR with an inter-porosity flow coefficient of 1E-3, the amount of drilling mud invaded between t_D=1E-2 and t_D=5E-2 shows a significant increase (higher slope) compared to later times (t_D=5E-2). Therefore, it can be observed that due to the earlier onset of the transition period, the loss volume increases more substantially for NFRs with a higher inter-porosity flow coefficient than for those with a lower coefficient. The dotted line in Fig 5.2 shows the transient period for the dimensionless rate and volume of NFR with different inter-porosity coefficient factors. Other parameters, including ω=1E-3, n=0.1, and D=1E3, are kept constant.

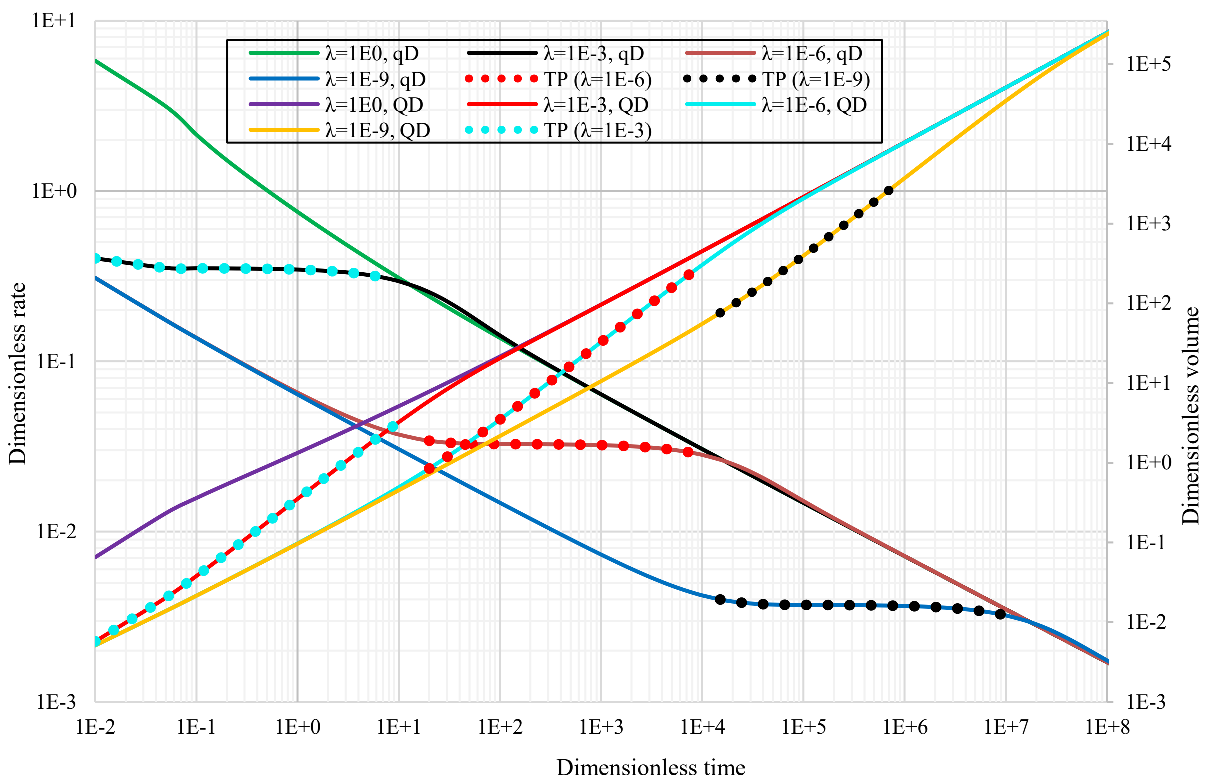

Fig 5.2 Dimensionless rate and volume for NFR with different interporosity flow coefficients.

5.3.1.3 Dimensionless Matrix Contribution Impact on Leak-off and Mud-Loss Phenomenon

The influence of Non-Newtonian inter-porosity transfer function (described by dimensionless Matrix contribution) on the leak-off phenomenon, drilling fluid rate, and volume during different periods have been studied in this section. The other three reservoir parameters are held constant to examine the effect of dimensionless matrix contribution on total loss volume. A sensitivity analysis is conducted on the dimensionless matrix contribution and its effect on the drilling fluid rate. The result shows that NFR with higher dimensionless matrix contribution experienced a transient period at earlier times compared to those with lower contributions. This is due to a higher rate of drilling-fluid invasion into the matrix medium, as the matrix medium accepted the drilling fluid with higher quantities. It should be noted that during the transition period in which the fracture supplies the matrix, a higher dimensionless matrix contribution results in the earlier drilling-fluid invasion from the fracture into the matrix medium, causing the drilling fluid rate to not decrease abruptly and remain high for a longer duration. As a consequence, the drilling fluid invades the fractured medium at higher rates during the transition period. As illustrated in Fig 5.3, for NFR with D=1E3, the mud invasion through the fractured medium exhibits a sharp decreasing trend between t_D=1E-2 and t_D=5E-2, followed by a constant rate of mud loss due to the transition zone between t_D=5E-2 and t_D=1E1. After t_D=1E1, the mud-loss incident continues in the entire system as the equilibrium condition is established. In summary, the higher the Non-Newtonian inter-porosity transfer function, the higher the NFR susceptibility to severe losses. This underscores the importance of monitoring mud rheology during each drilling period to manage or reduce loss to an acceptable level.

In the case of cumulative loss, it has been investigated how dimensionless matrix contribution affects total loss volume under the mentioned assumption. As previously stated, the higher the dimensionless matrix contribution factor, the earlier the transient period begins, resulting in a greater quantity of drilling fluid invading the matrix medium and total system. As a result, the mud-loss volume is higher for greater dimensionless matrix contribution. The reason is that the matrix system accepts greater mud quantities (higher qm). The total loss volume for NFR with different dimensionless matrix contributions shows a significant difference at earlier times, indicating the sensitivity of the dimensionless matrix contribution factor during this period. However, this difference gradually decreases and vanishes after t_D=1E4 when the mud-loss behavior becomes similar in the total system. This suggests that the dimensionless matrix contribution factor plays a crucial role in controlling early mud losses. As depicted in Fig 5.3, for NFR with D=1E3, the drilling fluid loss occurred mainly in the fractured system during the early times (1E-2<t_D<5E-2). Then, the loss volume increases intensively due to the onset of the transient period and the mud invasion from the fracture into the matrix medium (5E-2<t_D<1E1). Finally, the drilling fluid loss invades the entire system at t_D>1E1. The dotted line in Fig 5.3 shows the transient period of dimensionless rate and volume for NFR with varying dimensionless matrix contributions. It is important to note that λ=1E-3, ω=1E-3, and n=1E-1 are constant parameters in this analysis.

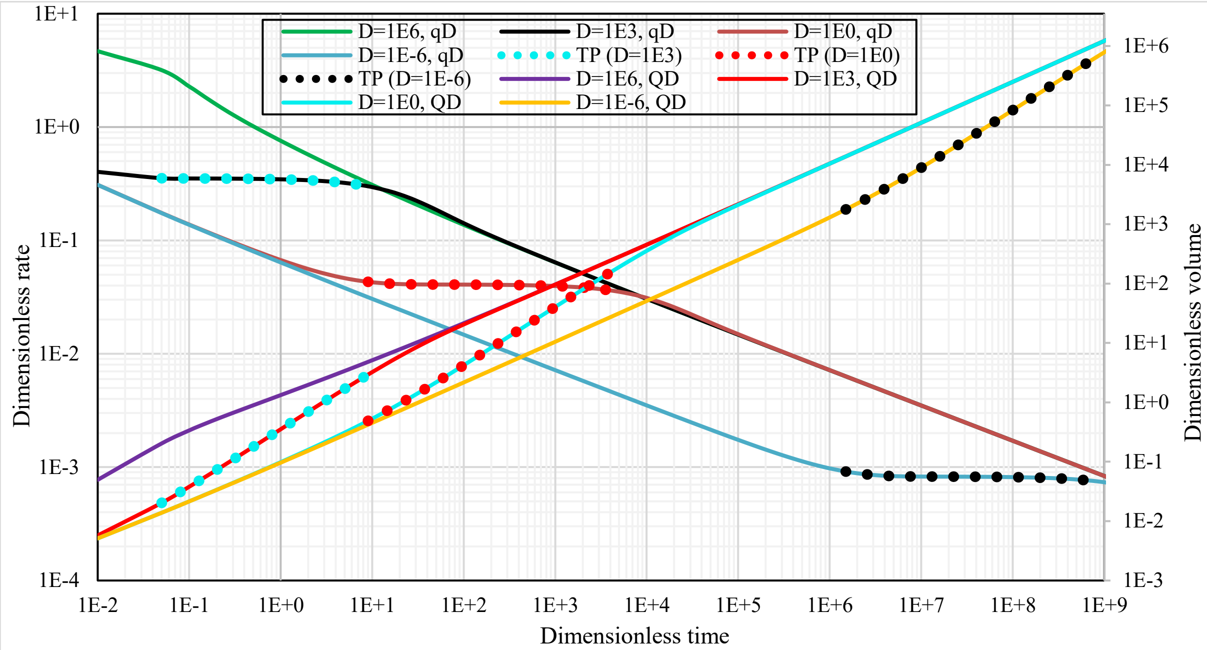

Fig 5.3 Dimensionless rate and volume for NFR with different dimensionless matrix contributions.

5.3.1.4 Drilling-Fluid Rheology Impact on Leak-off and Total Loss Volume

Depending on the pseudo-plasticity of the drilling fluid, dimensionless rate, and volume are varied for each case through NFR while the inner constant pressure assumption is considered inside the wellbore. The sensitivity analysis of drilling-fluid pseudo-plasticity and its effect on drilling fluid rate and total cumulative volume can be separated into three distinct periods. The results show that drilling fluids with greater pseudo-plastic behavior led to a slower reduction of dimensionless rate during early times (in this case, $t_D < 2E\text{-}2$). This is because the high velocity of drilling fluid flowing through the fracture decreases the viscosity of Non-Newtonian drilling fluid due to the relationship between shear rate and viscosity in pseudo-plastic fluids. As a result, the changes in dimensionless rate are minimal. In other words, the decreasing trend in dimensionless rate is less pronounced for pseudo-plastic drilling fluids than for Newtonian fluids when passing through a fractured system. Despite a sudden decrease in the drilling fluid rate through a fractured medium for drilling fluids with lower pseudo-plasticity, the total drilling fluid loss remains higher during early times due to greater invasion of drilling fluid at the start. Therefore, for drilling fluids with high pseudo-plasticity, the rate of invasion decreases significantly during earlier times. Fig 5.4 depicts the outcome. During the transient period (in this case, 3E-2 < t_D < 1E3), the dimensionless rate increases with higher pseudo-plasticity (lower n) of the drilling fluid. This is because higher pseudo-plasticity drilling fluids experience a significant decrease in viscosity during a mud-loss exchange between the fracture and matrix medium. Therefore, drilling fluid inside fracture medium invades through matrix medium at a higher rate (because the mud with higher pseudo-plasticity is highly sensitive to velocity and its viscosity decreases abruptly compared to Newtonian-mud type). As a result, the dimensionless rate remains at maximum points for drilling fluids with high pseudo-plasticity. As shown in Fig 5.4, drilling fluid with higher pseudo-plasticity experienced less change in dimensionless rate and maintained a lower viscosity during the transient period. It also reveals that the transient period for drilling fluid with higher pseudo-plasticity is shorter and terminates earlier but at a higher rate, leading to a higher loss volume of drilling fluid compared to the lower pseudo-plasticity fluid during the transient period. While minimizing the transient period is important, it is preferable to use a drilling fluid that maintains its pseudo-plasticity at a lower level temporarily during this period, resulting in a lower drilling fluid rate. At late times, once the matrix and fracture system reaches equilibrium, the dimensionless rate for drilling fluid with higher pseudo-plasticity decreases more rapidly than that of a Newtonian fluid. Therefore, after the transient period, the trend changes abruptly. After this period, the viscosity of pseudo-plastic drilling fluid increases significantly due to the saturation of the matrix medium with drilling fluid and the establishment of an equilibrium condition. Consequently, the velocity of the fluid decreases, leading to a sharp decline in the dimensionless rate for drilling fluid with this type of rheology.

The effect of drilling fluid pseudo-plasticity on cumulative mud loss can be classified into three categories: early time, transition period, and late time. Fig 5.4 illustrates that at early times (in this case, t_D < 2E-1), the dimensionless rate decreases sharply for drilling fluid with lower pseudo-plasticity, while the cumulative loss remains higher. As mentioned earlier, during the transition period, drilling fluid with higher pseudo-plasticity exhibits a higher invasion rate into the matrix system, leading to increased loss volume for mud with this rheology. During late times, the equilibrium condition is established in the total system (matrix+fracture), causing a shift in the trend of drilling fluid volume. The decrease in volume for the case with higher pseudo-plasticity is more abrupt than for the lower one. Furthermore, the effect of drilling fluid pseudo-plasticity on the overall system is considerably distinguishable during the late times compared to other periods. The dotted line in Fig 5.4 indicates the transient period of dimensionless rate and volume for drilling fluid with different pseudo-plasticity. In this section, we assume that λ=1E-3, ω=1E-3, and D=1E3 remain constant.

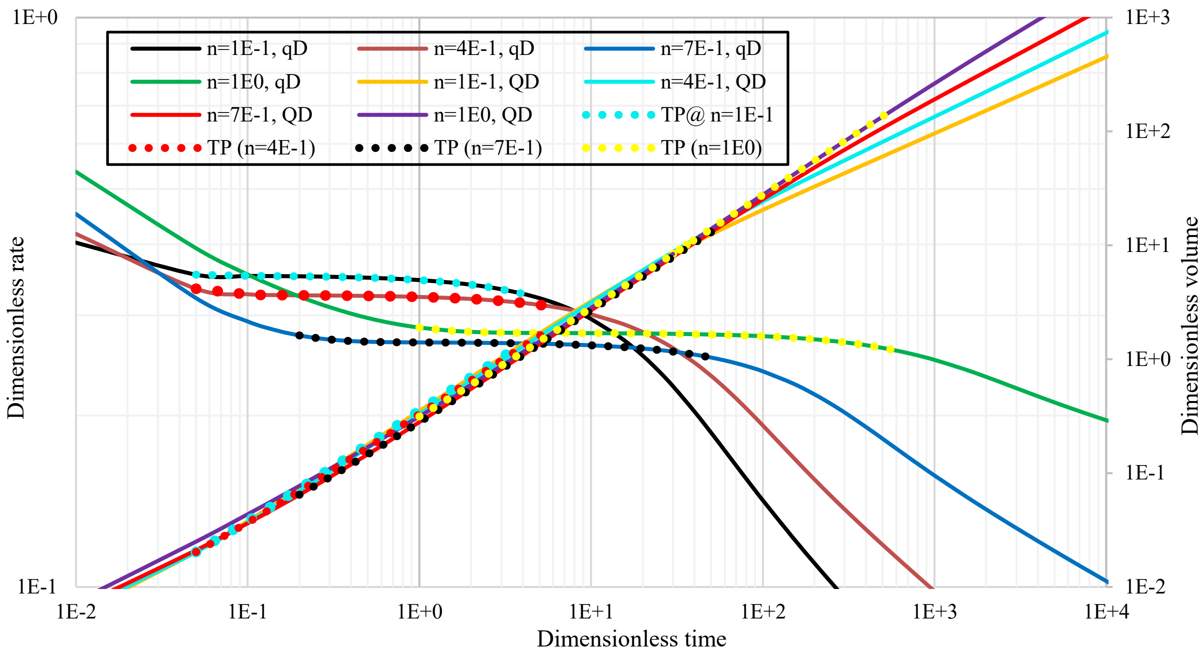

Fig 5.4 Dimensionless rate and volume for different drilling-fluid pseudo-plasticity through NFR.

5.3.2 Simultaneous Influence of Mud Rheology and Dimensionless Matrix Contribution on Total Loss Volume

This section presents a comprehensive investigation of the simultaneous effects of the Non-Newtonian inter-porosity transfer function and drilling-fluid pseudo-plasticity on mud-loss rate and volume. In this regard, NFRs with four different Non-Newtonian inter-porosity transfer functions are subjected to drilling fluid with varying pseudo-plasticity (achieved by adjusting the flow behavior index from n=0.1 to n=1) to assess how these critical reservoirs and drilling-fluid parameters interact and impact drilling fluid rate and volume. An infinite-acting reservoir is considered an outer boundary condition. The findings reveal that a decrease in drilling-fluid pseudo-plasticity leads to a more uniform drilling fluid rate across NFRs with different Non-Newtonian inter-porosity transfer functions (the impact of the Non-Newtonian inter-porosity transfer function on the dimensionless rate is more pronounced in the presence of a higher pseudo-plastic-drilling fluid). This is supported by the observed similarity in the dimensionless rate versus dimensionless time graphs illustrated in Fig 5.5. The results indicate that the transient period duration is shorter for drilling fluids with higher pseudo-plasticity. This can be attributed to the rapid decrease in drilling-fluid viscosity during invasion through the matrix medium at a higher rate, leading to a faster establishment of the equilibrium between the matrix and fractured medium. Furthermore, for NFRs with similar Non-Newtonian inter-porosity transfer functions, the onset of the transient period occurs earlier for drilling fluids with higher pseudo-plasticity, while the duration of this period shortens. In the mud-loss phenomenon, the worst-case scenario may arise for NFRs with a higher dimensionless matrix contribution. This is due to the transient period occurring at earlier times and higher rates, leading to an increased growth rate of mud loss. Fig 5.5 illustrates the transient period of the dimensionless rate for both scenarios, which is represented by the dotted line. The parameters λ=1E-3 and ω=1E-3 are held constant.

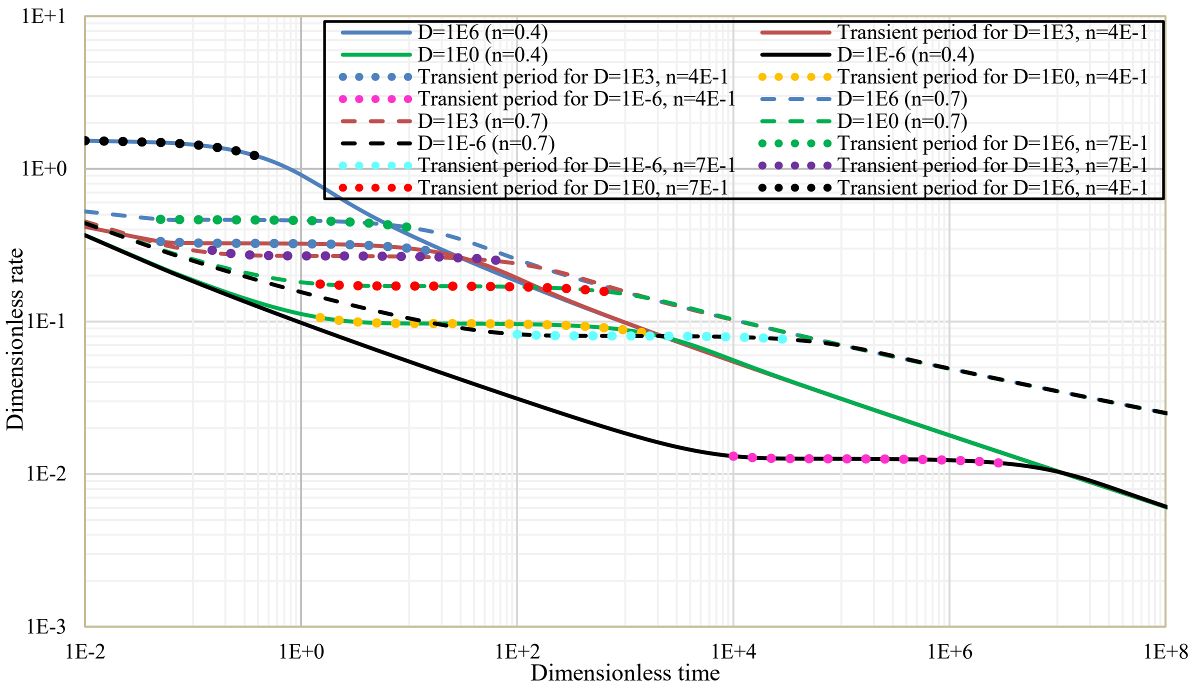

Fig 5.5 Dimensionless rate while considering both dimensionless matrix contribution and mud pseudo-plasticity.

Subsequently, the combined impact of drilling-fluid pseudo-plasticity and Non-Newtonian inter-porosity transfer function on drilling fluid volume is analyzed. The results demonstrate that an increase in drilling-fluid pseudo-plasticity leads to a decrease in total drilling fluid loss volume, attributable to the shortened transient period. Additionally, the drilling fluid with higher pseudo-plasticity experiences transient periods at lower rates and concludes the period earlier, which results in a lower cumulative loss. When both of these parameters are taken into account, the cumulative loss reaches its minimum since the drilling fluid has higher pseudo-plasticity, and the NFR has a lower dimensionless matrix contribution. Under such circumstances, the dimensionless rate exhibits a sudden decrease, while the transient period occurs with a delay at lower rates. In the case of two NFRs having equal Non-Newtonian inter-porosity transfer function, the total loss volume is greater for mud with higher pseudo-plasticity during the transient period due to the earlier start of this period at a higher rate. However, once the equilibrium situation is achieved in the matrix-fracture system, cumulative loss becomes similar for all cases. The dotted line in Figs 5.6 and 5.7 illustrates the transient period during dimensionless volume for both scenarios. The parameters λ=1E-3 and ω=1E-3 are held constant in these figures.

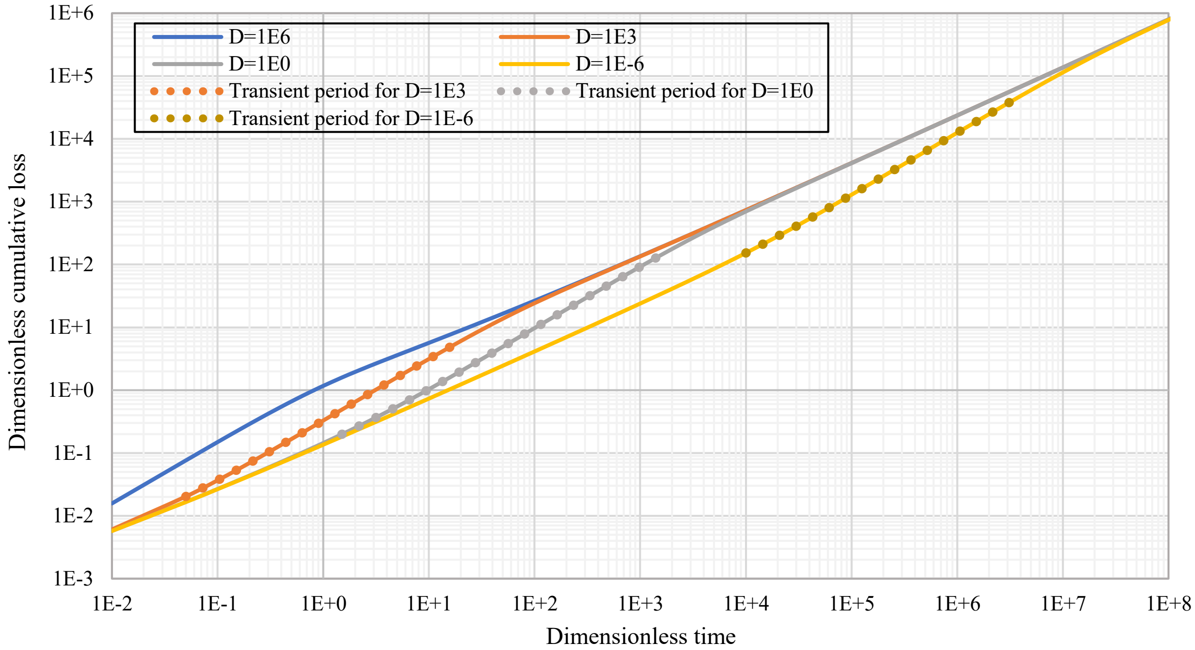

Fig 5.6 Dimensionless cumulative loss for various dimensionless matrix contribution and n= 4E-1.

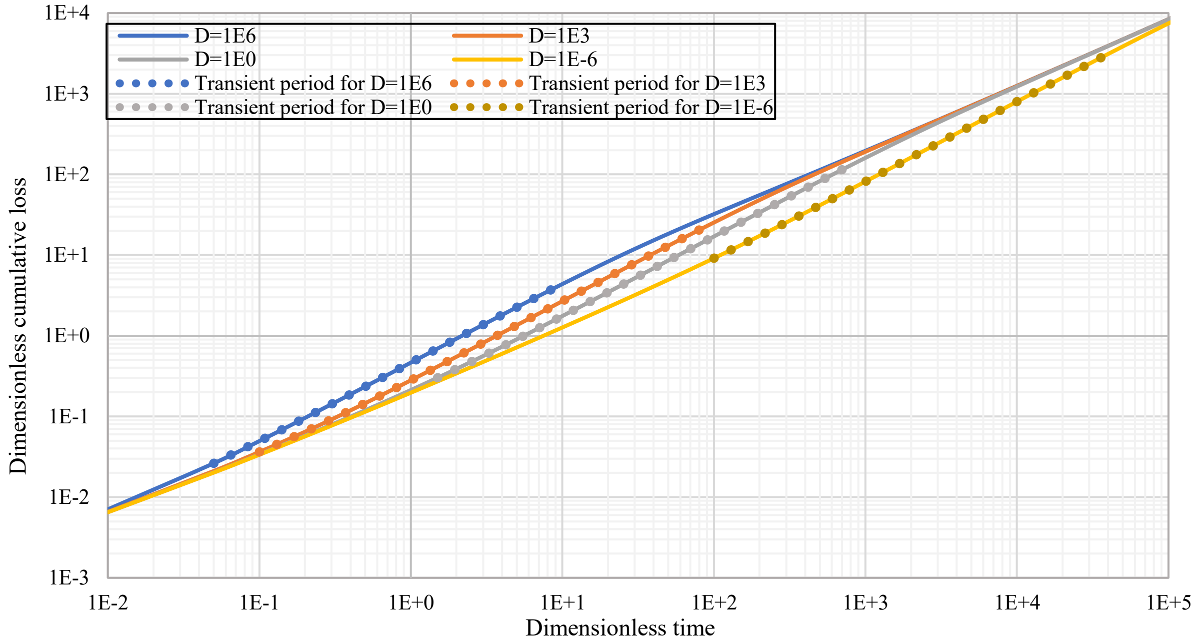

Fig 5.7 Dimensionless cumulative loss for various dimensionless matrix contribution and n= 7E-1.

5.3.3 Wellbore Boundary Impact on Mud Loss

The influence of the wellbore boundary conditions on the total loss volume is undeniable. Therefore, a sensitivity analysis is conducted on the characteristics of NFR and the rheology of drilling fluid, using dimensionless parameters such as storativity ratio, inter-porosity flow coefficient, dimensionless matrix contribution, and flow behavior index. The analysis is performed under two different wellbore boundary conditions (constant pressure and constant rate). The evaluated dual-porosity model under constant rate assumption proposed by Garcia-Pastrana et al. (2017) compared with the presented results. The comparison shows that, while the constant rate assumption established inside the wellbore, reservoir and drilling-fluid characteristics do not significantly affect the leak-off phenomenon, drilling fluid rate, and total loss volume. However, the presented solution reveals that while constant pressure is established inside the wellbore (as the main assumption to solve the general solution), it significantly impacts the drilling fluid rate and total loss volume. Therefore, under this assumption, effective management of the leak-off phenomenon and total loss volume can be achieved. Additionally, in the case of a differential pressure inside the wellbore, it is confirmed that a higher wellbore differential pressure results in a greater drilling fluid rate. This underscores the significance of drilling-fluid rheology in reducing the total cumulative loss volume, particularly under wellbore constant pressure conditions.

5.3.4 Categorization of drilling fluid rate and total loss volume

The drilling fluid rate and volume can be categorized under two distinct criteria: the severity of the drilling fluid and the period time of mud loss. This is an aspect that has been neglected in previous studies on drilling fluid loss. To elucidate this point, the rate and loss of drilling fluid are measured through a specific field case, and categorization is applied to this case. This process is detailed in the methodology section of the thesis (see Fig 4.5 and Fig 4.7). The purpose of this categorization is to better characterize the mud loss incident and to facilitate the mitigation of further loss in each scenario, especially during earlier times.

5.3.5 Dimensionless rate and volume through homogenous and NFR under wellbore constant pressure conditions while comparing cases

In this study, sensitive analysis on drilling fluid loss and volume is done by two procedures.

Primarily, sensitive analysis on dimensionless rate and volume for NFR with different properties and drilling-fluid parameters such as relative storage and expansion capacity, matrix-fracture communication, mud pseudo-plasticity, and Non-Newtonian inter-porosity transfer function to observe how they affect total loss volume.

Secondly, sensitive analysis on drilling fluid loss and volume in real-time after converting the dimensionless parameters to real-time (while converting it to be applicable for field data), by this procedure, it is possible to do sensitive analysis on both previous reservoir parameters plus fracture permeability and storativity as well as total storativity.

In the two above procedures, the influence of these parameters is observable in two ways, measuring the surface under a drilling fluid volume of each case (By Trapezoidal rule) or directly applying the introduced evaluated drilling fluid volume equation (solving by MATLAB).

In this study, procedure one has been applied to do a sensitive analysis to facilitate the process. While drilling fluid loss advances through NFR and homogenous reservoirs, the mud-loss rate decreases for all types of drilling fluid with different pseudo-plasticity.

In the case of a homogenous reservoir, as Fig 5.8 shows, the dimensionless rate declines rapidly for mud type with higher pseudo-plasticity in comparison with Newtonian one; the difference appears clearly after $t_D>1$. Moreover, the influence of pseudo-plasticity on the drilling fluid rate is more obvious when inner-constant pressure is established inside the wellbore than the inner-constant rate. Therefore, under this assumption, increasing mud pseudo-plasticity can effectively remedy loss volume. Figs. 5.8 and 5.9 show, how mud pseudo-plasticity affects the dimensionless drilling fluid rate and cumulative loss through homogenous reservoirs. In this regard, dimensionless rates for six types of mud with different pseudo-plasticity have been considered.

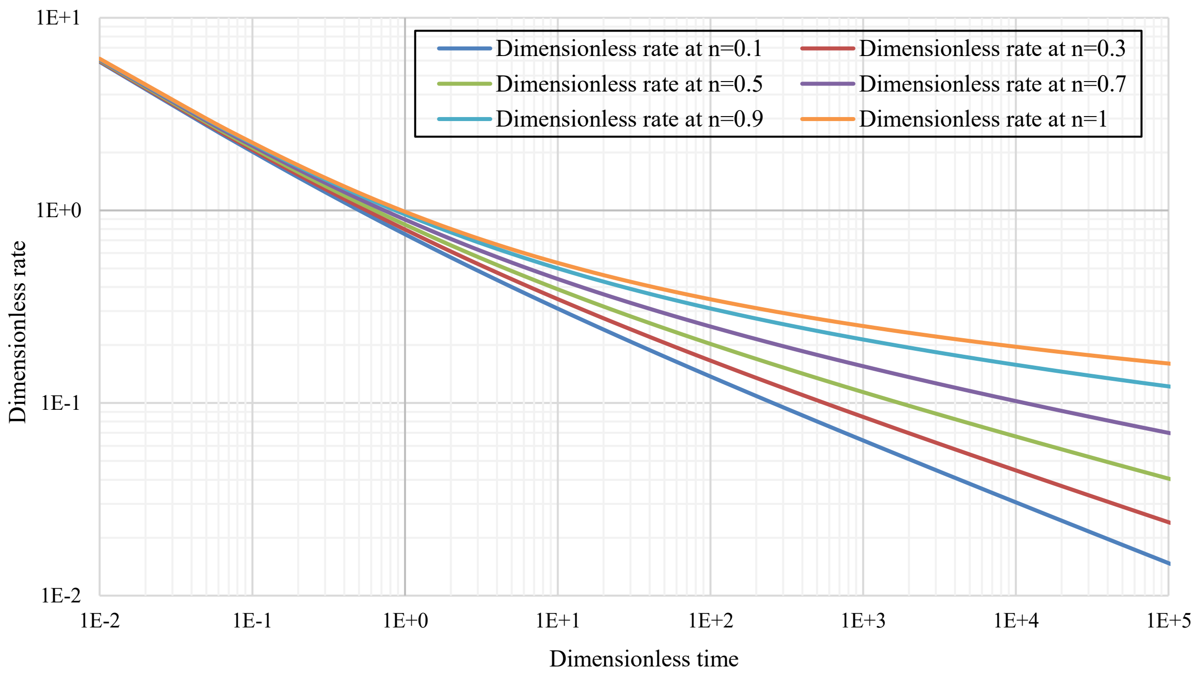

Fig 5.8 Influence of flow behavior index on dimensionless rate through homogenous reservoir under inner-constant pressure boundary.

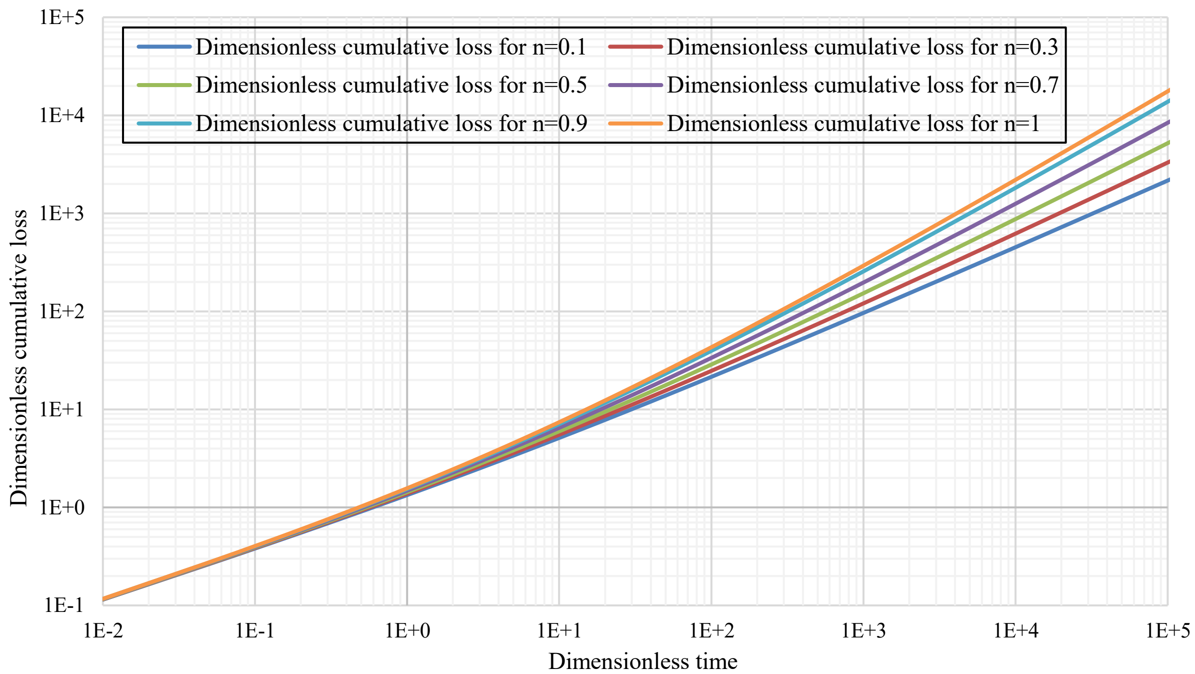

Fig 5.9 Influence of flow behavior index on dimensionless cumulative loss through homogenous reservoir under inner constant pressure boundary.

In the case of NFR, at short times, the flow behavior index does not affect the dimensionless rate of mud invasion considerably, but it becomes noticeable after $t_D = 10$, which shows since the fluid becomes more pseudo-plastic, the drilling fluid rate in a formation decreases dramatically for a higher flow behavior index (Fig 5.10), the reason is that while mud advancement occurs through fractured-medium, the velocity of mud with higher pseudo-plasticity decreases quickly, resulting in a sharp increase in viscosity, which it intensified decreasing mud-loss volume; therefore, as can be seen at Figs 5.10 and 5.11, the higher the drilling-fluid pseudo-plasticity, the lower the dimensionless rate and volume experienced.

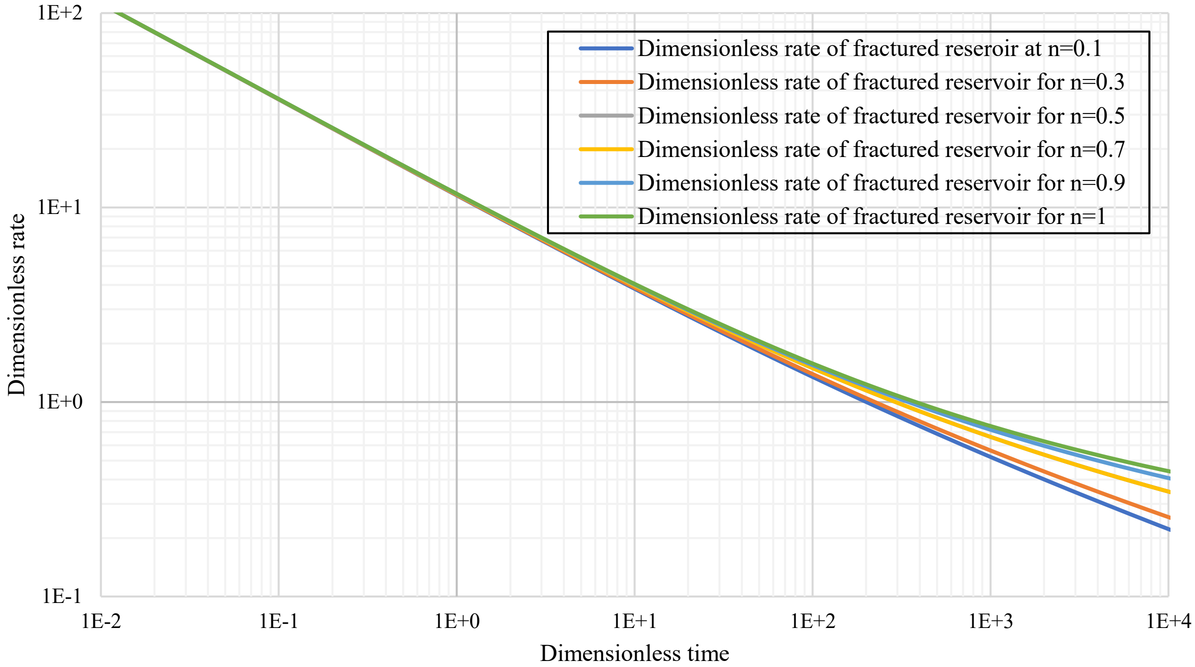

Fig 5.10 Influence of flow behavior index on dimensionless rate through NFR under inner-constant pressure boundary.

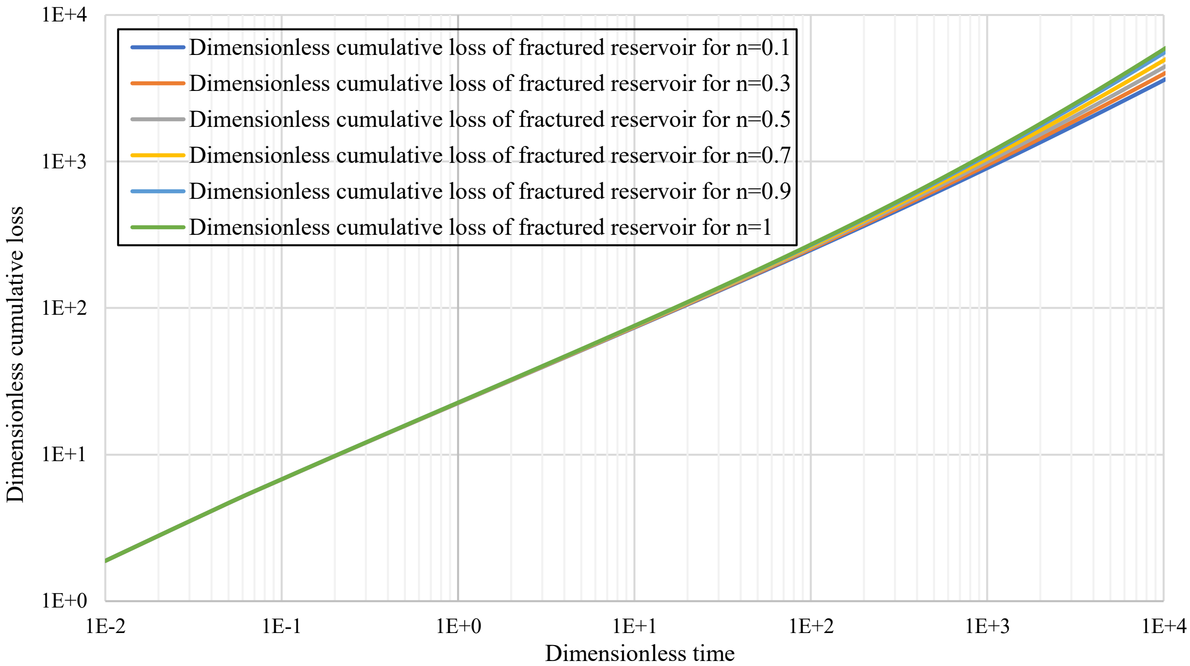

Fig 5.11 Influence of flow behavior index on dimensionless rate through NFR under inner-constant pressure boundary.

5.3.5.1 Pseudo-plasticity influence on loss rate and volume through NFR and homogenous reservoir

This part shows how drilling-fluid pseudo-plasticity affects drilling fluid rate and loss volume on two different types of reservoirs. As it cleared, the rate of drilling-fluid advancement is higher at earlier times through NFR than homogenous reservoir due to the easiness of drilling-fluid advancement through fractured-medium. As can be seen in Fig 5.12, the dimensionless rate experienced a sharp change between t_D=0.01 and t_D=100 through NFR; after t_D=1E2 the dimensionless rate for both reservoir types became almost similar (decreasing rate) due to the homogeneity of both systems after this period. In the case of cumulative drilling-loss volume, it increases intensively at earlier times in NFR than the homogenous one; in this regard, the dimensionless loss volume through NFR increases rapidly after t_D>1E2 while it happens after t_D>1E3 for the homogenous reservoir. The assumption considered is (ω= 4E2; λ= 1E-5; D=1E-4; n=0.1).

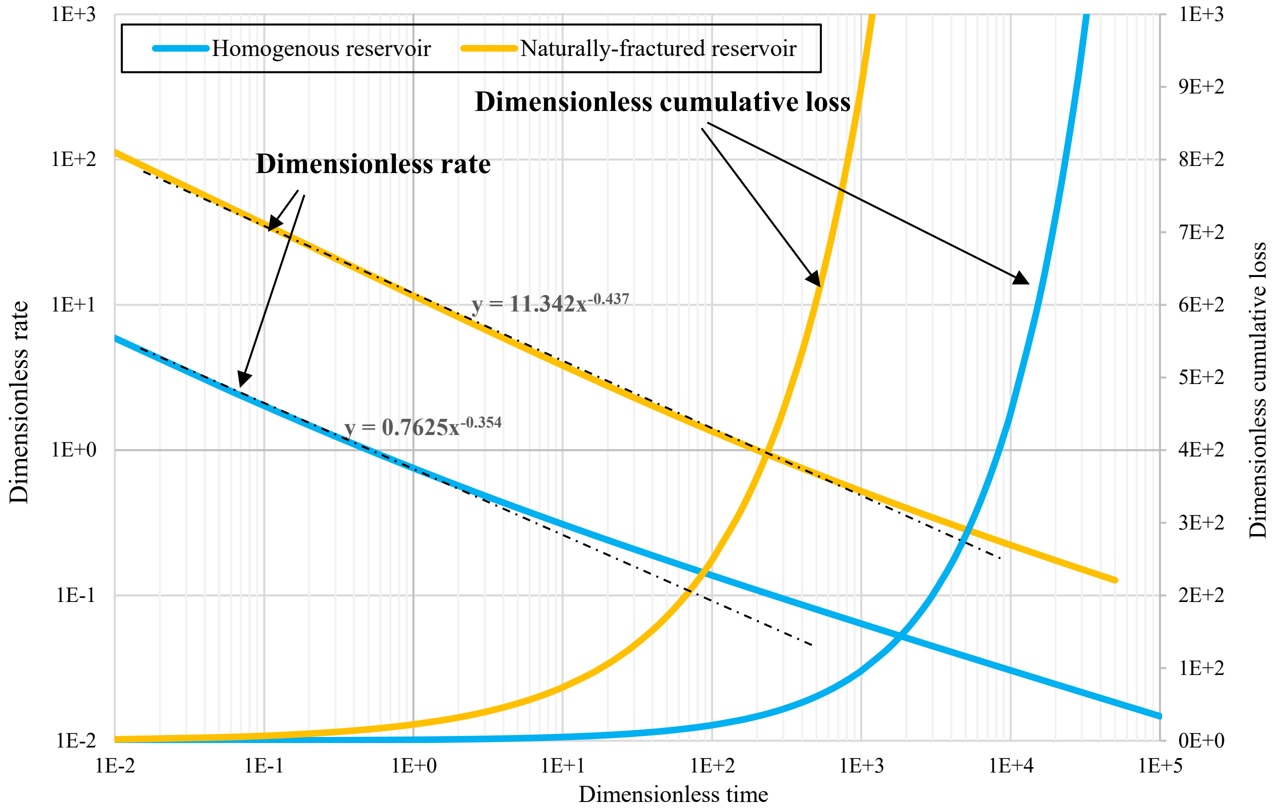

Fig 5.12 Dimensionless rate and cumulative volume through homogenous and NFR.

6 CONCLUSIONS

In this research, we propose a comprehensive and evaluated solution, advancing the estimation accuracy of fluid losses through NFRs, and thereby improving upon existing models. This solution considers the leak-off phenomenon and an inter-porosity transfer model that encapsulates the Non-Newtonian effects resulting from the interaction between the fracture and the matrix. The application of generated type-curves aims to facilitate quantitative and qualitative analysis while maintaining the complexity inherent in NFR cases. The significant outcomes from this study can be summarized as follows:

- NFR properties and mud pseudo-plasticity significantly affect the drilling-fluid rate, total loss volume, and leak-off phenomenon. When constant pressure is maintained inside the wellbore, these factors can be effectively controlled, enabling the operator to utilize drilling-fluid pseudo-plasticity as a tool to mitigate volume loss.
- Drilling-fluid pseudo-plasticity can be utilized as a tool to manage transient periods and leak-offs during drilling operations. The impact of drilling-fluid rheology on total loss volume is more pronounced for NFRs with higher leak-offs than for those with lower leak-off. Furthermore, the significance of mud rheology becomes more prominent under higher differential pressure conditions inside the wellbore compared to lower pressure conditions.
- A higher relative storage and expansion capacity of the fracture-to-matrix system leads to an earlier transient period and increased drilling-fluid invasion through the fractured medium. Applying drilling fluid with higher pseudo-plasticity is considered an effective procedure in mitigating further loss during earlier times.
- For NFRs with specific Non-Newtonian inter-porosity transfer functions, the relationship between mud pseudo-plasticity and the transient period's duration is inversely proportional, an increase in mud pseudo-plasticity results in a shorter transient period, initiating earlier. Furthermore, a sensitive analysis of the Non-Newtonian inter-porosity transfer function uncovers that the influence of this function on the drilling fluid rate becomes increasingly discernible as the pseudo-plasticity of the drilling fluid increases.
- An increase in the Non-Newtonian inter-porosity transfer function, indicative of enhanced matrix-fracture communication, results in an earlier occurrence of the transient period at higher rates. This in turn leads to an increase in the volume of drilling fluid loss.
- Total drilling fluid loss volume can be investigated during three distinct periods. During the early hours, despite the drilling-fluid rate through the fractured medium abruptly decreasing

for mud with lower pseudo-plasticity, the total mud loss remains higher (due to greater mud invasion at early times). Consequently, drilling fluid with higher pseudo-plasticity is deemed a more appropriate option for mitigating mud loss during this period. During the transient period, although this period is shorter when we use mud with higher pseudo-plasticity, using such mud resulted in a higher total loss volume. This increase in loss volume is attributed to the higher drilling fluid rate during this period when compared to using mud with lower pseudo-plasticity. At late times, drilling fluid with higher pseudo-plasticity experienced a sharp decrease in dimensionless rate when compared to drilling fluid with lower pseudo-plasticity. This led to a notable decrease in cumulative loss volume after the termination of the transient period. Overall, it is recommended to utilize a drilling fluid with a specific pseudo-plasticity during each stage of drilling to effectively mitigate further loss at earlier times.

- In all cases of NFRs, it is advised to implement a procedure that diminishes the transient period while simultaneously maintaining a lower rate of mud advancement. This strategy should be complemented by a tailored design of the drilling fluid, ensuring it sustains higher pseudo-plasticity during the early and late stages and exhibits reduced pseudo-plasticity during the transient period.
- When the pseudo-plasticity of the drilling fluid is maintained constant, an increase in the Non-Newtonian inter-porosity transfer function is found to elevate the volume of mud loss. This rise can be attributed to the transient period occurring at higher rates and starting at earlier times. These two factors intensify the total cumulative loss, especially in the early stages of the process.
- While the rate of drilling-fluid flow through the fractured medium decreases notably for mud with lower pseudo-plasticity, an increase in total mud loss is recorded during the early stages. This surge in loss can be chiefly attributed to the amplified invasion of mud at the onset of the mud-loss phenomenon.
- The workflow introduced in this study facilitates decision-making processes, enabling the measurement of NFR properties and the projection of decline curves for Non-Newtonian drilling fluid under various scenarios.
- The larger the differential pressure inside the wellbore, the greater the importance of mud rheology in mitigating loss volume.
- The significance of drilling-fluid rheology becomes particularly pronounced in NFRs with larger fracture apertures, highlighting its crucial role in managing fluid losses and reservoir

behavior. This underscores the importance of accurate rheological characterization in drilling operations, especially in reservoirs with substantial fracture apertures.

- The impact of Non-Newtonian fluid properties on ROI is more readily discernible at earlier stages in NFRs with higher leak-off rates. Consequently, this parameter demonstrates an accelerated increase in NFRs with a larger inter-porosity flow parameter, underscoring the crucial interplay between fluid properties and reservoir behavior.
- The current model, designed primarily for pseudoplastic fluid types, inherently limits its application to a narrow range of Non-Newtonian drilling fluids. Moreover, not incorporating the effect of reservoir fluids on drilling fluid invasion constrains the model's capability in accurately predicting mud loss rates, volumes, and NFR parameters in various drilling fluid loss scenarios.

7 RECOMMENDATIONS FOR FUTURE WORK

The limitation of this approach is that it might not accurately predict the performance of other types of drilling fluids. For future work, it is recommended to extend the applicability of the model to various drilling fluids. This could be achieved by deriving a specific rheological model for each drilling fluid. Once the rheological model is derived, it can be integrated into the COMSOL program. The COMSOL program, coupled with the double-porosity model, will enable the accurate measurement of the drilling fluid loss volume for different types of drilling fluids. This expanded scope of analysis will contribute to a more comprehensive understanding of fluid dynamics in drilling operations.

REFERENCES

Abbasi, M., Izadmehr, M., Karimi, M., Sharifi, M., Kazemi, A., 2017. Analytical study of fluid flow modeling by diffusivity equation including the quadratic pressure gradient term. Computers and Geotechnics 89, 1–8. https://doi.org/10.1016/j.compgeo.2017.04.001

Albattat, R., AlSinan, M., Kwak, H., Hoteit, H., 2022. Modeling lost-circulation in natural fractures using semi-analytical solutions and type-curves. Journal of Petroleum Science and Engineering 216, 110770. https://doi.org/10.1016/j.petrol.2022.110770

Al-Hameedi, A.T.T., Alkinani, H.H., Dunn-Norman, S., Flori, R.E., Hilgedick, S.A., 2018. Real-time lost circulation estimation and mitigation. Egyptian Journal of Petroleum 27, 1227–1234. https://doi.org/10.1016/j.ejpe.2018.05.006

Alsaba, M.T., 2014. Review of Lost Circulation Materials and Treatments with an Updated Classification.

Archer, R., 2000. APPLIED MATHEMATICS IN RESERVOIR ENGINEERING.

Boukadi, F., Yaghi, B., Al-Hadrami, H., Bemani, A., Babadagli, T., De Mestre, P., 2004. A Comparative Study of Lost Circulation Materials. Energy Sources 26, 1043–1051. https://doi.org/10.1080/00908310490494612

Bychina, M., Thomas, G.M., Khandelwal, R., Samuel, R., 2017. A Robust Model to Estimate the Mud Loss into Naturally Fractured Formations, in: Day 1 Mon, October 09, 2017. Presented at the SPE Annual Technical Conference and Exhibition, SPE, San Antonio, Texas, USA, p. D011S005R008. https://doi.org/10.2118/187219-MS

Carlson, E.S., Venkataraman, M., Clark, P.E., Sifferman, T.R., Coffey, M.D., Seheult, J.M., 1996. Predicting the Fluid Loss of Drilling, Workover, and Fracturing Fluids into a Formation With and Without Filter Cake, in: Permian Basin Oil and Gas Recovery Conference. Presented at the Permian Basin Oil and Gas Recovery Conference, Society of Petroleum Engineers, Midland, Texas. https://doi.org/10.2118/35227-MS

Carlson, M.R., 1999. Reservoir Characterization Of Fractured Reservoirs In Western Canada. Journal of Canadian Petroleum Technology 38. https://doi.org/10.2118/99-13-64

Chan, A.W., Brem, A.G., Abd Rahim, M.H., Numpang, A., Chong, S., 2022. The Four Pillars for De-Risking Fluid Loss Potential Along Fault Damage Zone: A Framework for Well Designs and Drilling Operations. Presented at the 56th U.S. Rock Mechanics/Geomechanics Symposium, OnePetro. https://doi.org/10.56952/ARMA-2022-0197

Cook, J., 2011. Stabilizing the wellbore to prevent lost circulation.

Da Prat, G., 1990. Well test analysis for fractured reservoir evaluation, Developments in petroleum science. Elsevier, Amsterdam ; New York.

Dake, L.P., 2001. The Practice of Reservoir Engineering: Revised Edition. Elsevier, Burlington.

Dokhani, V., Ma, Y., Li, Z., Geng, T., Yu, M., 2019. Transient Effects of Leak-off and Fracture Ballooning on Mud Loss in Naturally Fractured Formations. p. ARMA-2019-1945.

Dyke, C.G., Wu, B., Milton-Tayler, D., 1995. Advances in Characterizing Natural-Fracture Permeability From Mud-Log Data. SPE Formation Evaluation 10, 160–166. https://doi.org/10.2118/25022-PA

Elkatatny, S., Ahmed, A., Abughaban, M., Patil, S., 2020. Deep Illustration for Loss of Circulation While Drilling. Arab J Sci Eng 45, 483–499. https://doi.org/10.1007/s13369-019-04315-6

Escobar, F.-H., Zambrano, A.-P., Giraldo, D.-V., Cantillo, J.-H., 2011. Pressure and pressure derivative analysis for Non-Newtonian pseudoplastic fluids in double-porosity formations. CT&F Cienc. Tecnol. Futuro 4, 47–60. https://doi.org/10.29047/01225383.238

Fakoya, M.F., Ahmed, R.M., 2018. A generalized model for apparent viscosity of oil-based muds. Journal of Petroleum Science and Engineering 165, 777–785. https://doi.org/10.1016/j.petrol.2018.03.029

Feng, Y.., Arlanoglu, C.., Podnos, E.., Becker, E.., Gray, K.E.. E., 2015. Finite-Element Studies of Hoop-Stress Enhancement for Wellbore Strengthening. SPE Drilling & Completion 30, 38–51. https://doi.org/10.2118/168001-PA

Feng, Y., Gray, K.E., 2018. Lost Circulation and Wellbore Strengthening, SpringerBriefs in Petroleum Geoscience & Engineering. Springer International Publishing, Cham. https://doi.org/10.1007/978-3-319-89435-5

Garcia-Pastrana, J.R., Valdes-Perez, A.R., Blasingame, T.A., 2017a. Flow of Non-Newtonian Fluids within a Double Porosity Reservoir under Pseudosteady State Interporosity Transfer Conditions. Presented at the SPE Latin America and Caribbean Petroleum Engineering Conference, OnePetro. https://doi.org/10.2118/185479-MS

Garcia-Pastrana, J.R., Valdes-Perez, A.R., Blasingame, T.A., 2017b. Flow of Non-Newtonian Fluids within a Double Porosity Reservoir under Pseudosteady State Interporosity Transfer Conditions, in: Day 1 Wed, May 17, 2017. SPE, Buenos Aires, Argentina, p. D011S004R001. https://doi.org/10.2118/185479-MS

Golghanddashti, H., 2011. A new analytically derived shape factor for gas–oil gravity drainage mechanism. Journal of Petroleum Science and Engineering 77, 18–26. https://doi.org/10.1016/j.petrol.2011.02.004

Guillot, D., Hendriks, H., Callet, F., Vidick, B., 1990. 5 Mud Removal, in: Developments in Petroleum Science. Elsevier, pp. 5-1-5–37. https://doi.org/10.1016/S0376-7361(09)70303-6

Ikoku, C.U., Ramey, H.J., 1979. Transient Flow of Non-Newtonian Power-Law Fluids in Porous Media. Society of Petroleum Engineers Journal 19, 164–174. https://doi.org/10.2118/7139-PA

Keshavarz, M., Moreno, R.B.Z.L., 2023. Qualitative Analysis of Drilling Fluid Loss Through Naturally-Fractured Reservoirs. SPE Drilling & Completion. https://doi.org/10.2118/215810-PA

Kostov, N., Ning, J., Gosavi, S.V., Gupta, P., Kulkarni, K., Sanz, P., 2015. Advanced Drilling Induced Fracture Modeling for Wellbore Integrity Prediction, in: Day 3 Wed, September 30, 2015. Presented at the SPE Annual Technical Conference and Exhibition, SPE, Houston, Texas, USA, p. D031S033R004. https://doi.org/10.2118/174911-MS

Kuhlman, K.L., 2013. Review of inverse Laplace transform algorithms for Laplace-space numerical approaches. Numer Algor 63, 339–355. https://doi.org/10.1007/s11075-012-9625-3

Lavrov, A., 2006. Modeling Flow of a Biviscous Fluid From Borehole Into Rock Fracture. Journal of Applied Mechanics 73, 171–173. https://doi.org/10.1115/1.2061927

Lavrov, A., TotalBoox, TBX, 2016. Lost Circulation. Elsevier Science.

Lavrov, A., Tronvoll, J., 2004. Modeling Mud Loss in Fractured Formations, in: All Days. Presented at the Abu Dhabi International Conference and Exhibition, SPE, Abu Dhabi, United Arab Emirates, p. SPE-88700-MS. https://doi.org/10.2118/88700-MS

Lee, J., Rollins, J.B., Spivey, J.P., 2003. Pressure transient testing, SPE textbook series. Henry L. Doherty Memorial Fund of AIME, Society of Petroleum Engineers, Richardson, Tex.

Li´etard, O., Unwin, T., Guillot, D.J., Hodder, M.H., Civan, F., Rasmussen, M., 2002. Fracture width logging while drilling and drilling mud/loss-circulation-material selection guidelines in naturally fractured reservoirs. SPE Drilling & Completion.

Liétard, O., Unwin, T., Guillo, D.J., Hodder, M.H., 1999a. Fracture Width Logging While Drilling and Drilling Mud/Loss-Circulation-Material Selection Guidelines in Naturally

Fractured Reservoirs. SPE Drilling & Completion 14, 168–177. https://doi.org/10.2118/57713-PA
Liétard, O., Unwin, T., Guillo, D.J., Hodder, M.H., 1999b. Fracture Width Logging While Drilling and Drilling Mud/Loss-Circulation-Material Selection Guidelines in Naturally Fractured Reservoirs. SPE Drilling & Completion 14, 168–177. https://doi.org/10.2118/57713-PA
Mahmoudi, M., Roostaei, M., Ghalambor, A., 2016. Sand Screen Design and Optimization for Horizontal Wells Using Reservoir Grain Size Distribution Mapping, in: Day 1 Wed, February 24, 2016. Presented at the SPE International Conference and Exhibition on Formation Damage Control, SPE, Lafayette, Louisiana, USA, p. D011S001R004. https://doi.org/10.2118/179036-MS
Majidi, Miska, S.Z.. Z., Yu, M.., Thompson, L.G.. G., Zhang, J.., 2010. Quantitative Analysis of Mud Losses in Naturally Fractured Reservoirs: The Effect of Rheology. SPE Drilling & Completion 25, 509–517. https://doi.org/10.2118/114130-PA
Mansour, A., Dahi Taleghani, A., Salehi, S., Li, G., Ezeakacha, C., 2019. Smart lost circulation materials for productive zones. J Petrol Explor Prod Technol 9, 281–296. https://doi.org/10.1007/s13202-018-0458-z
Miska, S.Z., Yu, M., Thompson, L.G., Zhang, J., 2008. Modeling of Drilling Fluid Losses in Naturally Fractured Formations, in: All Days. Presented at the SPE Annual Technical Conference and Exhibition, SPE, Denver, Colorado, USA, p. SPE-114630-MS. https://doi.org/10.2118/114630-MS
Moazzeni, A., Nabaei, M., Jegarluei, S.G., 2012. Decision Making for Reduction of Nonproductive Time through an Integrated Lost Circulation Prediction. Petroleum Science and Technology 30, 2097–2107. https://doi.org/10.1080/10916466.2010.495961
Moore, P.L., 1986. Drilling practices manual. Second edition. Pennwell Books,Tulsa, OK, United States.
Narr, W., 2011. Characterization of naturally fractured reservoirs. Society of Petroleum Engineers, Richardson, TX.
Okoro, E.E., Dosunmu, A., Iyuke, S.E., 2018. Data on cost analysis of drilling mud displacement during drilling operation. Data in Brief 19, 535–541. https://doi.org/10.1016/j.dib.2018.05.075
Olarewaju, 1992. A Reservoir Model of Non-Newtonian Fluid Flow. Society of Petroleum Engineers. https://doi.org/SPE-25301- MS
Ostroot, K., Shayegi, S., Zoontjes, D., Lovorn, R., 2007. Comparison and Advantages of Underbalanced and Managed-Pressure Drilling Techniques: When Should Each Be Applied?, in: All Days. Presented at the Offshore Technology Conference, OTC, Houston, Texas, U.S.A., p. OTC-18561-MS. https://doi.org/10.4043/18561-MS
Pilehvari, A.A., Nyshadham, V.R., 2002. Effect of Material Type and Size Distribution on Performance of Loss/Seepage Control Material, in: All Days. Presented at the International Symposium and Exhibition on Formation Damage Control, SPE, Lafayette, Louisiana, p. SPE-73791-MS. https://doi.org/10.2118/73791-MS
Razavi, O., Karimi Vajargah, A., van Oort, E., Aldin, M., Govindarajan, S., 2016. Optimum particle size distribution design for lost circulation control and wellbore strengthening. Journal of Natural Gas Science and Engineering 35, 836–850. https://doi.org/10.1016/j.jngse.2016.08.038
Razavi, O., Lee, H.P., Olson, J.E., Schultz, R.A., 2017a. Drilling Mud Loss in Naturally Fractured Reservoirs: Theoretical Modelling and Field Data Analysis, in: Day 1 Mon, October 09, 2017. SPE, San Antonio, Texas, USA, p. D011S005R003. https://doi.org/10.2118/187265-MS

Razavi, O., Lee, H.P., Olson, J.E., Schultz, R.A., 2017b. Drilling Mud Loss in Naturally Fractured Reservoirs: Theoretical Modelling and Field Data Analysis, in: Day 1 Mon, October 09, 2017. Presented at the SPE Annual Technical Conference and Exhibition, SPE, San Antonio, Texas, USA, p. D011S005R003. https://doi.org/10.2118/187265-MS

Razavi, O., Vajargah, A.K., van Oort, E., Aldin, M., Patterson, R., 2015. How to Effectively Strengthen Wellbores in Narrow Drilling Margin Wells: An Experimental Investigation, in: Day 3 Wed, September 30, 2015. Presented at the SPE Annual Technical Conference and Exhibition, SPE, Houston, Texas, USA, p. D031S033R002. https://doi.org/10.2118/174976-MS

Rehm, B. (Ed.), 2012. Underbalanced drilling: limits and extremes, Gulf drilling series. Gulf Pub. Co, Houston, TX.

Rezaee, R. (Ed.), 2015. Fundamentals of Gas Shale Reservoirs: Rezaee/Fundamentals of Gas Shale Reservoirs. John Wiley & Sons, Inc, Hoboken, NJ. https://doi.org/10.1002/9781119039228

Sageev, A., Da Prat, G., Ramey, H.J., 1985. Decline Curve Analysis for Double-Porosity Systems, in: SPE California Regional Meeting. Presented at the SPE California Regional Meeting, Society of Petroleum Engineers, Bakersfield, California. https://doi.org/10.2118/13630-MS

Society of Petroleum Engineers, 2012. Unconventional wisdom: SPE annual technical conference and exhibition 2012, (ATCE 2012) ; San Antonio, Texas, USA, 8 - 10 October 2012. Curran, Red Hook, NY.

Stehfest, H., 1970. Algorithm 368: Numerical inversion of Laplace transforms [D5]. Commun. ACM 13, 47–49. https://doi.org/10.1145/361953.361969

Sun, H. (Ed.), 2015. 3 - Fetkovich Decline Curves Analysis, in: Advanced Production Decline Analysis and Application. Gulf Professional Publishing, pp. 67–94. https://doi.org/10.1016/B978-0-12-802411-9.00003-X

Wang, L., Chen, X., Xia, Z., 2018. A Novel Semi-Analytical Model for Multi-branched Fractures in Naturally Fractured-Vuggy Reservoirs. Sci Rep 8, 11586. https://doi.org/10.1038/s41598-018-30097-2

Warren, J.E., Root, P.J., 1963. The Behavior of Naturally Fractured Reservoirs. Society of Petroleum Engineers Journal 3, 245–255. https://doi.org/10.2118/426-PA

Wennberg, O.P., Svånå, T., Azizzadeh, M., Aqrawi, A.M.M., Brockbank, P., Lyslo, K.B., Ogilvie, S., 2006. Fracture intensity vs. mechanical stratigraphy in platform top carbonates: the Aquitanian of the Asmari Formation, Khaviz Anticline, Zagros, SW Iran. Petroleum Geoscience 12, 235–246. https://doi.org/10.1144/1354-079305-675

Wu, X., Wan, F., Chen, Z., Han, L., Li, Z., 2020. Drilling and completion technologies for deep carbonate rocks in the Sichuan Basin: Practices and prospects. Natural Gas Industry B 7, 547–556. https://doi.org/10.1016/j.ngib.2020.09.012

Xu, C., Kang, Y., You, Z., Chen, M., 2016. Review on formation damage mechanisms and processes in shale gas reservoir: Known and to be known. Journal of Natural Gas Science and Engineering 36, 1208–1219. https://doi.org/10.1016/j.jngse.2016.03.096

Ziegler, F.E., Jones, J.F., 2014. Predrill pore-pressure prediction and pore pressure and fluid loss monitoring during drilling: A case study for a deepwater subsalt Gulf of Mexico well and discussion on fracture gradient, fluid losses, and wellbore breathing. Interpretation 2, SB45–SB55. https://doi.org/10.1190/INT-2013-0099.1

APPENDIX A

DERIVATION OF DUAL-POROSITY SOLUTION THROUGH NFR UNDER WELLBORE CONSTANT PRESSURE CONDITION

The Appendix presents the derivation of the solution to measure Non-Newtonian fluid through NFR (Double Porosity). Dimensionless form of the proposed model (Escobar et al., 2011) respectively, defined by

$$\frac{\partial^2 p_{fD}}{\partial r_D^2} + \frac{n}{r_D}\frac{\partial p_{fD}}{\partial r_D} = r_D^{1-n}\left(\omega \frac{\partial p_{fD}}{\partial t_D} + (1-\omega)\frac{\partial p_{mD}}{\partial t_D}\right), t_D > 0 \text{ ....Eq A.1}$$

For source term, dimensionless form defined by;

$$\frac{\partial p_{mD}}{\partial t_D} = \frac{n\lambda}{(1-\omega)}.D^{1-n}.(p_{fD} - p_{mD}) \text{ ....Eq A.2}$$

To solve Eq A.1 and Eq A.2, the Eq 4.3 to Eq 4.5 turning to dimensionless form as below,

Initial Condition: Uniform pressure distribution

$$p_{mD}(r_{mD}, 0) = p_{fD}(r_{fD}, 0) = 0 \text{ ....Eq A.3}$$

Inner Boundary Condition: Constant wellbore pressure

$$p_{fD}\text{-}S\left(\frac{\partial p_{fD}}{\partial tD}\right)=1 \text{......................................Eq A.4}$$

Outer Boundary Condition: Infinite-acting reservoir

$$\lim_{r_D \to \infty} p_{fD}(r_D, t) = 0 \text{......................................Eq A.5}$$

Taking the Laplace transform of Eq. A.2:

$$u\acute{p}_{mD}(r_D, u) - p_{mD}(r_D, 0) = \frac{n\lambda}{(1-\omega)} D^{1-n}(\acute{p}_{fD}(r_D, u) - \acute{p}_{mD}(r_D, u)) \text{......................Eq A.6}$$

If Eq A.6 is arranged based on $\acute{p}_{mD}(r_D, u)$ function, it become

$$\acute{p}_{mD}(r_D,u)=\frac{n\lambda D^{1-n}}{u(1-\omega)+n\lambda D^{1-n}}\acute{p}_{fD}(r_D,u)\ldots\ldots\ldots\text{Eq A.7}$$

Then, taking the Laplace transform of Eq A.1:

$$\frac{d^2\acute{p}_{fD}(r_D,u)}{dr_D^2}+\frac{n}{r_D}\frac{d\acute{p}_{fD}(r_D,u)}{dr_D}=r_D^{1-n}[\omega(u\acute{p}_{fD}(r_D,u))+(1-\omega)(u\acute{p}_{mD}(r_D,u))]\ldots\ldots\ldots\text{Eq A.8}$$

Then, Eq A.7 substituting in Eq A.8

$$\frac{d^2\acute{p}_{fD}(r_D,u)}{dr_D^2}+\frac{n}{r_D}\frac{d\acute{p}_{fD}(r_D,u)}{dr_D}=r_D^{1-n}\left[\omega(u\acute{p}_{fD}(r_D,u))+(1-\omega)[u\frac{n\lambda D^{1-n}}{u(1-\omega)+n\lambda D^{1-n}}\acute{p}_{fD}(r_D,u)]\right]\ldots\ldots\ldots\text{Eq A.9}$$

The $u\acute{p}_{fD}(u)$ factored from Eq A.9 results in

$$\frac{d^2\acute{p}_{fD}(r_D,u)}{dr_D^2}+\frac{n}{r_D}\frac{d\acute{p}_{fD}(r_D,u)}{dr_D}=r_D^{1-n}\left[u\acute{p}_{fD}(r_D,u)\frac{u(1-\omega)\omega+n\lambda D^{1-n}}{u(1-\omega)+n\lambda D^{1-n}}]\right]\ldots\ldots\ldots\text{Eq A.10}$$

The interporosity flow function is introduced as

$$g(u)=\frac{\omega(1-\omega)u+n\lambda D^{1-n}}{(1-\omega)u+n\lambda D^{1-n}}\ldots\ldots\ldots\text{Eq A.11}$$

Since Eq A.11 substitute in Eq A.10, it become

$$\frac{d^2\acute{p}_{fD}(r_D,u)}{dr_D^2}+\frac{n}{r_D}\frac{d\acute{p}_{fD}(r_D,u)}{dr_D}=r_D^{1-n}[ug(u)\acute{p}_{fD}(r_D,u)]]\ldots\ldots\ldots\text{Eq A.12}$$

r_D^2 factor is multiplying in Eq A.12 which results in

$$r_D^2\frac{d^2\acute{p}_{fD}(r_D,u)}{dr_D^2}+nr_D\frac{d\acute{p}_{fD}(r_D,u)}{dr_D}=r_D^{3-n}[ug(u)\acute{p}_{fD}(r_D,u)]]\ldots\ldots\ldots\text{Eq A.13}$$

For solving Eq A.13, the parameter δ introduced as

$\delta=\frac{1-n}{2}$..Eq A.14

Since δ term applied to Eq A.13, it become

$r_D^2\frac{d^2\acute{p}_{fD}(r_D,u)}{dr_D^2}+(1-2\delta)r_D\frac{d\acute{p}_{fD}(r_D,u)}{dr_D}=r_D^{3-n}[ug(u)\acute{p}_{fD}(r_D,u)]]$................................Eq A.15

Similar to Ikoku and Ramey (1979), the following transform function has been applied

$\acute{p}_{fD}(r_D,u)=\hat{H}_D(z)$..Eq A.16

Where this form uses the transformation variable (z):

$z=\frac{2\sqrt{ug(u)}}{3-n}r_D^{\frac{3-n}{2}}$..Eq A.17

By using the definitions prescribed by Eq A.16 and Eq A.17, it obtains

$z^2\frac{d^2\hat{H}_D(z)}{dz^2}+\frac{d\hat{H}_D(z)}{dz}=z^2\hat{H}_D(z)$...Eq A.18

As in the case of Ikoku and Ramey (1979), it obtained

$\nu=\frac{1-n}{3-n}$..Eq A.19

To set the coefficient of the first derivative term in Eq A.15 to one, the following equation is proposed:

$\hat{H}_D(z)=\frac{z^\nu}{\psi}\dot{B}_D(z)$..Eq A.20

Where

$\psi=\left[\frac{2\sqrt{ug(u)}}{3-n}\right]^{\frac{1-n}{3-n}}$..Eq A.21

Therefore Eq. A.15 can be expressed in terms of Eq. A.18 as:

$$z^2 \frac{d^2\dot{B}_D(z)}{dz^2} + z\frac{d\dot{B}_D(z)}{dz} = (\nu^2 + z^2)\dot{B}_D(z) \text{..} \text{Eq A.22}$$

Therefore, the solution is

$$\dot{B}_D(z) = C_1 I_\nu(z) + C_2 K_\nu(z) \text{..} \text{Eq.23}$$

Recalling the change of variable from Eq. A.20 and Eq. Eq A.22, therefore it becomes

$$\hat{H}_D(z) = r_D^{\frac{1-n}{2}} [C_1 I_\nu(z) + C_2 K_\nu(z)] \text{..} \text{Eq.24}$$

Then, Eq A.24 can be written as

$$\acute{p}_{fD}(r_D, u) = r_D^{\frac{1-n}{2}} [C_1 I_{\frac{1-n}{3-n}} \left[r_D^{\frac{3-n}{2}} \frac{2\sqrt{ug(u)}}{3-n} \right] + C_2 K_{\frac{1-n}{3-n}}\ r_D^{\frac{3-n}{2}} \frac{2\sqrt{ug(u)}}{3-n}] \text{...............................} \text{Eq A.25}$$

Then, the Laplace transform should be implied on boundary conditions to transform them in the Laplace domain.

Initial Condition: Uniform pressure distribution

$$\acute{p}_{fD}(r_D, u = 0) = 0 \text{..} \text{Eq A.26}$$

Inner Boundary Condition: Constant flow pressure

$$\acute{p}_{fD} - S\left(\frac{\partial \acute{p}_{fD}}{\partial r_D}\right) = \frac{1}{u} \text{..} \text{Eq A.27}$$

Outer Boundary Condition: Infinite-acting reservoir system

$$\lim_{r_D \to \infty} \acute{p}_{fD}(r_D, u) = 0 \text{..} \text{Eq A.28}$$

Outer boundary condition considered on Eq A.25 which results in C_1 equal to zero. At the same time, the inner constant pressure condition assumed inside the wellbore results in

$$\frac{1}{u} = r_D^{\frac{1-n}{2}} \left[C_2 . K_{\frac{1-n}{3-n}} r_D^{\frac{3-n}{2}} \frac{2\sqrt{u.g(u)}}{3-n} \right] \text{………………………..………..……………………...….Eq A.29}$$

After Eq A.29 solves for C_2, it equals

$$C_2 = \frac{1}{u.K_{\frac{1-n}{3-n}} \frac{2\sqrt{u.g(u)}}{3-n}} \text{……………………………..……......…...…………………………Eq A.30}$$

Since the Eq A.30 substitute in Eq A.25, the specific result under constant wellbore pressure assumption in the Laplace domain derived as

$$\acute{p}_{fD}(r_D, u) = \frac{r_D^{\frac{1-n}{2}} .K_{\frac{1-n}{3-n}}(\frac{2.\sqrt{u.g(u)}}{3-n}.r_D^{\frac{3-n}{2}})}{u\ .K_{\frac{1-n}{3-n}}(\frac{2.\sqrt{u.g(u)}}{3-n})} \text{……………………………...……...………………Eq A.31}$$

Then, Darcy's law applies to relate dimensionless pressure with dimensionless rate

$$q_D = -r_D . \frac{\partial p_D}{\partial r_D} \text{……………………………………..…………………………………...Eq A.32}$$

After that, the Eq A.32 transforms to the Laplace domain as below

$$\hat{q}_D = -r_D . \frac{\partial \hat{p}_D}{\partial r_D} \text{………………………...……...…………………………………………...Eq A.33}$$

After the Eq A.31 substitute in Eq A.33, the result will be

$$\hat{q}_D(r_D,u) = -r_D.\frac{\partial \hat{p}_D(r_D,u)}{\partial r_D} = -r_D.\frac{\partial}{\partial r_D}\left(\frac{r_D^{\frac{1-n}{2}}.K_{\frac{1-n}{3-n}}(\frac{2.\sqrt{u.g(u)}}{3-n}.r_D^{\frac{3-n}{2}})}{u\,.K_{\frac{1-n}{3-n}}(\frac{2.\sqrt{u.g(u)}}{3-n})}\right) =$$

$$\frac{(1-n).r^{\frac{1-n}{2}}.K_{\frac{1-n}{3-n}}\left(\frac{2.r^{\frac{3-n}{2}}.\sqrt{u.g(u)}}{3-n}\right)}{2.u.K_{\frac{1-n}{3-n}}\left(\frac{2.\sqrt{u.g(u)}}{3-n}\right)} -$$

$$\frac{r^{\frac{1-n}{2}+\frac{3-n}{2}}.\sqrt{u.g(u)}.[-K_{\frac{1-n}{3-n}-1}\left(\frac{2.r^{\frac{3-n}{2}}.\sqrt{ug(u)}}{3-n}\right)-K_{\frac{1-n}{3-n}+1}\left(\frac{2.r^{\frac{3-n}{2}}.\sqrt{ug(u)}}{3-n}\right)]}{2.u.K_{\frac{1-n}{3-n}}(\frac{2.\sqrt{u.g(u)}}{3-n})} \text{……………..................………Eq A.34}$$

Following by applying Theorem 7, (Jim Lambers, ENERGY 281, Spring Quarter 2007-08), to derive cumulative recovery as below

$$Q_D(r_D,t_D) = \int_0^{t_D} q_D(r_D,t_D)\, dt_D \text{………………..………….........……………………Eq A.35}$$

$$Q_D(r_D,u) = \frac{1}{u}.q_D(r_D,u) = -\frac{(1-n).r^{\frac{1-n}{2}}.K_{\frac{1-n}{3-n}}\left(\frac{2.r^{\frac{3-n}{2}}.\sqrt{u.g(u)}}{3-n}\right)}{2.u^2.K_{\frac{1-n}{3-n}}\left(\frac{2.\sqrt{u.g(u)}}{3-n}\right)} -$$

$$\frac{r^{\frac{1-n}{2}+\frac{3-n}{2}}.\sqrt{u.g(u)}.[-K_{\frac{1-n}{3-n}-1}\left(\frac{2.r^{\frac{3-n}{2}}.\sqrt{ug(u)}}{3-n}\right)-K_{\frac{1-n}{3-n}+1}\left(\frac{2.r^{\frac{3-n}{2}}.\sqrt{ug(u)}}{3-n}\right)]}{2.u^2.K_{\frac{1-n}{3-n}}(\frac{2.\sqrt{u.g(u)}}{3-n})} \text{………………...…......……..Eq A.36}$$

APPENDIX B

DERIVATION OF DIFFUSIVITY SOLUTION THROUGH HOMOGENOUS RESERVOIR UNDER WELLBORE CONSTANT PRESSURE CONDITION

This Appendix provides an evaluated solution suitable for measuring Non-Newtonian fluid flow through a homogenous reservoir.

Dimensionless form of Non-Newtonian fluid flow through a homogenous reservoir derived by (Ikoku, 1979) is

$$\frac{\partial^2 p_{DNN}}{\partial r_D^2} + \frac{n}{r_D}\frac{\partial p_{DNN}}{\partial r_D} = r_D^{1-n}\frac{\partial p_{DNN}}{\partial t_{DNN}} \quad \text{..........Eq B.1}$$

According to the cases that this study follows to measure drilling fluid rate and volume, the following initial and boundary conditions are considered,

Initial condition: Uniform pressure distribution

$$p_{DNN}(r_D, t_D = 0) = 0 \quad \text{..........Eq B.2}$$

Inner boundary condition: Constant flow pressure

$$p_{DNN}(r_D = 1, t_D) = 0 \quad \text{..........Eq B.3}$$

Outer Boundary Condition: Infinite-Acting Reservoir

$$\lim_{r_D \to \infty} p_{DNN}(r_D, t_D) = 0 \quad \text{..........Eq B.4}$$

Since the Laplace transforms apply to Eq B.1, it become

$$\frac{d^2 \acute{p}_{DNN}(r_D,u)}{dr_D^2} + \frac{n}{r_D}\frac{d\acute{p}_{DNN}(r_D,u)}{dr_D} = r_D^{1-n} u \acute{p}_{DNN} \quad \text{..........Eq B.5}$$

Then, to solve the Eq B.5 for our specific case, the Laplace transform should be exerted on Eq B.3 and Eq B.4.

Inner boundary condition in Laplace domain: Constant flow pressure

$p_{DNN}(r_D = 1, u) = \frac{1}{u}$ ………………………………………………………… Eq B.6

Outer Boundary Condition in the Laplace domain: Infinite-Acting Reservoir

$\lim_{r_D \to \infty} p_{DNN}(r_D, u) = 0$ ………………………………………………………… Eq B.7

Then, r_D^2 should be multiplied on Eq B.5

$r_D^2 \frac{d^2 \acute{p}_{DNN}(r_D,u)}{dr_D^2} + nr_D \frac{d\acute{p}_{DNN}(r_D,u)}{dr_D} = r_D^{3-n} u\acute{p}_{DNN}(r_D, u)$……………………………………Eq B.8

The δ defined as

$\delta = \frac{1-n}{2}$……………………………………………………………………Eq B.9

After considering Eq B.9 on Eq B.8, it results

$r_D^2 \frac{d^2 \acute{p}_{DNN}(r_D,u)}{dr_D^2} + (1 - 2\delta) r_D \frac{d\acute{p}_{DNN}(r_D,u)}{dr_D} = r_D^{3-n} u\acute{p}_{DNN}(r_D, u)$……………………………Eq B.10

Following transform function defined

$\acute{p}_{DNN}(r_D, u) = \hat{G}_D(z)$…………… ……………………………………………Eq B.11

While the transform variable is

$z = \frac{2\sqrt{u}}{3-n} r_D^{\frac{3-n}{2}}$ ……………………………………………………………Eq B.12

Then, Eq B.11 and Eq B.12 substituting in Eq B.10

$z^2 \frac{d^2 \hat{G}_D(z)}{dz^2} + (1 - 2\nu) z \frac{d\hat{G}_D(z)}{dz} = z^2 \hat{G}_D(z)$……………………………………………..Eq B.13

The ν parameter is defined as

$\nu = \frac{1-n}{3-n}$ ……………………………………………………………………Eq B.14

To arrange the first derivative term in Eq B.13 to one, the below equation suggests

$\hat{G}_D(z) = \frac{z^\nu}{\psi} B_D(z)$ ……………………………………..……….…………………..Eq B.15

While

$\Psi = \left[\frac{2\sqrt{u}}{3-n} r_D^{\frac{3-n}{2}}\right]^{\frac{1-n}{3-n}}$ ………………………………..……………………..……………………Eq B.16

The transformation is given by Eq B.15 and Eq B.16 applying to Eq B.13

$z^2 \frac{d^2 B_D(z)}{dz^2} + z\frac{dB_D(z)}{dz} = (\nu^2 + z^2) B_D(z)$ …………………………………………......……..Eq B.17

Therefore, the general solution of Eq B.17 become

$B_D(z) = C_1 I_\nu(z) + C_2 K_\nu(z)$ ……………………………………...……...……….....…Eq B.18

While Eq B.15 is considered, the Eq B.18 become

$\hat{G}_D(z) = \frac{z^\nu}{\psi} [C_1 I_\nu(z) + C_2 K_\nu(z)]$ ………………………..……….....………………......…Eq B.19

Therefore, the general solution for Eq B.10 obtain as

$\acute{p}_{DNN}(r_D, u) = r_D^{\frac{1-n}{2}} [C_1 I_{\frac{1-n}{3-n}} \left[r_D^{\frac{3-n}{2}} \frac{2\sqrt{u}}{3-n}\right] + C_2 K_{\frac{1-n}{3-n}} \left[r_D^{\frac{3-n}{2}} \frac{2\sqrt{u}}{3-n}\right]]$ ………………....………..Eq B.20

Since the outer boundary condition (infinite-acting behavior) applied on the general solution (Eq. B20) and the behavior of Modified Bessel functions of the first kind shows, the C1 becomes zero. Then, inner constant pressure is applied on Eq B.20 which results in

$C_2 = \frac{1}{u.K_{\frac{1-n}{3-n}} \frac{2\sqrt{u}}{3-n}}$ …………………………......……………...…………………………Eq B.21

While substituting C1 and Eq B.21 in Eq B.20, the dimensionless pressure through a homogenous reservoir for Non-Newtonian fluid under constant wellbore pressure equal to

$$\hat{p}(r_D, u) = \frac{r_D^{\frac{1-n}{2}} . K_{\frac{1-n}{3-n}}(\frac{2}{3-n}.\sqrt{u}.r_D^{\frac{3-n}{2}})}{u . K_{\frac{1-n}{3-n}}(\frac{2}{3-n}.\sqrt{u})} \quad \text{……………………………………………Eq B.22}$$

Applying the Laplace transform to both sides of the Darcy equation

$$q_D(r_D, u) = -r_D . \frac{\partial \hat{p}_D(r_D,u)}{\partial r_D} = -r_D . \frac{\partial}{\partial r_D} \left(\frac{r_D^{\frac{1-n}{2}} . K_{\frac{1-n}{3-n}}(\frac{2}{3-n}.\sqrt{u}.r_D^{\frac{3-n}{2}})}{u . K_{\frac{1-n}{3-n}}(\frac{2}{3-n}.\sqrt{u})} \right) \text{……………………………Eq B.23}$$

Then, the dimensionless rate in the Laplace domain for Non-Newtonian fluid in a homogenous reservoir will be

$$q_D(r_D, u) = \frac{r^{2-n}.K_{\frac{2}{3-n}}(\frac{2.r^{\frac{3-n}{2}}.\sqrt{u}}{3-n})}{u^{0.5}.K_{\frac{n-1}{n-3}}(\frac{2.\sqrt{u}}{3-n})} \text{……………………………………………………Eq B.24}$$

After that, dimensionless volume in the Laplace domain can be derived readily by recalling Theorem 7, therefore, it becomes

$$Q_D(r_D, u) = \frac{r^{2-n}.K_{\frac{2}{3-n}}(\frac{2.r^{\frac{3-n}{2}}.\sqrt{u}}{3-n})}{u^{1.5}.K_{\frac{n-1}{n-3}}(\frac{2.\sqrt{u}}{3-n})} \text{……………………………………………………Eq B.25}$$

To derive the solution in analytical form, Hankel developed asymptotic (short argument) expansions that have been applied to transform the numerical solution in the Laplace domain. As a result, we can derive dimensionless rate and volume approximate solutions for both conditions. To derive the analytical solution for a short time, Hankel developed asymptotic (short argument) expansions (Eq B.26) applied to approximate the Bessel functions (q_D as s $\rightarrow \infty$,) at early times,

$$K_\alpha(u) \sim \sqrt{\frac{\pi}{2u} e^{-u}} \left(1 + \frac{4\alpha^2 - 1}{8u} + \frac{(4\alpha^2-1)(4\alpha^2-9)}{2!(8u)^2}\right) \text{……………………………………Eq B.26}$$

Since the approximate quantity for Besselk for both numerator and denominator is derived, the equation simplifies and prepares for LaPlace inversion, consequently, the dimensionless rate for a short time is measured below

$$q_D(r_D,t_D)=\frac{r^{(1.25-0.75n)}.e^{-\frac{(1-r_D^{(1.5-\frac{n}{2})})^2}{(n-3)^2.t_D}}}{\sqrt{\pi}.\sqrt{t_D}}$$ ……………………..……...……………………Eq B.27

To derive the analytical solution for a long time, developed asymptotic (Large argument) expansions by Hankel (Eq B.28) have been applied for both numerator and denominator to approximate modified Besselk terms

$$K_\alpha(z)\sim\frac{\Gamma(\alpha)}{2}.(\frac{2}{z})^\alpha \quad \text{if } \alpha>0$$ ………………..…...………....………..............…..………..Eq B.28

Then, the LaPlace inverse is taken to obtain the analytical dimensionless rate, and it become

$$q_D(r_D,t_D)=\frac{(3-n)^{\frac{n+1}{3-n}}.r^{1-n}.t_D^{-\frac{2}{n-3}-1}}{\Gamma(\frac{n-1}{n-3})}$$ …………………………..……..…………………..Eq B.29

The analytical dimensionless cumulative loss in real short-time and long-time are deriving similarly as below respectively

$$Q_D(r_D,t_D)=-\frac{0.9\,.r_D^{2-n}.(r^w-1).(\frac{1.77245.t_D.|n-3|.1F1(-0.5;0.5;\frac{(r^w-1)^2}{(n-3)^2.t_D})}{|r^w-1|}-3.1416)}{\sqrt{3-n}\,.(n-3)}$$ ....……..….......Eq B.30

$$Q_D(r_D,t_D)=\frac{(3-n)^{\frac{n+1}{3-n}}.r^{1-n}.t_D^{-\frac{(5-n)}{n-3}-1}.\Gamma(\frac{2}{n-3})}{\Gamma\left(\frac{n-1}{n-3}\right).\Gamma(-\frac{5-n}{n-3})}$$ ……………………...……………………......Eq B.31